IOWA STATE UNIVERSITY
Digital Repository

2013

Automated inter-plant spacing sensing of corn plant seedlings and quantification of laying hen behaviors using 3D computer vision

Akash Dev Nakarmi
Iowa State University

Follow this and additional works at: http://lib.dr.iastate.edu/etd

Part of the Agriculture Commons, Behavior and Ethology Commons, Bioresource and Agricultural Engineering Commons, and the Computer Engineering Commons

Automated inter-plant spacing sensing of corn plant seedlings and quantification of laying hen behaviors using 3D computer vision

by

Akash D Nakarmi

A dissertation submitted to the graduate faculty

in partial fulfillment of the requirements for the degree of

DOCTOR OF PHILOSOPHY

Co-Majors: Agricultural and Biosystems Engineering;
Human Computer Interaction

Program of Study Committee:
Lie Tang, Co-Major Professor
Hongwei Xin, Co-Major Professor
Stuart Birrell
Suzanne T Millman
Brian L Steward

Iowa State University
Ames, Iowa
2013

DEDICATION

This dissertation is dedicated to my loving wife *Anupama Shrestha*

My son *Abhi D Nakarmi*

And my parents *Mr. Anand Nakarmi* and *Mrs. Ambika Nakarmi.*

TABLE OF CONTENTS

LIST OF FIGURES

Chapter 6

LIST OF TABLES

NOMENCLATURE

2D	Two Dimensional
3D	Three Dimensional
CAD	Computer Aided Design
CCD	Charged Coupled Device
CMOS	Complementary Metal Oxide Semiconductor
EU	European Union
FIFO	First In First Out
FOV	Field of View
FPS	Frames per Second
LED	Light Emitting Diode
PSV	Plant Standing Variability
RFID	Radio Frequency Identification
ROI	Region of Interest
RSME	Root Mean Squared Error
SBI	Suppression of Background Illumination
SD	Stocking Density
TCP/IP	Transmission Control Protocol/Internet Protocol
TOF	Time of Flight
UEP	United Egg Producers
USB	Universal Serial Bus

ACKNOWLEDGEMENTS

I would like to express the deepest appreciation to my major professor, Dr. Lie Tang, who continually and convincingly conveyed a spirit of adventure in regard to research and assistantship, and an excitement in regard to teaching. Without his guidance and persistent help, this dissertation would not have been possible.

I would like to thank my co-major professor Dr. Hongwei Xin, and my committee members Dr. Stuart Birrell, Dr. Suzanne T. Millman, and Dr. Brian L. Steward for their guidance and support throughout the course of this research.

In addition, I would also like to thank my friends, colleagues, the department faculty and staff for making my time at Iowa State University a wonderful experience. I also want to offer my appreciation to Tim Shepherd, without whom, this thesis would not have been possible.

Finally, thanks to my family for their encouragement and to my wife for her hours of patience, respect and love.

ABSTRACT

Within-row plant spacing plays an important role in uniform distribution of water and nutrients among plants, hence affects the final crop yield. While manual in-field manual measurements of within-row plant spacing is time and labor intensive, little work has been carried out to automate the process. An automated system is developed using a state-of-the-art 3D vision sensor that accurately measures within-row corn plant spacing. The system is capable of processing about 1200 images captured from a 61 m crop row containing approximately 280 corn plants in about three and half minutes.

Stocking density of laying hens in egg production remains an area of investigation from the standpoints of ensuring hen's ability to perform natural behaviors and production economic efficiency. It is therefore of socio-economic importance to quantify the effect of stocking density on laying hens behaviors and thus wellbeing. In this study, a novel method for automatic quantification of stocking density effect on some natural laying hen behaviors such as locomotion, perching, feeding, drinking and nesting is explored. Image processing techniques are employed on top view images captured with a state-of-the-art time-of-flight (TOF) of light based 3D vision camera for identification as well as tracking of individual hens housed in a 1.2 m × 1.2 m pen. A Radio Frequency Identification (RFID) sensor grid consisting of 20 antennas installed underneath the pen floor is used as a recovery system in situations where the imaging system fails to maintain identities of the hens.

CHAPTER 1

INTRODUCTION

Dissertation Outline

This dissertation is organized as a compilation of five journal articles related to

the research studies focusing on inter-plant spacing sensing and laying hen behavior

monitoring. Chapter 1 provides a brief introduction and also lists the research objectives

of the studies. (Chapter 2 and Chapter 3) discuss image processing techniques developed

for within-row inter-plant spacing sensing of corn plants in early growth stages. The

third article (Chapter 4) details image processing algorithm developed for identification

of cotton plant stems. The last two articles (Chapter 5 and Chapter 6) describe

algorithms for visual monitoring of laying hens to support automatic quantification of

stocking-density effects on their behavior. Final conclusions from the research and

recommendations for future research are presented in Chapter 7.

Inter-plant Spacing Sensing

Spacing variability, rate of emergence, and plant population are the most

common characteristics used by producers in evaluating planter performance.

Mechanisms and maintenance along with planting speed all may influence seed

singulation and placement and can additionally affect plant spacing and emergence

variability, and such variability may ultimately affect plant growth and grain yield.

Uniform plant spacing is always desired for equal distribution of water and nutrients

among plants, but the effect of within-row plant spacing variability on grain yield is unclear. Vanderlip et al. (1988) found that grain yield decreased when the standard deviation of within-row plant distribution exceeded 2.5 inches. Nielsen (1991) suggested that loss due to uneven plant spacing averaged 2.5 bu/acre if the standard deviation of within-row plant distribution was increased by an inch. Krall et al. (1977) and Doerge et al. (2002) documented similar effects of plant-spacing variability, with reported yield losses averaging 3.4 bu/acre for every inch of increase in the standard deviation of within-row plant distribution.

The gaps within crop rows not only cause higher plant space variability but also dramatically lower overall plant populations, thereby leading to lower grain yield. On the other hand, Nafziger (1996) concluded that double seed drops can actually have a positive effect on grain yield up to some undefined upper threshold of plant population. There are contradicting reports over the cumulative effects of gaps and multiple seed drops in a field, especially when the plant population is within the optimum range, 28,000 to 32,000 plants per acre.

Recently, Lauer and Rankin (2004) concluded that it appeared that effects of plant spacing variability on corn grain yield were negligible. Similar conclusions were reported in Liu et al. (2004a). A subsequent study by Liu et al. (2004b) contradicted this assertion with the conclusion that there is a significant linear yield loss of 1.5 bu/acre for every inch of increase in standard deviation of plant distribution due to uneven plant spacing. Nielsen (2005) validated his previous studies and documented the rate of yield loss of 2.2 bu/acre for every inch increase in standard deviation of plant distribution.

In contrast, uneven emergence almost always reduces grain yield, with early-emerging plants unable to compensate for the lower yield of late-emerging plants. Carter et al. (1989) and Nafziger at al. (1991) reported a yield loss of 6-9% and 6-8%, respectively, in corn plants when within-row emergence of one-half to three-quarters of plants was delayed by 1½ weeks. Ford and Hicks (1992) reported a yield loss of 9.4 bu/acre when emergence of one-half of the plants was delayed by a week and 23.4 bu/acre when it was delayed by 2 weeks. However, the authors also stated that the yield reduction was not significant enough to justify replanting since yields from uneven-emerging stands were similar to yields from late-planted uniformly-emerging stands.

As stated by Barge and Thomison (2001), the most friendly method for determining planters' spacing performance is to measure the distance between plants in the field. The ideal way would be to measure seed-to-seed distance, which would require uprooting of the plants to locate seeds. However, the process of acquiring manual measurements of plant-to-plant spacing is labor-intensive, time-consuming and prone to human errors. Therefore, development of an automated sensing system for collecting plant-to-plant spacing data is desirable.

Planter manufacturers and researchers have been working closely to develop computer vision-based automatic inter-plant spacing sensing systems. Current systems mostly utilize top-view images obtained from a stereo rig or a video camera. These systems are highly sensitive to color variations introduced by shadow formations and glares, making them usable only for a limited time frame, perhaps within a day. Color-based segmentation of top-view plant images becomes challenging when plant canopies

begin occluding each other and making it difficult to identify the plant centers. Specifically, current 2D color vision-based systems (Tang & Tian, 2008a, 2008b) use top-view images only, record crop-row video, generate a mosaicked crop row image by using the background portions, i.e., the soil surface, of the image frames, and then automatically measure the plant spacing utilizing color information. Plants and plant centers are then segmented and subsequently plant row center lines are fitted for plant identification. Though these systems perform well under well-controlled conditions (proper crop size and color, proper background composition and proper time of a day), their system performances are constrained by a range of external factors:

1) Image acquisition platform stability: Tang and Tian (2008a, 2008b) used a modified two-wheeled bicycle that required close operator attention to maintain the stability of the platform.

2) Controlled lighting and wind conditions: Tang and Tian (2008a, 2008b) used an umbrella for casting a shadow over the imaging area, while Shrestha and Steward (2003) did not cover the imaging area at all. Color rendering was poor and inconsistent when sun light components changed rapidly during early mornings and late afternoons. Severe wind conditions can also deform plant leaves, making corn plant center detection difficult and inaccurate.

3) Shrestha and Steward (2003) and, Tang and Tian (2008a, 2008b) both used a camcorder (a device not really designed for industrial computer vision) to record crop rows and then digitized the analog video signal into digital video frames. Color fidelity was adversely affected during multiple signal conversions.

4) Corn plant recognition and stem center detection: Current systems rely on color only for corn plant identification and center cluster detection. This approach generally works well when corn plants are between growth stages from V1 to V2 (about one week after emergence when plants contain 1-2 leaves), but it also requires good growth conditions, i.e., limited water and nutrient stresses, and ideal lighting and wind conditions upon sensing.

Using color alone appears to be inadequate to cope with the complexity of field conditions that lead to both color variations and color fading, e.g. drought, nutrient deficiency, spray damage, residue under decomposing, mossy soil patches, etc. Crop-row detection is important since it makes use of planting geometry (most generally a straight line) to enhance the capability for plant detection. The current crop-row detection method is constrained by color-based crop plant and center cluster identification. Though geometric features such as average plant size and compactness can be used, crop-row line fitting can fail drastically when background noise from weed patches, algae, or moisturized residue overpopulate the number of true corn plants during the process. Mistakenly-fitted crop rows can require a large number of manual corrections in using the current system. Jin and Tang (2009) proposed a real-time corn plant sensing approach using a stereo camera. They reported a 96% success rate in correctly detecting the corn plants, and a maximum distance error in locating the plant centers of 0.05 m and 0.01 m for 74.6% and 62.3% of detected plants, respectively.

Research Objectives

The overall goal of this research was to develop a methodology for automatic measurement of distances between corn plants in early growth stages using time-of-flight light based 3D camera. The objectives of the work were to:

1) Develop a system that automatically detects corn plants in a crop row and measures within-row spacing between the plants,

2) Determine the system's performance in detecting plant-stem centers, and

3) Determine the system's inter-plant distance measurement accuracy by comparing system measurements with ground distance measurements collected from the fields

Laying Hen Behavior Monitoring

In their natural environment, chickens are known to live in small groups spending considerable amount of time scratching and foraging for food. They also exhibit inheritable behaviors such as dust bathing and pre-laying nesting. Chickens and other domestic birds raised for commercial purpose are kept in a wide array of housing systems and the physical environment in these systems varies considerably. Farmyard and free-range housing systems allow birds to move more freely through their environment. In such systems birds typically have access to natural daylight, a variety of substrates, are usually kept at a lower stocking density (SD), and can be exposed to extreme weather conditions and predation. Most commercial housing systems, on the other hand, are complete confinement houses in which birds are generally kept at

relatively higher stocking densities, while their environment is automatically controlled in an effort to achieve optimal thermal conditions, nutrition, and protection from predator, pathogens and adverse weather conditions.

In the United States and globally laying hens are primarily housed in conventional cages also known as battery cages. Conventional cages provide smaller group size resulting in lower levels of aggression and cannibalism. Cage systems are known to improve overall well-being of the birds through improved hygiene (Appleby, 1998). The higher egg-production and stocking-density capacity of cage systems also make them economically favorable. In these housing systems large numbers of birds can be efficiently housed in confinement with highly-mechanized feed and water systems, and with manure collected and removed automatically (Cooper & Albentosa, 2003). However, cage systems restrict many natural behaviors such as foraging, roosting, nesting and perching, which decreases animal welfare. There is thus growing pressure from animal well-being and consumer groups advocating the banning of conventional cage systems in the poultry industry. The European Union (EU) imposed a ban on battery-cage systems starting early 2012. Alternative housing systems such as furnished cages and colony housing have become the de facto housing systems in the EU, and are emerging in North America and other countries.

In a study of White Leghorns, Cunningham and Vantienhoven (1983) showed that the number of occurrences of conspecific head-pecking was higher in shallow cages (31.8 cm from front to back) compared to deep cages (50.8 cm from front to back). Bareham (1976) designed an experimental furnished cage with a horizontal floor, an

extended height with access to food and water provided on two levels, and two perches and nesting boxes. The study showed that the White Leghorn laying-strain birds kept in the experimental cage exhibited more movement, reflex activity, preening and sitting, but less feeding, drinking, pecking, pushing and other stereotypical behavior compared to those kept in conventional cages.

Pohle and Cheng (2009) recently conducted a comparative study of effects of furnished cages and battery cages on White Leghorn chicken behavior. Their study showed that birds housed in battery cages spent more time walking than those housed in furnished cages. In contrast, the birds housed in furnished cages spent more time feeding than those housed in battery cages. Drinking behavior was significantly affected by age, with birds housed in the furnished cages showing a decreased in time spent drinking at 40 weeks of age. At the age of 50 weeks, the level of preening behavior was higher in the birds housed in the furnished cages, while the birds housed in battery cages spent more time performing exploratory pecking behavior. These researchers did not observe dust-bathing behavior in either housing system, while in furnished housing systems the hens exhibited exploratory pecking, resting, and preening behaviors in dust-bathing areas.

Appleby et al. (2002) reported that birds performed foraging, resting, and standing behaviors in the dustbath rather than dust-bathing behavior. Pohle and Cheng (2009) suggested that birds highly selected for egg production, such as White Leghorns in battery cage systems might have adapted to the production environment with reduced dustbathing behavior when compared with behavior in more natural environments.

Braastad (1990) reported that birds spent 25% to 41% of each day on perches. In a similar study, Appleby (1998) reported that more than 80% of birds perched at night, while Duncan et al. (1992) reported that up to 99% of birds perched at night. Pohle and Cheng (2009) also reported that the hens in their study spent a considerable amount of time on perches. Birds are known to use branches for resting and avoiding predators or aggressive peers in their natural environments, so perching is considered to be an inherent behavior.

Yue and Duncan (2003) reported that birds without nestboxes exhibited frustration behavior (stereotyped pacing) compared to those provided with nestboxes. Cooper and Appleby (1997) indicated that birds were motivated to lay eggs in nestboxes and exhibited nest-searching behavior when nestboxes were not available.

Visual monitoring of laying-hen movements for behavioral analysis appears to be unsatisfactory for several reasons. First, the presence of human observers affects behavior and movement of laying hens. Second, during night-time, when lights are off, it is difficult to observe their movements. Third, it is both time and labor intensive to observe laying hens for a prolonged period of time, although video cameras can be used to avoid the effects of human presence on laying-hen behavior and movement. Similarly, infrared cameras can be used for low or no-light conditions. However, the time-consuming nature of human analysis of video recordings is still a problem. Therefore, a system to automatically track individual laying hens and extract their behavior and movement data is indispensable.

Monitoring laying hens is particularly difficult since their behaviors are unpredictable and their movements cannot be expected to follow regular paths. The behavior of laying hens consists of sporadic walking, feeding, and drinking, interspersed by resting and less frequent activities that include wing-flapping, dust-bathing, and peer interaction.

Tracking multiple laying hens for behavior monitoring is a challenging task with interesting features from a computer-vision perspective. Segmenting laying hens from the background can be difficult because the litter on which the hens live can often be of similar intensity to that of their feathers. Laying hens tend to flock together, and because they are not highly-mobile animals, difficulty in separating individual hens can persist and be prolonged. Conversely, hens may make sudden and quick moves, thereby creating a discontinued trajectory that can create difficulty in tracking.

The literature on classical multi-target tracking is based on the use of data-association after foreground detection in the image. Uchida et al. (2000) proposed a robust method for tracking many pedestrians by viewing them from an upper oblique angle. They extracted individuals using background subtraction. When pedestrians overlapped each other, they robustly tracked targets based on their trajectories. However, poultry do not move for long time periods while remaining in contact, and they may alter their trajectories randomly.

Computer vision has been applied to tracking animals. Sumpter et al. (1997) tracked a group of animal at a high frame rate. Sergeant et al. (1998) developed a poultry-tracking system in which a camera was placed above the poultry group. They

detected poultry silhouettes based on color information and segmented these silhouettes

by using the information on the contours of the silhouette. Fujii et al. (2009) used a

computer-vision technique based on particle filters to track multiple laying hens, but that

system was not able to track laying hens over a prolonged period of time.

<u>Research Objectives</u>

The primary goal of this study was to develop a methodology for automatic

quantification of stocking density effects on common laying-hen behaviors using light

based time-of-flight camera and RFID antenna network. The objectives were to:

1) Develop a tracking system capable of tracking individual laying hens housed

in groups of 5 and 10,

2) Extract common laying-hen behaviors such as locomotion, perching, nesting,

feeding, and drinking, and

3) Analyze the effects of stocking density on extracted laying-hen behaviors

References

Appleby, M. C. (1998). Modification of laying hen cages to improve behavior. *Poultry Science, 77*(12), 1828-1832.

Appleby, M. C., Walker, A. W., Nicol, C. J., Lindberg, A. C., Freire, R., Hughes, B. O., & Elson, H. A. (2002). Development of furnished cages for laying hens. *British Poultry Science, 43*(4), 489-500.

Bareham, J. R. (1976). A comparison of the behaviour and production of laying hens in experimental and conventional battery cages. *Applied Animal Ethology, 2*(4), 291-303.

Barge, G. L., & Thomison, P. (2001, 04/25/2010). Tips to reduce planter performance effects on corn yield. *Extensions Factsheet.* Retrieved April 25, 2010, from http://ohioline.osu.edu/agf-fact/0150.html.

Braastad, B. O. (1990). Effects on behavior and plumage of a key-stimuli floor and a perch in triple cages for laying hens. *Applied Animal Behaviour Science, 27*(1-2), 127-139.

Carter, P. R, Nafziger, E. D, & Lauer, J. G. Uneven emergence in corn. North Central Regional Extension Publication No. 344.

Cooper, J. J., & Appleby, M. C. (1997). Motivational aspects of individual variation in response to nestboxes by laying hens. *Animal Behaviour, 54*, 1245-1253.

Cooper, J. J., & Albentosa, M. J. (2003). Behavioural priorities of laying hens. *Avian and Poultry Biology Reviews, 14*(3), 127-149.

Cunningham, D. L., & Vantienhoven, A. (1983). Relationship between productions factors and dominance in white leghorn hens in a study on social rank and cage design. *Applied Animal Ethology, 11*(1), 33-44.

Doerge, T., Hall, T., & Gardner, D. (2002). New research confirms benefits of improved plant spacing sensing in corn. *Crop Insights, 12*(2).

Duncan, E. T., Appleby, M. C., & Hughes, B. O. (1992). Effect of perches in laying cages on welfare and production of hens. *British Poultry Science, 33*(1), 25-35.

Ford, J. H., & Hicks, D. R. (1992). Corn growth and yield in uneven emerging stands. *Journal of Production Agriculture, 5*(1), 185-188.

Fujii, T., Yokoi, H., Tada, T., Suzuki, K., Tsukamoto, K., & Ieee. (2009). Poultry Tracking System with Camera Using Particle Filters. *2008 Ieee International Conference on Robotics and Biomimetics, Vols 1-4*, 1888-1893.

Jin, J., & Tang, L. (2009). Corn plant spacing sensing using real-time stereo vision. *Journal of Field Robotics, 26*(6-7), 591-608.

Krall, J. M., Esechie, H. A., Raney, R. J., Clark, S., Teneyck, G., Lundquist, M., . . . Vanderlip, R. L. (1977). Influence of within-row variability in plant spacing on corn grain yield. *Agronomy Journal, 69*(5), 797-799.

Lauer, J. G., & Rankin, M. (2004). Corn response to within row plant spacing variation. *Agronomy Journal, 96*(5), 1464-1468.

Liu, W. D., Tollenaar, M., Stewart, G., & Deen, W. (2004a). Within-row plant spacing variability does not affect corn yield. *Agronomy Journal, 96*(1), 275-280.

Liu, W. D., Tollenaar, M., Stewart, G., & Deen, W. (2004b). Impact of planter type, planting speed, and tillage on stand uniformity and yield of corn. *Agronomy Journal, 96*(6), 1668-1672.

Nafziger, E. D., Carter, P. R., & Graham, E. E. (1991). Response of corn to uneven emergence. *Crop Science, 31*(3), 811-815.

Nafziger, E. D. (1996). Effects of missing and two-plant hills on corn grain yield. *Journal of Production Agriculture, 9*(2), 238-240.

Nielsen, R. L. (1991). Stand establishment variability in corn. from http://www.agry.purdue.edu/ext/pubs/AGRY-91-01_v5.pdf.

Nielsen, R. L. (2005). Effect of plant spacing variability on corn grain yield. from http://www.kingcorn.org/research/psv/Report2005.pdf.

Pohle, K., & Cheng, H. W. (2009). Furnished cage system and hen well-being: Comparative effects of furnished cages and battery cages on behavioral exhibitions in White Leghorn chickens. *Poultry Science, 88*(8), 1559-1564.

Sergeant, D., Boyle, R., & Forbes, M. (1998). Computer visual tracking of poultry. *Computers and Electronics in Agriculture, 21*(1), 1-18.

Shrestha, D. S., & Steward, B. L. (2003). Automatic corn plant population measurement using machine vision. *Transactions of the Asae, 46*(2), 559-565.

Sumpter, N., Boyle, R. D., & Tillett, R. (1997). Modelling collective animal behaviour using extended point-distribution models. University of Leeds, School of Computer Studies.

Tang, L., & Tian, L. F. (2008a). Real-time crop row image reconstruction for automatic emerged corn plant spacing measurement. *Transactions of the Asabe, 51*(3), 1079-1087.

Tang, L., & Tian, L. F. (2008b). Plant identification in mosaicked crop row images for automatic emerged corn plant spacing measurement. *Transactions of the Asabe, 51*(6), 2181-2191.

Uchida, K., Miura, J., & Shirai, Y. (2000). *Tracking multiple pedestrians in crowd.* Paper presented at the Proc. Workshop of Machine Vision and its Applications, Tokyo, Japan.

Yue, S., & Duncan, I. J. H. (2003). Frustrated nesting behaviour: relation to extra-cuticular shell calcium and bone strength in White Leghorn hens. *British Poultry Science, 44*(2), 175-181.

CHAPTER 2

AUTOMATIC INTER-PLANT SPACING SENSING AT EARLY GROWTH
STAGES USING A 3D VISION SENSOR

A. D. Nakarmi[2], L. Tang[3]

Abstract

An inter-plant spacing sensing system using a TOF (time of flight) of light based
3D sensor was developed. The 3D sensor was capable of capturing distance information,
intensity and amplitude data in a single shot. The side view depth images captured were
stitched together using distance information from a wheel encoder in conjunction with a
feature-based image sequencing process for the stem location identification. One
obvious advantage of the system over current color-based 2D systems was the use of
depth images for plant identification, which was less sensitive to color variations. A
covered cart was designed to prevent the sunlight from directly shedding on the plants
and reduce the interference from the wind, which in turn made the system usable
throughout the day. The vertical camera position was easily adjustable making the
system suitable to work with plants at different growth stages.

The use of side-view images made the system capable of detecting inclined
plants and therefore, boosted the performance of the system in precisely locating the
stem centers, which in turn minimized the measurement errors. The measurement

[2.]Department of Agricultural and Biosystems Engineering, Iowa State University, Ames, IA 50011.
[3.]Corresponding author. Phone: 515-294-6778; Fax: 515-294-6633; Email: lietang@iastate.edu.

accuracy demonstrated the system superiority over the current systems which make use of top-view images for inter-plant spacing sensing.

The use of side-view images made the system capable of detecting inclined plants and therefore, boosted the performance of the system in precisely locating the stem centers, which in turn minimized the measurement errors. The measurement accuracy demonstrated the system superiority over the current systems which make use of top-view images for inter-plant spacing sensing. The system achieved an overall mean root mean squared error (RMSE) of 0.017 m with a mean plant misidentification ratio of 2.2 %. The coefficient of determination (R^2) was 0.95 between the in-field manual distance measurements and the system distance estimates.

Keywords. *3D, machine vision, corn plant spacing sensing, early growth stages, image processing*

Introduction

Uniform plant spacing is always desired for equal distribution of water and nutrients among plants. Researchers in the past have shown that variations in plant spacing result in significant variation in final crop yields. Vanderlipet al. (1988) found that grain yield decreased when standard deviation of within-row plant distribution exceeded 2.5 inches. Nielsen (1991) suggested that loss due to uneven plant spacing averaged 2.5 bushels per acre for every inch increase in standard deviation of within-row plant distribution. Doerge et al. (2002) documented similar effects of plant space

variability, with reported yield losses averaging 3.4 bushels per acre for every inch increase in standard deviation of within-row plant distribution.

The gaps within crop rows not only cause higher plant space variability but also dramatically lower overall plant populations, thereby leading to lower grain yield. On the other hand, Nafziger (1996) concluded that double seed drops can actually have a positive effect on grain yield up to some undefined upper threshold of plant population. There are contradicting reports over the cumulative effects of gaps and multiple seed drops in a field, especially when the plant population is within the optimum range, 28,000 to 32,000 plants per acre.

Recently, Lauer and Rankin (2004) concluded that the effects of plant spacing variability on corn grain yield were negligible. Similar conclusions were reported in Liu et al. (2004a). Subsequent study by Liu et al. (2004b) contradicted this with the conclusion that a significant linear yield loss of 1.5 bushels per acre for every inch increase in standard deviation of plant distribution due to uneven plant spacing. Nielsen (2005) validated his previous studies and documented the rate of yield loss of 2.2 bushels per acre for every inch increase in standard deviation of plant distribution.

As stated in Barge and Thomison (2001), the friendliest method to determine planters' spacing performance is by measuring the distance between plants in the field. The ideal way would be to measure seed-to-seed distance, which would require uprooting of the plants to locate seeds. However, the process of acquiring manual measurements of plant-to-plant spacing is labor intensive, time consuming and prone to

human errors. Therefore, an automated sensing system for collecting plant-to-plant spacing data is desirable.

Planter manufacturers and researchers have been working closely to develop computer vision-based automatic inter-plant spacing sensing systems. Current systems mostly utilize top-view images using a stereo rig, or a video camera. These systems are highly sensitive to color variations introduced by shadow formations and glares, making them usable only for a limited time frame within a day. Color-based segmentation of top-view plant images becomes challenging when plant canopies start occluding each other, thereby making it difficult to identify the plant centers. Specifically, the current 2D color vision-based systems (Tang & Tian, 2008a, 2008b) use top view images only, record crop row video, generate a mosaicked crop row image by using the background portions, i.e., the soil surface, of the image frames; and then automatically measure the plant spacing via utilizing color information, where plants and plant centers are segmented and subsequently plant row center-line are fitted for plant identification. Though the systems perform well under well controlled conditions (proper crop size and color, proper background composition and proper time of a day), the systems performances are constrained by a range of external factors: 1) Image acquisition platform stability: Tang and Tian (2008a, 2008b) used a modified two-wheeled bicycle which required a close attention from operators to maintain the stability of the platform. 2) Controlled lighting and wind conditions: Tang and Tian (2008a, 2008b) made use of an umbrella for casting a shadow over imaging area, whereas Shrestha and Steward (2003) did not cover the imaging area at all. Color rendering was poor and inconsistent

when sun light components change rapidly during early mornings and late afternoons. Severe wind conditions can also deform plant leaves, making corn plant center detection difficult and inaccurate. 3) Shrestha and Steward (2003) and, Tang and Tian (2008a, 2008b) both used a camcorder (a device not really designed for industrial computer vision) to record crop rows and then digitized analog video signal into digital video frames. Color fidelity was adversely affected during multiple signal conversions. 4) Corn plant recognition and stem center detection: Current systems rely on color only for corn plant identification and center cluster detection. Generally it works well when corn plants are between growth stages from v1 to v2 (about one week after emergence when plants contain 1-2 leaves), but it also requires good growth conditions, i.e., limited water and nutrient stresses, and ideal lighting and wind conditions upon sensing. Using color alone appears to be inadequate to cope with the complexity of field conditions that lead to both color variations and color fading, e.g. drought, nutrient deficiency, spray damage, residue under decomposing, mossy soil patches, etc. Crop row detection is important as it makes use of planting geometry (most times a straight line) to enhance the ability of plant detection. The current crop row detection method is constrained by color-based crop plant and center cluster identification. Though geometric features such as average plant size and compactness are used, crop row line fitting can fail drastically when background noise from weed patches, algae, moisturized residue over populate the number of true corn plants during the process. Mistakenly fitted crop rows can lead to a large number of manual corrections in using the current system. Jin and Tang (2009) proposed a real-time corn plant sensing using a stereo camera. The authors reported 96%

success rate in correctly detecting the corn plants, and maximum distance error, in locating the plant centers of 0.05 m and 0.01 m for 74.6% and 62.3% of detected plants respectively.

The overall goal of the research was to develop a system for automatic measurement of distances between corn plants in early growth stages. The objectives of the work were to: 1) determine the system's performance in detecting plant stem centers, and 2) determine the system's inter-plant distance measurement accuracy by comparing the system measurements with the ground distance measurements collected from the fields.

Materials and Methods

The system consists of five major steps: 1) image acquisition; 2) image pre-processing; 3) stem location identification; 4) image mosaicking; and5) inter-plant distance measurement. The side-view images of plants along crop rows were captured. The acquired images were pre-processed to differentiate plant segments from background and soil. The segmented images were used to identify stem locations, mosaic them together and finally measure distance between the identified plants. Sub-steps involved in each step are shown in figure 1. The image acquisition component was written in C++ whereas the components for offline processing (steps 2-5) were written in C#. The major steps involved are described in details in the following sections.

Image Acquisition	a. Side view images were acquired at every 100 encoder counts (approximately 0.05 m along the crop row direction)
Image Pre-processing	a. Radial distortion was corrected. b. Distance information was used to remove background from depth image. c. Region-of-interest, for further processing, was defined. d. Smaller regions were discarded and smaller holes were filled. e. Morphological closing was performed to obtain smooth object boundaries.
Stem Location Identification	a. Object skeleton was generated and pruned. b. Terminal points of the skeleton were found. c. Starting from the bottom point, segmented depth image was traversed to find the candidate stem location.
Image Mosaicking	a. Mosaicked image was generated either by matching the identified stems in two consecutive images or by using the encoder reading to calculate distance traveled by the cart between the images.
Inter-plant Distance Measurement	a. Inter-plant distances between the identified plants were calculated. b. The calculated distances were compared with manual measurements from the field to compute measurement accuracy.

Figure 1. Steps involved in automatic inter-plant distance measurement algorithm

Image Acquisition

A state-of-the-art 3D imaging sensor, SwissRanger SR4000 (MESA Imaging AG, Zuerich, Switzerland), based on TOF (time of flight) of light principle was used to capture 3D spatial data plus intensity and amplitude images of the scene simulataneously. SR4000 measures distance using indirect (phase-shift based) TOF measurement. Continuously modulated light waves are sent out from illumination light emitting diodes (LEDs). Charged coupled device (CCD)/complementary metal oxide (CMOS) imaging sensor measures the phase shift of returned signal at each pixel. The returned signal amplitude A is smaller than the emitted signal amplitude E as shown in figure 2. There is an offset of B with respect to emitted signal mainly due to additional

background light. The received signal is modulated four times per cycle with each

sample shifted by 90° phase angle. Phase shift φ and the distance are calculated using

equations 1 and 2, respectively (Buttgen et al., 2005).
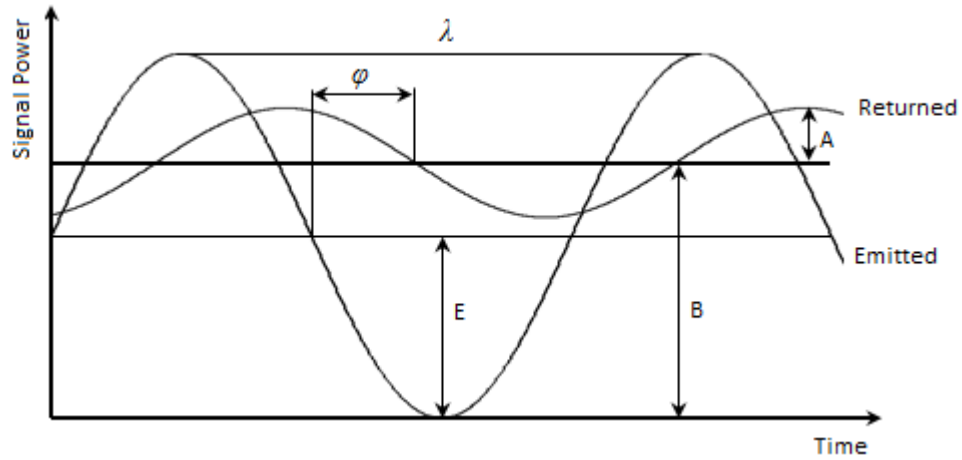
Figure 2. Principle of the time of flight measurement based on continuously modulated signals

$$\varphi = \arctan\left(\frac{A_0 - A_2}{A_1 - A_3}\right) \tag{1}$$

$$R = \frac{c}{4\pi f_{mod}}\varphi = \frac{\varphi}{2\pi}\frac{\lambda}{2} \tag{2}$$

where A_0, A_1, A_2 and A_3 are four samples of received signal, c is the speed of light, f_{mod} is

the modulation frequency of the emitted signal and λ is its wavelength. The spatial data

are acquired in Cartesian coordinates with its origin at the center of the frontal face of

the camera. The 3D TOF sensor is superior to conventional stereo vision sensor as it

does not rely on non-uniform texture feature for non-ambiguous disparity map

generation, which is particularly useful for the application as plant leaves often present

somewhat uniform texture. The self-calibrating optical design of the sensor automatically corrects for environmental fluctuations such as illumination conditions. The camera has rather small, $43.6°(h) \times 34.6°(v)$ FOV (field of view). With this FOV, it can capture an area of 0.40 m x 0.31 m if placed 0.50 m away from the scene. The camera is capable of capturing x, y, z (or depth) images along with intensity and amplitude images with a resolution of 176 x 144 pixels. The amplitude image contains for each pixel a 16-bit integer representing the strength of the reflected signal by the object. Its values are low when the strengths of the reflected signals are weak.

A three-wheeled steerable cart was designed. The imaging area was fully covered to avoid undesired effects of direct sunlight during image acquisition. The covered platform also minimized the effect of wind on plant postures. A high-resolution (4096 counts/rev.) encoder was mounted on the rear left wheel of the cart. The wheel circumference was 2.02 m. The encoder reading was used to trigger the camera to capture side view images at every 100 encoder counts, which was equivalent to approximately 0.05 m translation along the crop row. A leveler was used in front of the wheel, on which the encoder was mounted, to allow a smooth rolling as shown in figure 3. The cart was pushed manually at about 1.5 m/s. The sensor was mounted at about 0.10 m from the ground and about 0.55 m away from the crop row, with the frontal face of the camera facing the crop row. The vertical and lateral positions of the camera from the crop row were adjustable. The camera and the encoder were connected to a tablet laptop through USB 2.0 interfaces. Two 12 V batteries were used to power the devices. The batteries were connected in parallel.

(a)   (b)

Figure 3. Three-wheeled inter-plant distance measurement platform: (a) CAD model showing an encoder attached to the rear wheel and a leveler mounted in front of it; and (b) the real cart in action in one of the test fields

Image Pre-processing

The images captured from the camera suffered radial distortion, specifically, Barrel distortion, where the points moved from their correct positions towards the center of the image, as if the image was projected on a spherical surface. Some cameras do in-camera distortion correction, before any file is written, while others such as SR4000 require post-processing of the images to correct the distortion. Lens parameters need to be known to correct the distortion. Barrel distortion inherent to the images captured by SR4000 was adequately corrected by applying a simple transformation using equations 3 and 4 provided by the camera manufacturer.

$$x_i = \frac{f}{p} \times \frac{x_w}{(z_w + c)} \tag{3}$$

$$y_i = \frac{f}{p} \times \frac{y_w}{(z_w + c)} \tag{4}$$

where, (x_i, y_i) are the corrected image coordinates corresponding to the scene points (x_w, y_w), f is the focal length and p is the pixel-pitch of the camera, and c is the distance from the frontal face of the camera to the imaging area inside the camera. The equations project the measured points in Cartesian coordinates onto their respective image locations in X-Y image plane. The projected image (figure 4b) was larger in size than the originally captured image (figure 4a). The missing points along the curves were recovered using averaging based interpolation method in both horizontal and vertical directions. The interpolated image was then cropped from the center to obtain the corrected image in its original size, i.e., 176 x 144 pixels as shown in figure 4c.

(a)   (b)   (c)
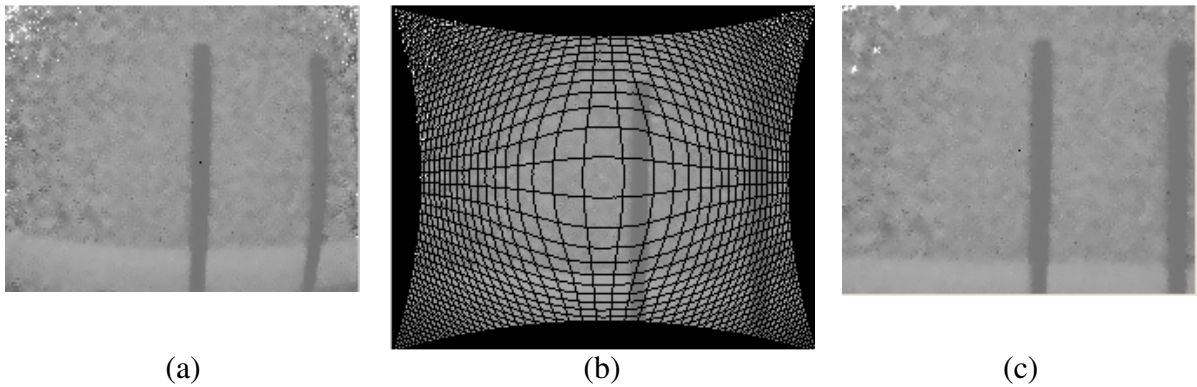
Figure 4. Barrel distortion correction: (a) original (distance) image with visible distortion; (b) size of the image increased after distortion correction; and (c) final corrected image after interpolation and cropping

The background was removed from the depth image using distance threshold of 0.6 m (i.e., about 0.05 m behind the crop row). Any pixel beyond the threshold value was considered a background pixel (figure 5b). The image was scanned from the bottom until the number of foreground pixels along the scan line were less than 50% of the image width (figure 5c). The scanning removed nearly all the soil content from the

image. ROI (region of interest) was defined from this line to one-third of image height

above the line, where the influence of the leaves was minimal. The ROI boundary was

10 pixels, which is equivalent to the half the diameter of plant stem, inside from both left

and right edges of the image (figure 5d). As the final pre-processing step, morphological

closing operation was carried out within the ROI to remove noisy regions and obtain

smooth object boundaries (figure 5e).

(a)　　　　　　　　　　　(b)　　　　　　　　　　　(c)

(d)　　　　　　　　　　　　　　　(e)
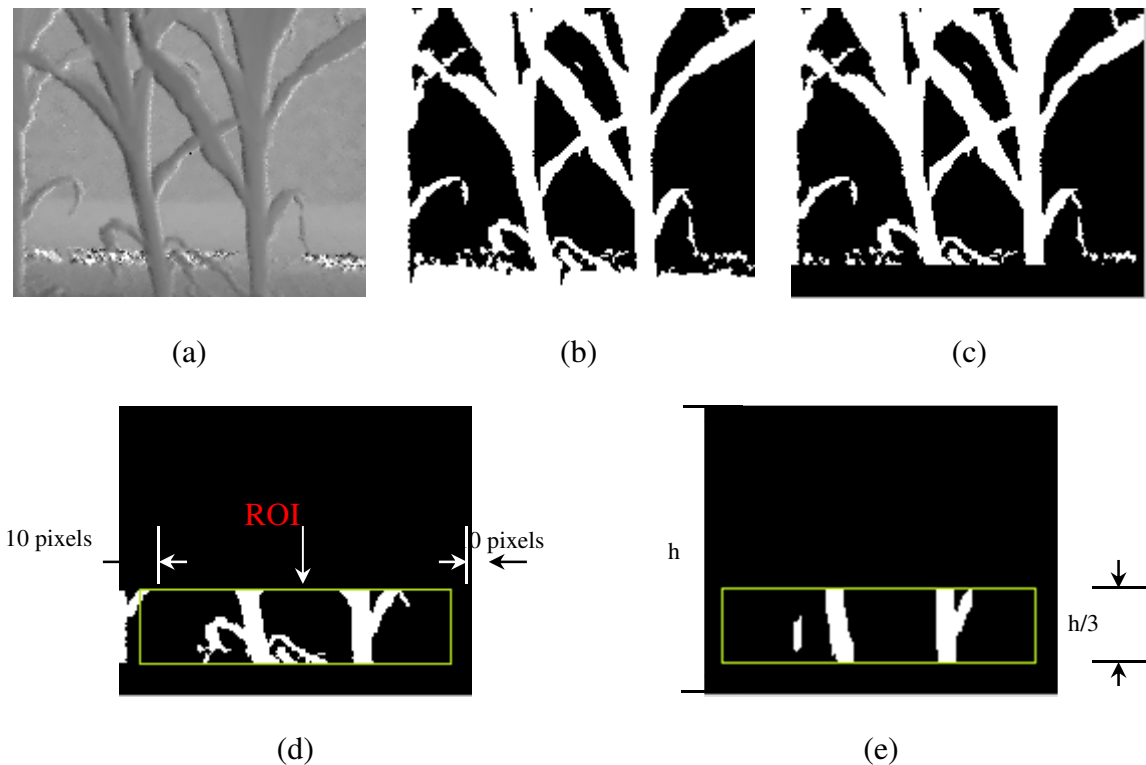
Figure 5. Image pre-processing: (a) corrected distance image; (b) segmented image after
background removal; (c) soil region removed; (d) ROI defined; and € noise removed
<u>Stem Identification</u>

The foreground regions within the ROI were labeled and processed individually.

First, skeleton of a region was generated by using a parallel thinning algorithm based on

8-connectivity (Rosenfeld, 1975) and noisy protrusions were pruned. Regions containing

less than half the height of the ROI in their skeletons were deemed unimportant and discarded. Next, terminal points of the skeleton were determined. Points which lied above the center line of the ROI were grouped as top points and those below the center line were grouped as bottom points (figure 6a). Depending on the number of top and bottom points two different approaches were used to determine stem locations.

Scenario 1: When there was one top point and one bottom point, centroid and orientation of the skeleton were determined. Starting from the bottom point, the segmented depth image was traversed upwards passing through the centroid in the direction guided by the orientation of the skeleton. The region was considered a candidate stem, if the number of pixels along the traverse line was more than two-third of the height of the image (figure 6b, left plant).

Scenario 2: When there were multiple top points, the segmented depth image was traversed so that the traverse lines originating from the bottom point passed through all the top points. The longest traverse line which met the length threshold, i.e., two-third of the height of the image was considered as the probable stem location and its direction gave the orientation of the plant (figure 6b, right plant).
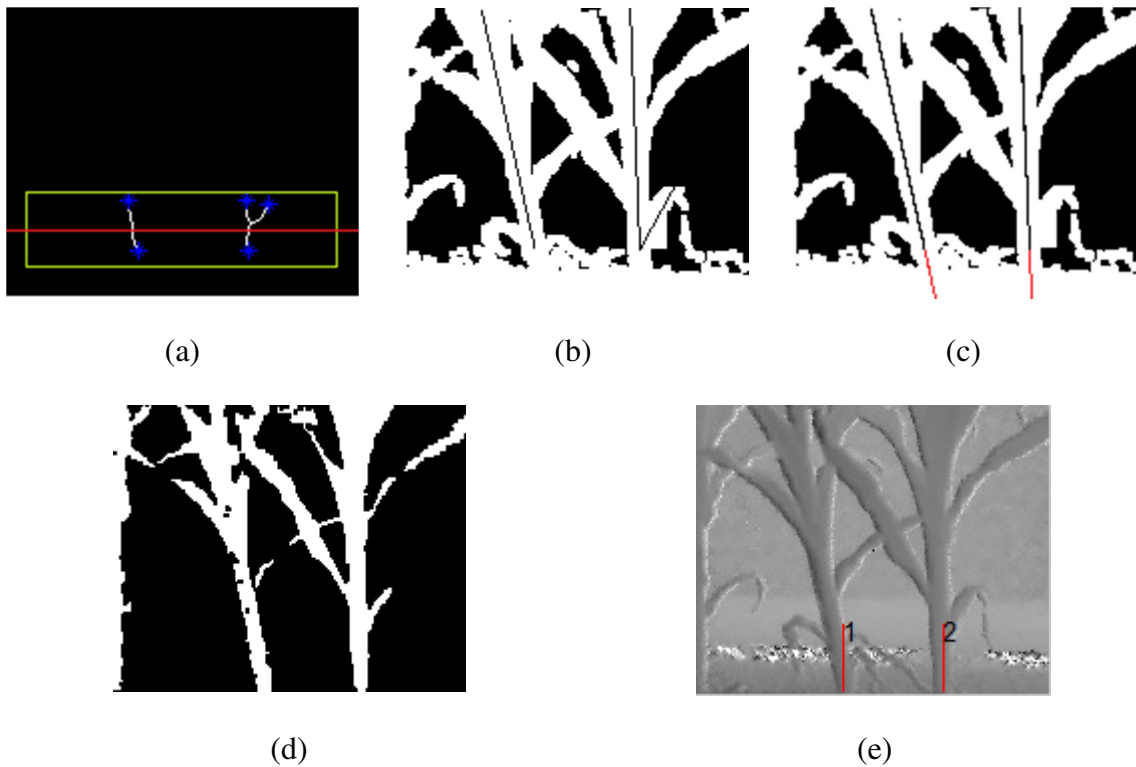
Figure 6. Stem location identification: (a) skeletonization of objects within the ROI; (b) upward traverse lines approximating candidate stem locations; (c) downward traverse lines finding the soil-plant intersection; (d) image generated by taking 8 most significant bits of intensity image that adequately suppressed background and soil regions; and (e) identified stem locations

If the orientation of the candidate stem location, given by the direction of the line connecting the bottom and the top points, was within ±15° from the vertical, it was processed further to determine stem center, i.e., point where stem intersect with soil surface. From the bottom point, along the direction guided by the orientation of the traverse line, it was traversed down to locate the intersection point. The most significant 8-bit values of the amplitude image (figure 6d) which adequately suppressed soil and background regions was used to identify the stem-soil intersection. The image was

traversed downward starting from the bottom point along the stem orientation until a black pixel was found. The identified stem-soil intersection point was the stem center (figure 6c).

Image Mosaicking

There was significant overlapping between the images when they were captured at approximately 100 encoder counts (i.e., approximately 0.05 m along the crop row direction). These images were stitched together to recover spatial information of each plant in the crop row. Mosaicking was required for distance measurement between the plants especially when the plants came from two different images. One of the common methods used to mosaic images is correlation-based template matching. In this method, a template window is chosen on an image and its best match is searched on the next image.The effectiveness of this method depends on the stability of the chosen template. Plant regions, especially the leaves, are not stable in the sense that wind tends to blow them and their postures change from frame to frame. Tang and Tian (2008a, 2008b) used soil surface to find a window with the highest variance and searched its match in the next image. With side view images the soil surface occupied less than 10% of the images and has a perspective view that can change drastically at slightly different camera view angles, therefore it was not possible to use soil surface for correlation-based matching and hence image mosaciking.

A new image mosaciking algorithm based on encoder data and the results of stem identification was developed. Though a high resolution encoder was used, the encoder

data was not sufficient for mosaicking images. First, there was inherent cummulative distance measurement error associated with encoder sensing. Second, there occurred counting error depending on soil conditions, error due to slippage when the soil was wet and error due to bumps when the soil was rough. Third, the plants in the crop row did not lie in the same plane along the camera's viewing direction and they appeared different from different viewing angles. When mosaiked based on encoder data alone, the mosaicked image appeared unrealistic (splits and halves) at places where the mosaicking took place on plant regions. Therefore, a sensor fusion approach was adapted where the encoder reading was used to approximate horizontal distance traveled by the cart between the images. The stem locations sensed by the image processing algorithm were then matched using the information provided by the encoder. A 30 pixel wide search space was created with the probable stem location as its center. The image being processed is termed as *current* image, and the one that was processed immediately before is termed as *previous* image.The mosaicking algorithm is explained with the help of some examples below:

Scenario 1: In the simplest case, when at least one stem was identified in both the previous and the current images, the location of last stem in the previous image was matched with one of the identified stems in the current image. The probable stem location was identified based on the fact that there was certain offset between the two image as they were captured from the view points which were approximately 0.05 m apart. The encoder reading was used to define a search space around the probable stem location. The two images were stitched at the matched stem location (figure 7).
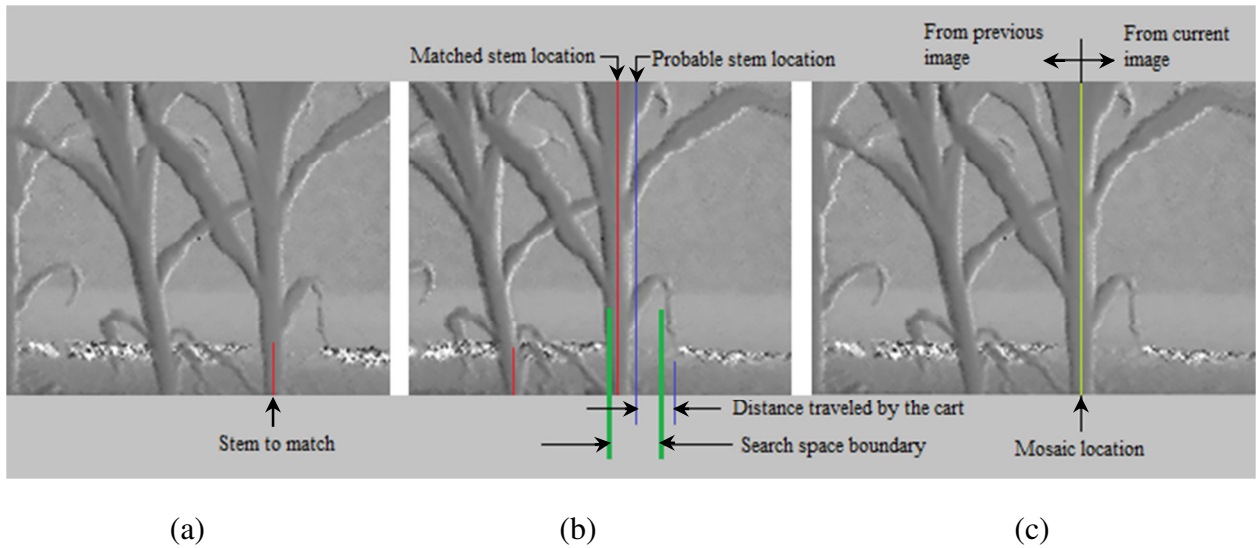
Figure 7. Mosaicking when stem match was available: (a) Last stem in the previous image; (b) search space boundary defined in the current image based on encoder reading; (c) mosaicked image, left portion came from the previous image and right portion came from the current image

Scenario 2: When there was only one stem identified in the previous image and it was not visible in the current image, the center of the previous image was used at the mosaic location. The encoder reading was used to determine the distance covered by the cart between the two images, which in turn was used to approximate the corresponding mosaic location on the current image (figure 8). Similar approach was utilized when there was no stems identified in the previous image but at least one stem was found in the current image (a plant was identified after a large gap) and also in the situation when no stems were identified in both the previous and the current images (images between the plants separated by a large gap) (figure 8).
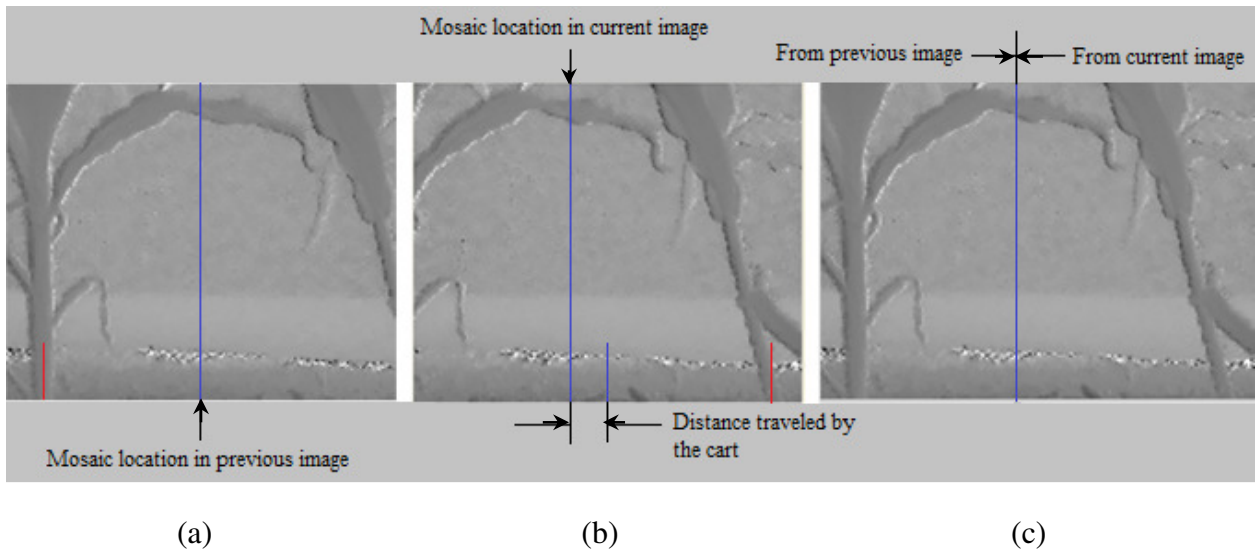
Figure 8. Mosaicking when stem match was not available: (a) center of the previous image was chosen as mosaic location; (b) corresponding mosaic location on the current image was found using encoder reading, and (c) mosaicked image, left portion was from the previous image and right portion was from the current image

Inter-plant Distance Measurement

An algorithm was developed to measure distances between the identified stem locations. The distance between any two plants were calculated along the same horizontal line. Among the two plants, one with the stem center further from the bottom edge of the image was used as the basis and a point on the other plant along the direction of the traverse line was found (figure 9). These points in image coordinates were then transformed to world coordinates using equations 5 and 6, which were derived from equations 3 and 4 respectively. The Euclidean distance formula given by equation 7 was used to calculate the distance between the plants.

Distance between
the plants
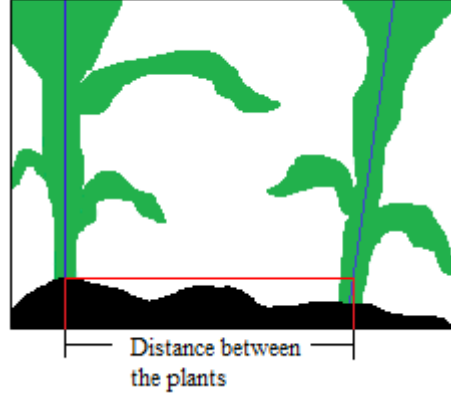
Figure 9. Distance between the plants was calculated along the same horizontal line

$$x_w = x_i \times \frac{p}{f} \times (z_w + c) \tag{5}$$

$$y_w = y_i \times \frac{p}{f} \times (z_w + c) \tag{6}$$

$$d = \sqrt{(x_{1w} - x_{2w})^2 + (y_{1w} - y_{2w})^2 + (z_{1w} - z_{2w})^2} \tag{7}$$

where (x_w, y_w) are the scene points corresponding to the image points(x_i, y_i), f is the focal

length and p is the pixel-pitch of the camera, and c is the distance from the frontal face

of the camera to the imaging area inside the camera. Since the distance was calculated

on the same horizontal line, the middle term of equation 5 turned out to be zero. The

algorithm took different approaches to deal with different situations in order to

accurately calculate the distances. The distance measurement was not trivial especially

when the plants came from two different images. The horizontal distance traveled by the

cart between the plants was required to be tracked before it was possible to measure

distance between these plants. Some of the interesting situations are described below with examples:

Scenario 1: When the last stem identified in the previous image was closer to the left edge of the image than the distance covered by the cart, there was a possibility that the stem was not identified in the current image. The center of the previous image was used as the mosaicking location and its corresponding location on the current image was found using encoder data. The distance between the first stem identified in the current image and the mosaicking location in that image was calculated. It was then added to the distance between the last stem identifed in the previous image and the mosaicking location in that image. This gave the distance between the last plant in the previous image and the first plant identified in the current image (figure 10).

(a)   (b)   (c)
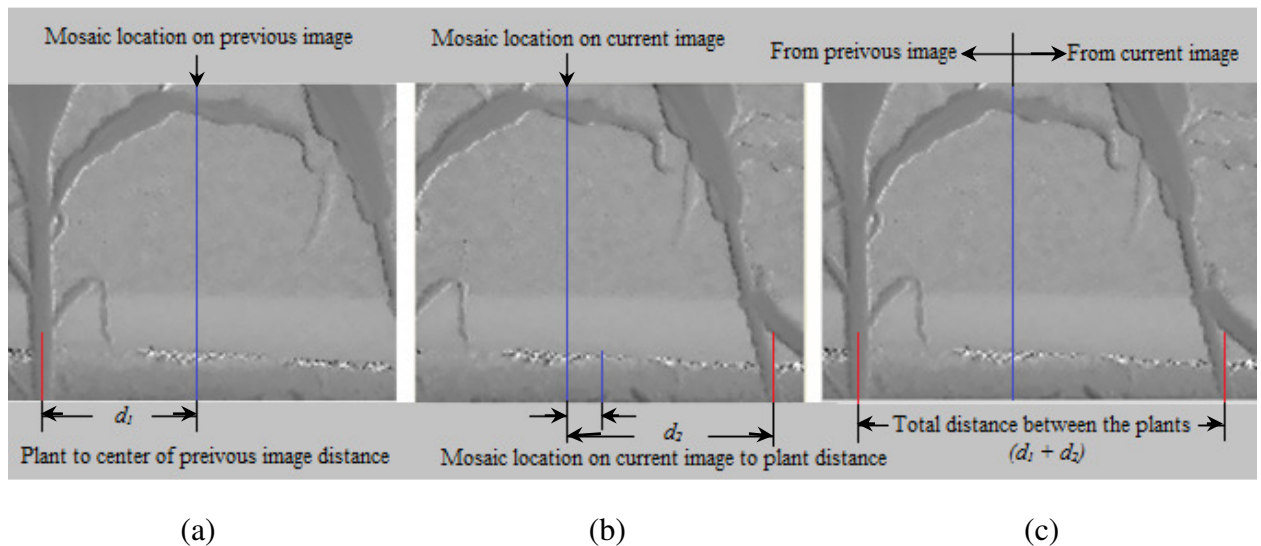
Figure 10. Distance calculation between plants appearing in different images: (a) distance of the last plant in previous image to its center, i.e., the mosaic location; (d) distance of the corresponding mosaic location in current image to the first plant identified in it; and (d) total distance between then plants in mosaicked image

Scenario 2: When a plant was identifed in an image after one or many images were processed without any plants identified, the distance between the last plant identified and the newest plant identified were calculated using equation 8. First, the distance between the last stem identifed and the mosaicking location, i.e., the center of the image on which the plant was identified, was calculated. Next, for each image where the stem identification algorithm did not find a plant, the distance between the point that corresponded to the previous mosaic location and its center was calculated. Finally, the distance between the point that matched with the previous mosaic location and the first plant identified after the gap was calculated. The sum of all the distances gave the distance between the two plants separated by at least one blank image.

$$d = d_1 + \sum_{i=1}^{n} \Delta d_i + d_2 \tag{8}$$

where d_1 is the distance of the last stem identified to the mosaic location of the image, each Δd_i represents the distance traveled by the cart between the images, and d_2 is the distance of the mosaic location on the current image to the first stem identified on it. Scenario 1 is a special case of scenario 2, when the middle term of equation 6 becomes zero, i.e., when there is no blank image between the plants, but the plants still appear in two different images.

Experiments and Results

Images were captured from three different test fields located in Ames, IA, Moline, IL, and Carlyle, IL. In Ames and Carlyle test fields manual weeding was carried

out, where as in Moline test field weeds were controlled using herbicides (4-5 days prior to planting and 20-21 days after planting) before the images were captured. When the images were captured, corn plants were between v4-v6 growth stages in Ames (September 2009), between v3-v4 in Moline (October 2009) and Carlyle (July 2010). Images captured from nine 6 m long segments, three from each test field, were used for the experiment. In-field manual measurement was taken by laying down tape measure along a crop row and speaking the distances out loud to an audio recorder. The manual measurement was later used to calculate error in distance measured by the system. A processed crop row segment with all correctly identified corn plants are shown in figure 11. The shorter lines at top portion of the images represent the mosaic locations and the labeled longer lines at the bottom portion of the images represent stem locations.
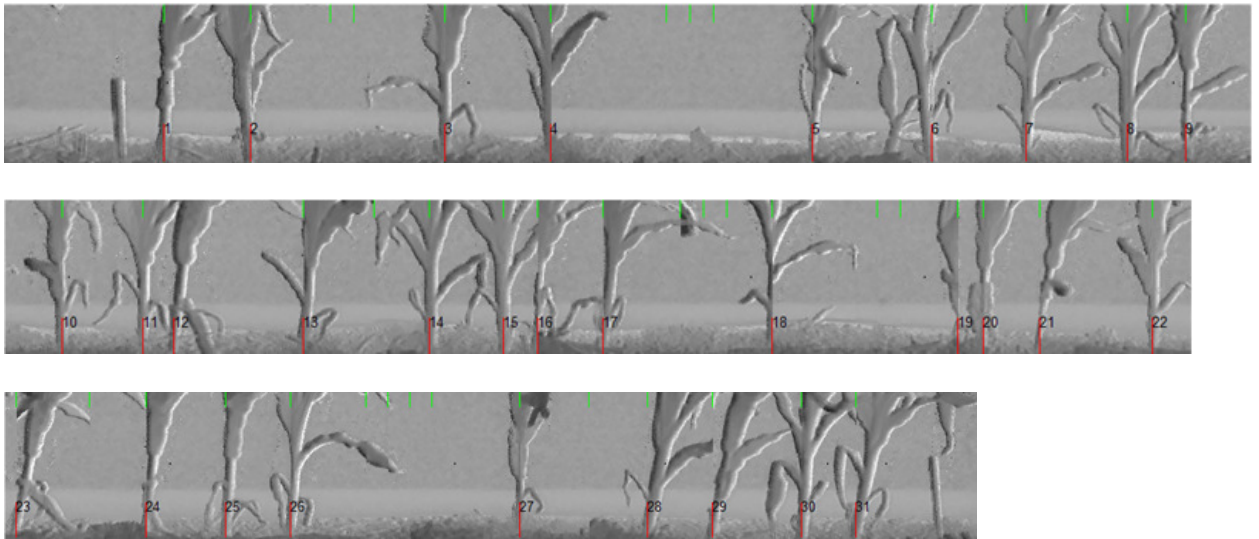
Figure 11. A processed crop row segment consisting of 31 corn plants: the objects before the first and the last plants are the segment markers.

The experimental results are shown in table 1, where L_m is manually measured crop row segment length, i.e., from the first plant to the last plant in the segment, L_c is system calculated crop row segment distance, N is total number of plants in the segment, N_f is total number for non-plants detected falsely as plants, N_m is total number missed or undetected plants, R_m is plant misidentification ratio calculated using equation 9, and RMSE is root mean squared error in inter-plant distance measurement.

$$R_m = \left(\frac{N_f + N_m}{N} \right) * 100\% \tag{9}$$

Table 1. Inter-plant distance measurement field test results

Location	L_m (m)	L_c (m)	N	N_f	N_m	R_m (%)	RMSE (m)
Ames, IA	6.11	6.04	33	0	1	3.03	0.017
	6.02	5.95	32	1	0	3.12	0.016
	6.26	6.19	30	1	0	3.33	0.017
Moline, IL	5.90	5.97	35	0	0	0.00	0.017
	5.98	6.03	31	0	0	0.00	0.021
	5.70	5.81	37	0	1	2.70	0.023
Carlyle, IL	6.05	6.08	38	1	0	2.63	0.018
	6.03	6.25	40	0	0	0.00	0.014
	6.10	6.28	41	0	2	4.88	0.013
Overall						2.21	0.017

The system achieved a mean plant misidentification ratio of 2.21% across the crop row segments. The false-positive plant identification often occurred due to long plant canopies hanging sideways (figure 12a). Plant identification errors due to undetected plants occurred in situations where one of the plants was not detected by the system when. For example, when two plants were growing less than one hundredth of a

meter away from each other (figure 12b), or when a plant was considerably short (figure 12c), or when a plant was tilted by more than ±15° (figure 12d).

(a)

(b)

(c)

(d)
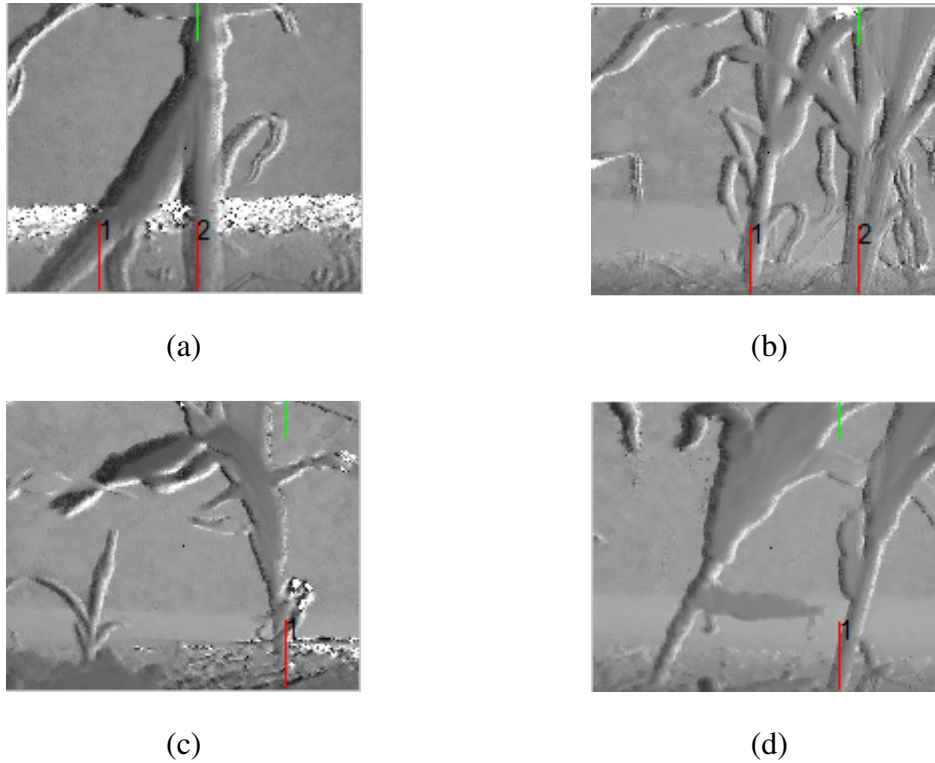
Figure 12. Plant misidentification situations: (a) long plant canopy identified as a plant; (b) two plants growing too close to each other identified as one; (c) considerably short plant undetected, and (d) considerably tilted plant undetected

Overall mean RMSE of 0.017 m was achieved with the maximum being 0.023 m and the minimum being 0.013 m. The algorithm was able to estimate lengths of the crop row segments, at the end of inter-plant distance measurement, with an accuracy of up to +0.03 m (i.e., 0.5 %). The maximum error in the estimation of +0.22 m (i.e., 3.6 %) occurred when most of the plants in the row segment were tilted in one direction

resulting in inter-plant distance measurement errors between most of the plant pairs to be positive.

The system was able to measure inter-plant distance with minimum error of ±0.03 m with maximum error being ±0.06 m. The larger error occurred when the system failed to use plant pixel, and instead used a pixel from the soil while calculating the distance, or the system failed to determine the plant center accurately due to clutters near the plant soil intersection. More than 70 % of the measurements errors were between ±0.02 m. The system measured distance estimates were regressed onto manual in-field measurements, the linear model coefficient of determination (R^2) was found to be 0.95.

Conclusions

The results demonstrate that the use of 3D vision system can accurately measure the spacing between the plants in a crop row with overall mean RMSE of 0.017 m and mean plant misidentification ratio of 2.2%. If the imaging area is covered properly and the camera is protected from the direct sunlight, the camera can capture images at any point of the day, in any illumination condition. The working mechanism of TOF cameras is color independent and is free from the limitations of systems which rely on color only for plant identification and center cluster detection. Using color alone appears to be inadequate to cope with the complexity of field conditions that lead to both color variations and color fading.

The system captures images from the side so that plants and soil intersections are always visible. This approach allows the system to accurately detect the stem centers

when the plants are inclined within $\pm 15°$ from the vertical axis. The performances of systems which work on top view images are severely affected when the plants are inclined. These systems fail to accurately identify the stem centers and hence measure the inter-plant spacing.

The system, however, cannot precisely locate the doubles or triples. The system can be modified to process more than one image at a time. When multiple images are processed at a time, the same plant is actually being viewed from more than one angle, which increases the chances of finding the plants which are occluded by other plants.

Currently, the system is tested on fields where weeds were completely removed either manually of using herbicides. As for the future work the authors plan to make the system robust enough to perform satisfactorily in real field conditions with weeds and residues from previous crops.

References

Barge, G.L., Thomison, P., 2001. Tips to reduce planter performance effects on corn yield, Extensions Factsheet. Horticulture and Crop Science Dept., The Ohio State University.

Buttgen, B., Oggier, T., Lehmann, M., Kaufmann, R., Lustenberger, F., 2005. CCD/CMOS lock-in pixel for range imaging: challenges, limitations and state-of-the-art. Mesa Imaging AG.

Doerge, T., Hall, T., Gardner, D., 2002. New research confirms benefits of improved plant spacing sensing in corn. Crop Insights 12.

Jin, J., Tang, L., 2009. Corn plant spacing sensing using real-time stereo vision. Journal of Field Robotics 26, 591-608.

Lauer, J.G., Rankin, M., 2004. Corn response to within row plant spacing variation. Agronomy Journal 96, 1464-1468.

Liu, W.D., Tollenaar, M., Stewart, G., Deen, W., 2004a. Within-row plant spacing variability does not affect corn yield. Agronomy Journal 96, 275-280.

Liu, W.D., Tollenaar, M., Stewart, G., Deen, W., 2004b. Impact of planter type, planting speed, and tillage on stand uniformity and yield of corn. Agronomy Journal 96, 1668-1672.

Nafziger, E.D., Carter, P.R., Graham, E.E., 1991. Response of corn to uneven emergence. Crop Science 31, 811-815.

Nielsen, R.L., 1991. Stand establishment variability in corn, Retrieved from: http://www.agry.purdue.edu/ext/pubs/AGRY-91-01_v5.pdf on 09/01/2011.

Nielsen, R.L., 2005. Effect of plant spacing variability on corn grain yield, Retrieved from: http://www.kingcorn.org/research/psv/Report2005.pdf on 04/25/2010.

Rosenfeld, A., 1975. A characterization of parallel thinning algorithms. Information and Computation/Information and Control 29, 286-291.

Shrestha, D.S., Steward, B.L., 2003. Automatic corn plant population measurement using machine vision. Transactions of the Asae 46, 559-565.

Tang, L., Tian, L.F., 2008a. Real-time crop row image reconstruction for automatic emerged corn plant spacing measurement. Transactions of the Asabe 51, 1079-1087.

Tang, L., Tian, L.F., 2008b. Plant identification in mosaicked crop row images for automatic emerged corn plant spacing measurement. Transactions of the ASABE 51, 2181-2191.

Vanderlip, R.L., Okonkwo, J.C., Schaffer, J.A., 1988. Corn response to precision of within-row plant spacing. Applied Agricultural Research 3, 116-119.

CHAPTER 3

WITHIN-ROW SPACING SENSING OF CORN PLANTS USING 3D COMPUTER
VISION

A manuscript prepared for submission to Biosystems Engineering

A. D. Nakarmi[1], L. Tang[1,2]

Abstract

Within-row plant spacing plays important role in uniform distribution of water and nutrients among plants, hence affects the final crop yield. While manual in-field measurements of within-row plant spacing is time and labor intensive, little work has been carried out to automate the process. We have attempted to develop an automatic system making use of a state-of-the-art 3D vision sensor that accurately measures within-row corn plant spacing. The system is robust to outdoor illumination conditions and can be used at any point of time on a given day. Based on small scale experiments in fields, this system can measure the within-row corn plant spacing with a mean ($\pm$ standard deviation) error of 1.60 ± 2.19 cm. The root mean squared error was 2.19 cm.

Keywords. Spacing Sensing, Inter-plant Spacing, Within-row, 3D Computer Vision, Time-of-flight

Introduction

Plants compete among themselves for water and nutrients. Evenly spaced plants

[1.] Department of Agricultural and Biosystems Engineering, Iowa State University, Ames, IA, 50010
[2.] Corresponding author. Phone: 515-294-9778; Fax: 515-294-6633; e-mail: lietang@iastate.edu

therefore, plays an important role in uniform distribution of the water and nutrients required for proper growth. Researchers have studied the effect of plant standing variability (PSV) on final crop yield. Most notably, Nielsen (1991) reported that there was a reduction of about 2.5 bushels per acre for every inch increase in standard deviation of within-row plant spacing. Doerge et al. (2001) found similar effects of plant space variability on grain yield, where they reported a loss of 3.4 bushels per acre for every inch increase in standard deviation of within-row plant distribution. The effect of PSV on final crop yield however, is not conclusive as there exists some studies (Lauer & Rankin, 2004 and Liu et al. 2004a) where the authors reported that the effects of plant spacing variability on corn grain yield was negligible. Subsequent studies by Nielsen (2005) and Liu et al. (2004b), reported a yield loss of 2.2 bushels per acre and 1.5 bushels per acre, respectively, for every inch increase in standard deviation of plant spacing.

While planter manufacturers are concerned about the performance of their planters, till today they rely on in-field manual measurements of within-row plant spacing for evaluation of planter performance. Typically, manual measurements are carried about by laying down a tape measure along a crop row and recording inter-plant spacing on a notebook or an audio recorder. Manual methods are time and labor intensive, and at the same time subject to human error. It takes about 25 minutes to manually measure inter-plant spacing of a typical 200 feet crop row with around 280-290 plants, including time of recording and entering measurement data into a spreadsheet.

Little work has been done in automating the inter-plant spacing sensing process. Shrestha and Steward (2003) and Tang and Tian (2008a, 2008b) used image processing techniques using top view images to automatically measure inter-plant spacing. Their approach relied solely on color information to detect plants on images, which affected the robustness of the system when the outdoor illumination conditions changed. Also the accuracy of locating stem centers suffered, especially when the canopies of adjacent plants got interconnected. Jian and Tang (2009) developed a corn plant sensing system using a stereo camera with a 96 % correct detection rate. In previous work, Nakarmi and Tang (2012), the authors took a different approach using a state-of-the-art 3D sensor based on time-of-flight (TOF) of light to automatically measure within-row corn plant spacing. The system did not rely on color information and used side view images instead to accurately locate stem centers on the images. The system performance however, was affected by outdoor illumination conditions, long hanging plant canopies and multiple plants growing together.

In this paper, a new within-row corn plant spacing sensing system is presented that can perform at any point of time on a given day without being affected by outdoor illumination conditions, and at the same time whose performance is not severely affected by hanging canopies. The system performance was validated against manual measurements taken from multiple 61 m (200 feet) long corn plant rows.

Materials and Methods

A three-wheeled cart, as depicted in figure 1, was designed such that the imaging area was covered to prevent direct sunlight shining on the plants. A tunnel like structure was made. While pushing the cart along a crop row, special attention was given so that crop row always remained more or less at the center of the tunnel. The tunnel also ensured minimum effect of the wind on plant postures. The wall of the tunnel facing the camera was covered by a soft fabric material which resulted in uniform depth data on the wall. A high resolution, 4096 counts per revolution encoder was mounted on one of the rear wheels of the cart and was used to trigger image capturing.
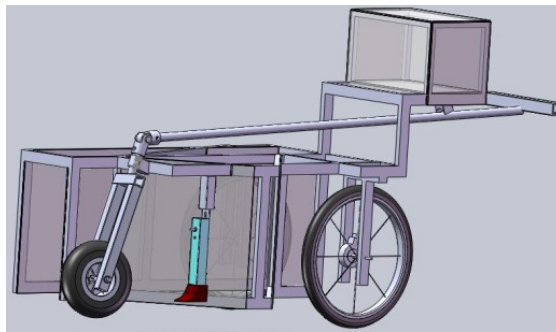
Figure 1. CAD model of a three-wheeled data acquisition platform

A time-of-flight (TOF) of light based 3D camera (CamCube2^{TM} from PMD Technologies, Siegen, Germany) was mounted about 10 cm above the ground and at about 50 cm away from crop row. Each image was captured at about 100 encoder counts which was approximately 5 cm along the crop row direction. The corn plants were in v3-v4 (3-4 weeks) growth stage, and herbicides were used kill weeds a week prior to capturing images from the field. The system was developed using C# as a programming

language and Microsoft Visual Studio 2010 development environment in Microsoft

Windows 7 platform. An algorithm for within-row corn plant spacing sensing was

developed which consisted of a four-step process as listed in table 1. First, the captured

images were segmented to separate plants from the background. In the next step, the

plant stem centers were localized. The images were then mosaicked together and finally

inter-plant spacing was computed. For the sake of completeness, the operating principle

of the 3D camera will be presented in the next section and a detailed description of the

algorithm will be presented in the following sections.

Table 1. Four-step within-row corn plant spacing sensing algorithm

Image segmentation	a. Discard upper quarter of image to reduce the effect of long plant canopies b. Separate plants from background and soil using depth and amplitude values, respectively. c. Group foreground regions into separate plants and discard smaller regions
Stem center identification	a. Find Hough lines on segmented image b. Group Hough lines for each plant on the image c. Select Hough line that approximates stem center d. Trim plant regions around the Hough lines
Image mosaicking	a. Find common plant in three consecutive images b. If found, mosaic at common plant location, otherwise use encoder data to mosaic them
Inter-plant spacing measurement	a. Calculate variance of depth values along stem skeleton and use it as a score for each identified plant b. For two plants appearing in an image, sum the plant scores to assign score to the distance between them c. Calculate distance scores for the plants in every image they appear d. Use the distance with the lowest variance as the best available distance between the plants

The sensor sends out modulated light waves from light emitting diodes (LEDs), and the imaging sensor measures the phase shift of returned signal at each pixel to calculate distance of the target object (Buttgen et al, 2005, Ringbeck, 2007 & Hansard et al, 2012). The sensor comes pre-calibrated and by default operates at a 20 MHz modulating frequency. Suppression of background illumination (SBI) implemented in the camera model allows the sensor to automatically correct for environmental fluctuations such as illumination conditions and makes it suitable for outdoor applications. This TOF sensor and other similar TOF sensors are superior to conventional stereo vision systems as they do not rely on non-uniform texture feature for non-ambiguous disparity map generation, which is particularly useful for the application as plant canopies that often present somewhat uniform texture. The sensor captures spatial data in Cartesian coordinates with its origin at the center of the frontal face of the camera. Along with spatial data, the camera also captures amplitude image, which contains for each pixel a value representing the strength of the reflected signal by the object. The amplitude values are low when the strengths of the reflected signals are weak. The camera has a rather small field of view (FOV), $40°$ (h) $\times$ $40°$ (v) and captures images with 204×204 pixel spatial resolution.

Integration time is one of the most important and only available internal camera parameter that could be adjusted. It describes the time period in which incoming photons are detected for one measurement cycle to derive phase shift and the corresponding distance. If the integration time is set too low, the amplitudes of related pixels decrease and distances for distance objects cannot be measured. On the other hand, if the

integration time is too high, oversaturation is observed and measurements fail.

Therefore, integration time needs to be carefully selected before acquiring images.

Image Segmentation

Samples of depth image, amplitude image, background and soil removed image
and final segmented image are shown in figure 2. The captured images were processed
to separate plants from the background and soil. The top quarter of the images were
discarded to reduce the effect of leaves in plant localization and stem center
identification.


(a)

(b)

(c)

(d)
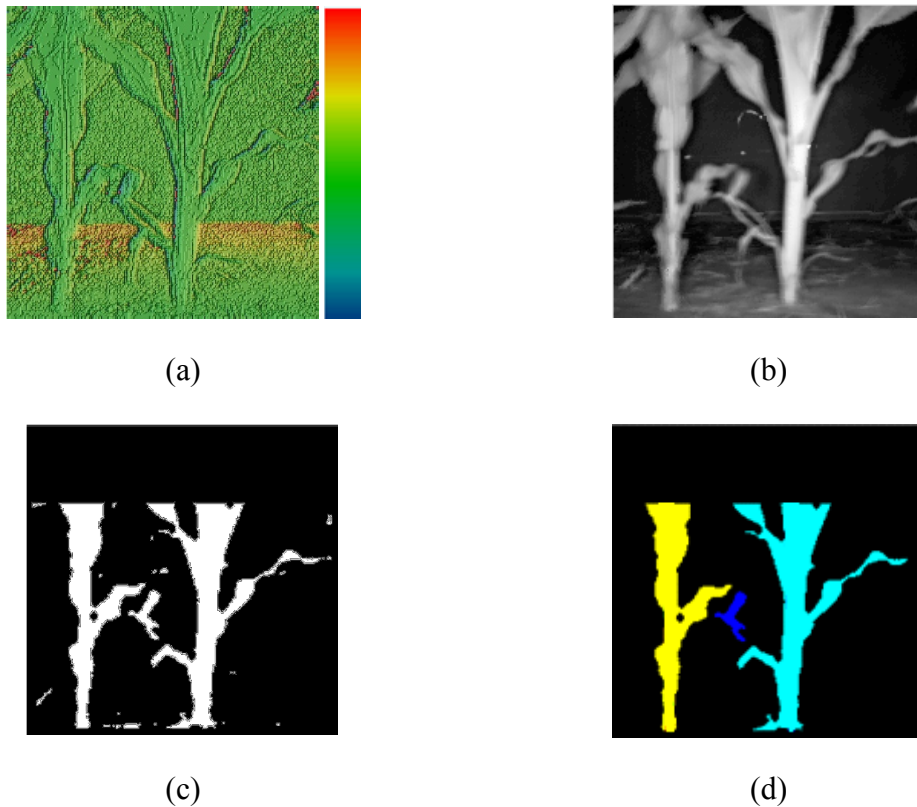
Figure 2. Image segmentation: (a) depth image with pseudocolor, blue color represents
closer and red represents farther pixels; (b) amplitude image; (c) image with upper
quarter discarded, background and soil removed; (d) final segmented image

A depth threshold at 5 cm in front of the tunnel wall was used to segment the middle half of the image. The fact that the lower quarter of the image mostly contained soil region and that amplitude values of soil pixels were significantly lower than those of plant pixels, an amplitude threshold of 500 was used to separate plant regions from the soil. Basically, depth and amplitude values were used to segment plants from the background and the soil, respectively. Region growing algorithm was used to group connected pixels together and smaller isolated region were removed (Heijden, 1995).

Stem Center Identification

For stem center identification Hough lines (Duda and Hart, 1972) were found on segmented images. Search for the Hough lines were limited to $\pm15°$ from the vertical, which allowed for the identification of plants inclined up to $15°$ left and right of the vertical and also improved the computation time. Identified Hough lines were grouped together based on their proximity. X values of the lower ends of the Hough lines in each group were sorted and one with the median value was used as the best line passing through the center of the plant stem. The plant regions were then trimmed around the best Hough line by taking 10 pixels on each side of the line. Skeleton of the trimmed plant regions were computed and the lower most point on the skeleton was used as the stem center. A sample of a segmented image, its identified Hough lines, plant regions trimmed around the best Hough lines, and skeletons of the trimmed plant regions are illustrated in figure 3.
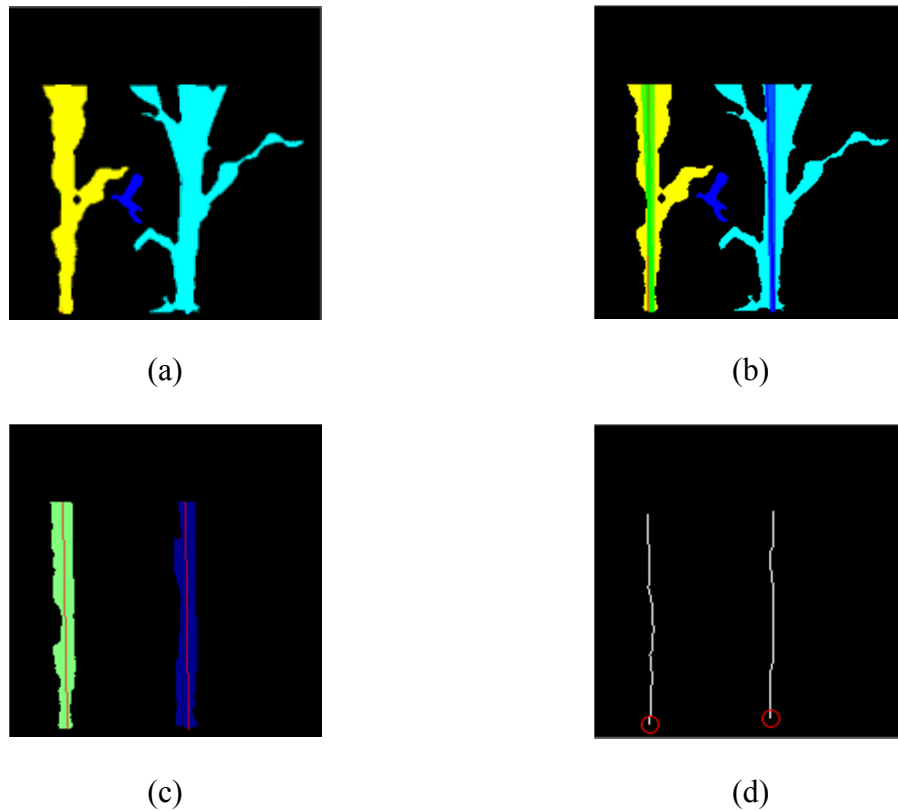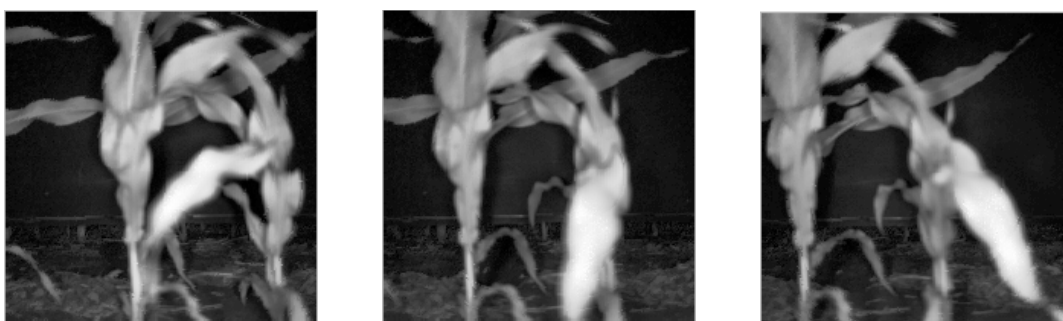
Figure 3. Stem center identification: (a) segmented image; (b) identified Hough lines; (c) plant regions trimmed around the best Hough lines; (d) skeletons of trimmed plant regions

Challenges in Accurately Locating Stem Centers

Figure 5 depicts two typical cases which were required to be resolved for the robustness in stem center identification and hence for improving inter-plant spacing measurement accuracy of the system. In the first case, it was observed that plant leaves at times occluded the stems, which prevented the system from accurately locating the stem center. When the adjacent images were processed, the system however, was able to locate the stem centers without difficulty. The scenario is illustrated in figure 4a. In the second case, a few cases of multiple plants growing together were observed. The system

was not able to detect two plants on the first two images shown in figure 4b, while it was able to detect both the plants in the third image. To resolve the issues, for subsequent image mosaicking and inter-plant spacing measurement steps, an algorithm was developed such that the system considered multiple images, image in hand and its two neighbors, instead of relying on a single image for identification of plant centers.


(a)

(b)

Figure 4. Typical issues in stem center identification: (a) plant leaves occluding a stem; (b) multiple plants growing together

Image Mosaicking

The images were stitched together to form a mosaicked image. In each step three images were considered for mosaicking. Image grouping scheme is shown in figure 5.

The identified stem locations were used to mosaic the images where possible, and encoder data was used when stem location information was not available. The multi-view approach was used to account for cases shown in figure 5 as well as to improve distance calculation accuracy, which will be discussed in the next section. The mosaicking scheme was based on the flowchart shown in figure 6.
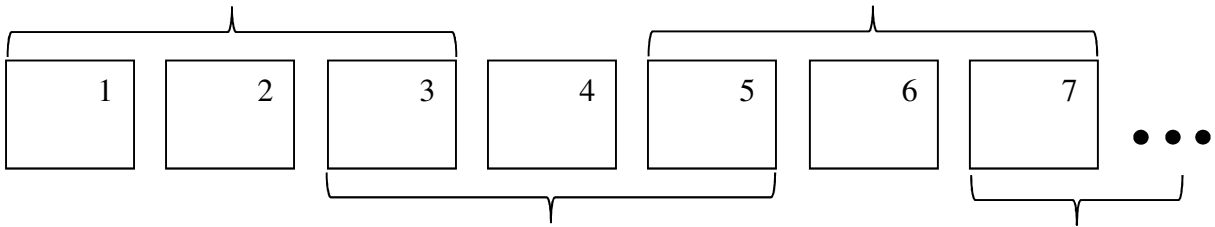
Figure 5. Image grouping: three images at a time

First, a common plant was searched in the three images in hand. If it was found, the first and the third images were stitched at the common plant location and the mosaic image was formed from these two images, while the second image was completely discarded for image mosaicking purpose. Figure 7 illustrates the scenario where (a) a common plant in the three images is marked and (b) identified stem locations are marked by lower lines and a mosaic location is marked by the upper line.
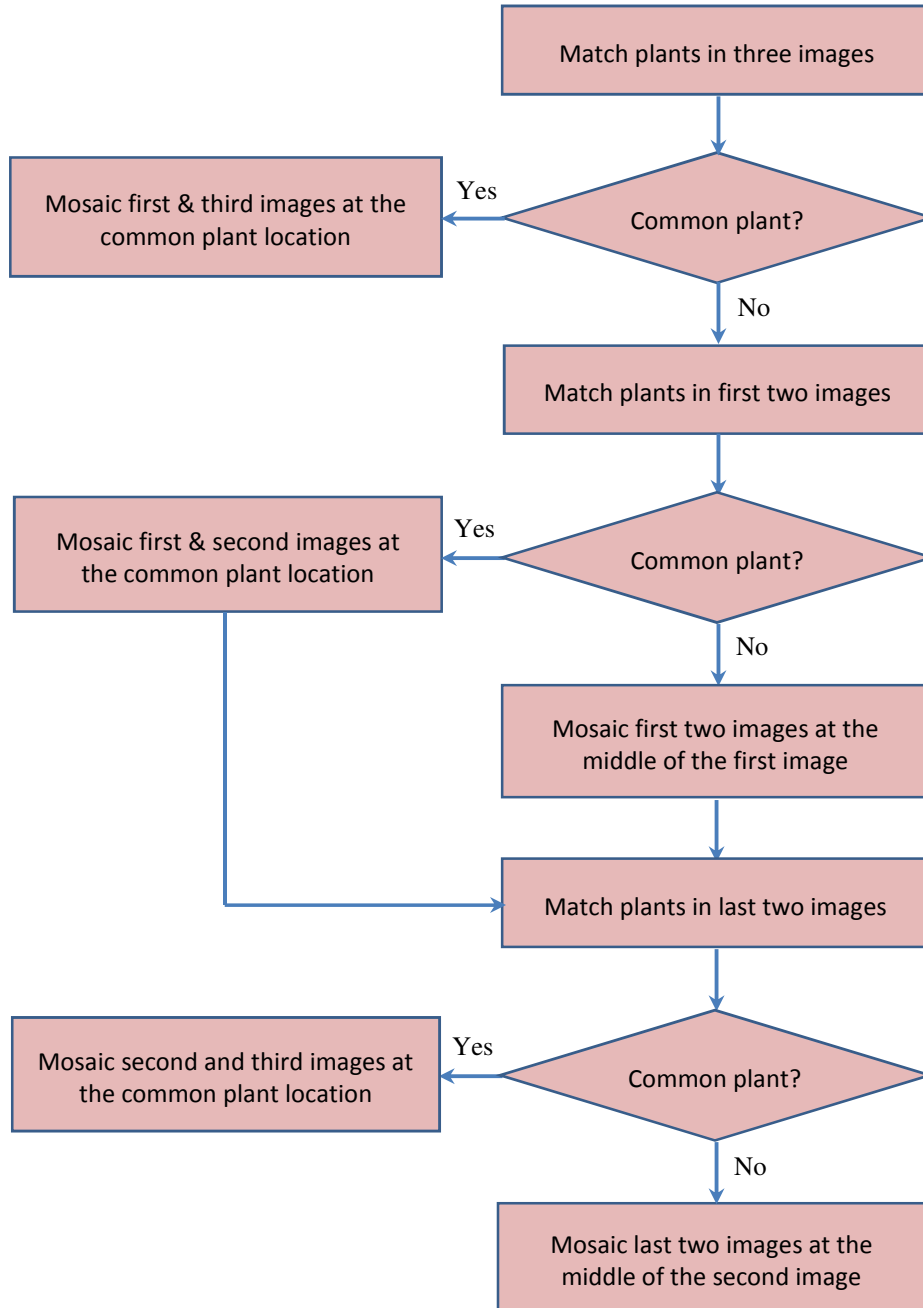
Figure 6. A flowchart of image mosaicking scheme
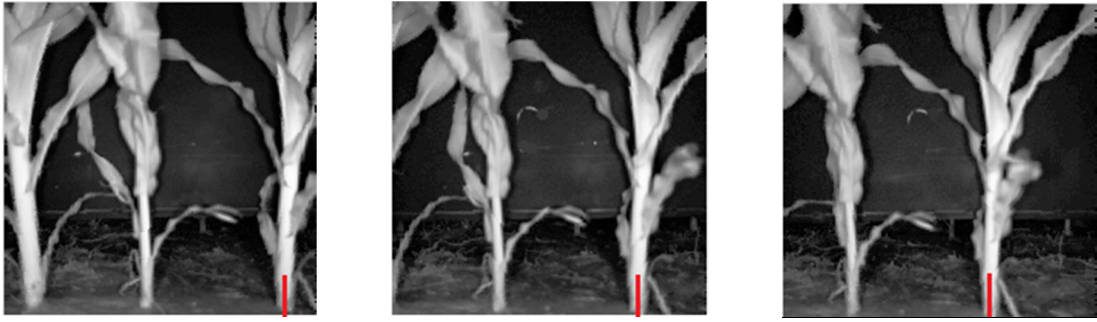
(a)
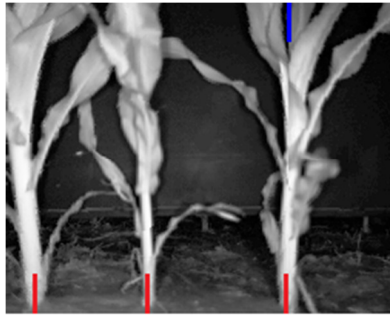
(b)

Figure 7. Image mosaicking when there is a common plant: (a) three consecutive images with a common plant; (b) mosaicked image formed by stitching the first and the third images

When a common plant was not found in all three images, a common plant was searched between the first and the second images. If found the two images were stitched at the common plant location. In order to stitch the second and the third image, a mosaic location on the third image was determined as a location corresponding to the middle of the second image. For this purpose, encoder data was used to calculate the translation between the two images along the crop row direction. The case is depicted in figure 8. Similar scheme was used, when there was no common plant between the first and the second images.

(a)

(b)

Figure 8. Image mosaicking when there is a common plant between two images: (a) three consecutive images with a common plant in the first and the second images; (b) mosaicked image formed by stitching the first and the second images at their common plant location (upper left line) and, the second and the third images at the middle of the second image and its corresponding location in the third image (upper right line)

When there was no common plant between all three images, the images were mosaicked entirely based on the encoder data. The case is shown in figure 9. The first and the second images were mosaicked at the middle of the first image and its corresponding location on the second image. Similarly, the second and the third images were mosaicked at the middle of the second image and its corresponding location on the third image.
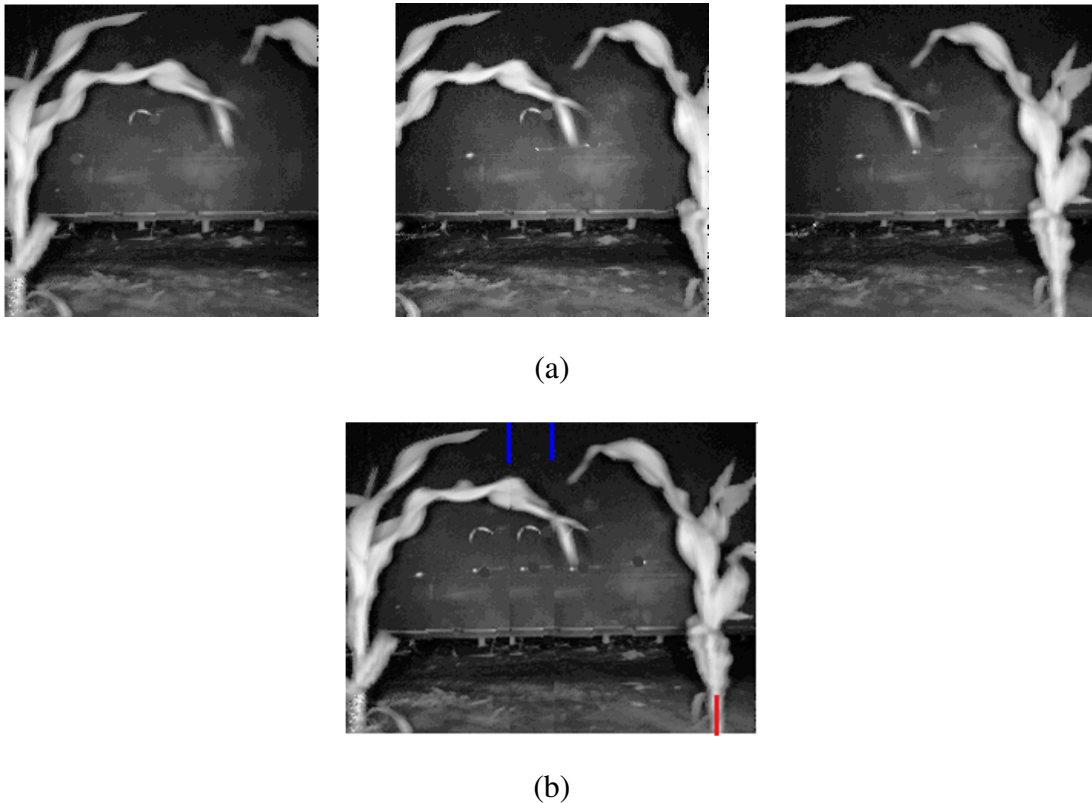
(a)

(b)

Figure 9. Image mosaicking when there is no common plant between images: (a) three consecutive images with no common plant between them; (b) mosaicked image formed by stitching the first and the second images at the middle of the first image and its corresponding location in the second image (upper left line) and, the second and the third images at the middle of the second image and its corresponding location in the third image (upper right line)

Inter-plant Spacing Measurement

The multi-view approach was used in used to calculate the distances between the plants as well. The idea was to calculate distances between any two plants in all the images in which they were visible and pick the one that the algorithm indicated as the best. The identified stems were assigned with scores based on the variation of depth values along the skeletons up to 5 cm up from the lowermost point of the skeleton. In

absence of noise, due to occluding leaves, direct sunlight etc., depth variance along a

stem was expected to be small. Therefore, smaller the depth variance higher is the

chance of having good inter-plant spacing measurement. While measuring the distances

between any two plants, the depth variances of the plants were summed up to assign

score to the distance measured between them. Every time the same two plants appeared

on different images, the distance scores were saved, and the distance with the lowest

score was selected to be the best available measurement. The process is illustrated in

figure 10. The distance measured between the plants on the first image was selected as

the best available distance as the calculated depth variance along the stems was the

lowest. The depth variance on the third image was the highest due to the leaf that

occluded the stem of the first plant. The distance between the plants measured in the

field was 20.21 cm, and the system measured distance was 20.09 cm.

(a)   (b)   (c)
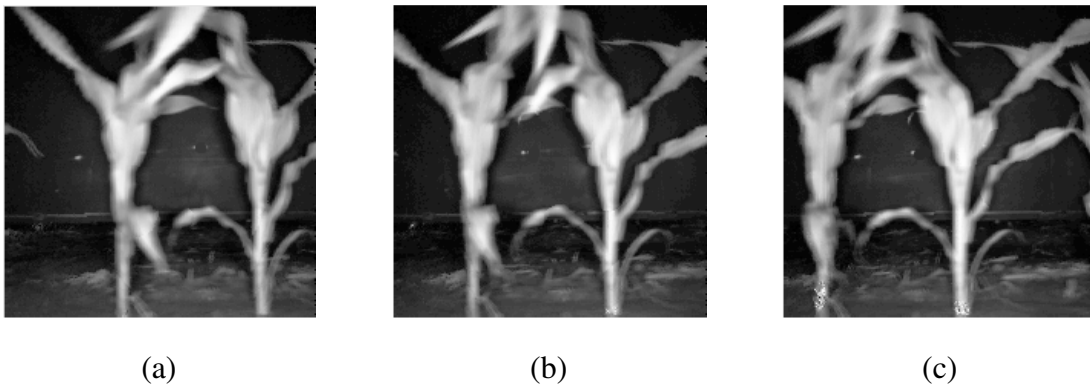
Figure 10. Inter-plant spacing measurement using multi-view approach: (a) with depth variance of 6.32 and measured distance 20.09 cm; (b) with depth variance of 10.87 and measured distance 20.38 cm; (c) with depth variance of 4070.37 and measured distance 26.41 cm. In-field manual measurement was 20.21 cm which is closest to the distance selected by the system in the first image

Four 61 m (200 ft) long corn rows were used for the performance evaluation of the system. Data collection was done in June, 2011 on a test field in Illinois. The system measurements were compared against in-field manual measurements to calculate mean and standard deviation of error. Misidentification rate was calculated to determine the percentage of manual correction. The misidentification rate was computed using Equation 3.

$$R_m = \frac{N_m + N_f}{N} \tag{3}$$

where N_m is total number of missed plants, N_f is total number of false-positive detection and N is total number of plants in a row.

Results and Discussion

There were no false detection in all the rows, while the system did not detect some plants which were shorter than the threshold used. The average mean $\pm$ standard deviation of error was 1.60 ± 2.19 cm, and the root mean squared error (RMSE) was 2.54 cm. The results of the experiment are listed in table 2, where N_c is number of correct plant detections.

Table 2. Average within-row corn plant distance measurement error.

Row	N	N_c	N_m	N_f	R_m	Mean error (cm)	RMSE (cm)
1	288	284	4	0	1.38 %	1.20	2.12
2	273	265	8	0	2.93 %	1.14	2.03
3	270	267	3	0	1.10 %	2.14	3.25
4	266	264	2	0	0.75 %	1.43	2.77
Average	274				1.54 %	1.60	2.54

Conclusions

With the multi-view approach, the system was able to resolve issues imposed by long hanging plant canopies and doubles (two plants growing together). The multi-view approach also helped to improve the accuracy of the stem center identification, and hence inter-plant spacing measurements. The average misidentification rate was 1.54 % with no false detections. The missed plants were mostly the shorter plants. The presence of shorter weeds and dead but standing weeds did not affect the performance of the system. The system took about three minutes to capture images from a typical 61 m (200 ft) crop row containing an average of 275 plants and about 3 and ½ minutes which was significantly compared to 25 minutes required to collected manual measurements.

The use of TOF camera as opposed to conventional stereo camera proved advantageous as TOF camera was robust to outdoor illumination conditions. However, the imaging area was needed to be properly covered so that direct sunlight did not shine on plants. It was noticed that integration time needed to be adjusted depending on the sunlight conditions so as to capture better data. While in the morning and the evening hours integration time of 800 - 1000 μs was found to give better data, during middle of the day when the sunlight intensity was very strong in the month of June, when the data was collected, integration time of 300 - 500 μs was used.

References

Buttgen, B., Oggier, T., Lehmann, M., Kaufmann, R., Lustenberger, F., 2005. CCD/CMOS lock-in pixel for range imaging: challenges, limitations and state-of-the-art. Mesa Imaging AG.

Doerge, T., Hall, T. and Gardner, D. 2001. New Research Confirms Benefits of Improved Plant Spacing in Corn. Pioneer Hi-Bred. Available at: https://www.pioneer.com/home/site/us/agronomy/library. Accessed 08 May 2012.

Duda, R. O., & Hart, P. E. (1972). Use of Hough tranformation to detect lines and curves in pictures. *Communications of the Acm, 15*(1), 11-15.

Hansard, M., Lee, S., Choi, O. & Horaud, R. 2012. Time-of-Flight Cameras: Principles, Methods and Applications. Springer.

Heijden, F. van der. 1995. *Image Based Measurement Systems: Object Recognition and Parameter Estimation.* West Sussex, England: John Wiley and Sons.

Jian, J. and Tang, L. 2009. Corn Plant Sensing Using Real-time Stereo Vision. *Journal of Field Robotics. 26(6-7): 591-608.*

Lauer, J. and Rankin, M. 2004. Corn Response to Within-row Plant Spacing Variation. *Agron. J., 96: 1464-1468.*

Liu, W., Tollenaar, M., Stewart, G. and Deen, W. 2004a. Within-row Plant Spacing Variability Does Not Affect Corn Yield. *Agron. J., 96: 275-280.*

Liu, W., Tollenaar, M., Stewart, G. and Deen, W. 2004b. Impact of Planter Type, Planting Seed and Tillage on Stand Uniformity and Yield of Corn. *Agron. J., 96: 1668-1672.*

Nakarmi, A.D. and Tang, L. 2012. Automatic Inter-plant Spacing Sensing at Early Growth Stages using a 3D Vision Sensor. *Computers and Electronics in Agriculture, 82: 23-31.*

Nielsen, R.L. 1991 (Rev. 2001). Stand Establishment Variability in Corn. Purdue University, Agronomy Department. Publication AGRY-91-01. Available online at http://www.agry.purdue.edu/ext/pubs/AGRY-91-01_v5.pdf. (URL verified 05/07/2012).

Nielsen, R.L. 2004 (rev. 2005). Effect of Plant Spacing Variability on Corn Grain Yield. Purdue University, Agronomy Department. Available online at http://www.agry.purdue.edu/ext/corn/research/psv/Report2005.pdf (URL verified 05/08/2012).

RingBeck, T. 2007. A 3D Time of Flight Camera for Object Detection. *Optical 3-D Measurement Techniques, Plenary Session 1: Range Imaging I.*

Tang, L. and Tian, L. F. 2008a. Plant Identification in Mosaicked Crop Row Images for Automatic Emerged Corn Plant Spacing Sensing. *Transactions of ASABE. 51 (6): 2181-2191.*

Tang, L. and Tian, L. F. 2008b. Real-time Crop Row Image Reconstruction for Automatic Emerged Plant Spacing Measurement. *Transactions of ASABE. 51(3): 1079-1087.*

CHAPTER 4

STEM DETECTION ALGORITHM FOR COTTON PLANTS: PROOF OF CONCEPT

A manuscript prepared for submission to Computers and Electronics in Agriculture

A. D. Nakarmi, L. Tang

Abstract

Plant population, row spacing, and within-row interplant distance can affect final yield. Automated plant population measurement and within-row interplant distance measurement have potential for assessments of in-field variation of plant emergence and planter performance. A non-invasive machine vision system was developed to detect cotton plants in side-view images. A time-of-flight of light based 3D camera was used to capture images of cotton plants at V3 to V4 stages. The image processing algorithm developed was capable of detecting cotton plants in low weed infestation field conditions. The acquired images were processed to compute "vesselness" measure. Curvilinear structures were detected on "vesselness" image. The center pixels of the curvilinear structures were computed followed by line-fitting and edge-linking step. Finally, Hough lines were computed to detect the cotton stem profiles. Over a set of sample images containing 100 cotton plants, the system correctly detected 93 plants and misidentified seven of them, with two false-positive detections.

Keywords: cotton plant; stem detection; image processing; vesselness; Hough line

[1.] Department of Agricultural and Biosystems Engineering, Iowa State University, Ames, IA 50011, USA.
[2.] Corresponding author. Phone: 515-294-6778; Fax: 515-294-2255; Email: lietang@iastate.edu.

Introduction

Plant population, row spacing, and within-row interplant distance can affect final yield. Researchers in the past have investigated automated population measurement and within-row interplant spacing sensing systems. Suduth et al. (2000) developed a combine-mounted mechanical sensor to map corn plant population at harvest. Shrestha and Steward (2003) developed image processing algorithms for automatic corn plant population measurement system. Tang and Tian (2008a, 2008b), Jin and Tang (2009), and Nakarmi and Tang (2012) developed image processing algorithms for interplant spacing sensing of corn plants within a row using video camera, stereo camera, and light based time-of-flight 3D camera, respectively.

Detection of cotton stems from images is particularly challenging as leaves tend to occlude their stem profiles. McCarthy et al. (2009) used image processing techniques to detect stems and measure internode length. In their research, images were captured by forcing the main stem into a glass window which allowed the leaves to move away from the stem, thereby getting clear stem profile.

The objective of the study was to develop image processing algorithms for automatic detection of cotton plant stems using a time-of-flight of light based 3D sensor.

Materials and Methods

An image processing algorithm has been developed to automatically detect cotton stem centers from images acquired in non-invasive manner using a time-of-flight of light based 3D camera.

The algorithm developed for detection of cotton plant stems involves three major steps: (a) computation of "vesselness" measure; (b) detection of curvilinear structures; and (c) edge linking and line fitting on detected curvilinear structures.

In the first step, significant lines, which most likely correspond to stems and/or branches, were extracted from the images. Amplitude images, which provide the strength of signals returned back to camera sensor, were used for the image processing purpose. Eigenvalues of Hessian matrix (H) was implemented to extract curvilinear structures.

$$H = \begin{bmatrix} I_{xx} & I_{xy} \\ I_{xy} & I_{yy} \end{bmatrix} \tag{1}$$

where $I_{ab} = \dfrac{\partial^2 I}{\partial a \partial b}$ for each image pixel, and I is the pixel amplitude value. The eigenvalues detect the principal direction of local second-order image structure. The image second-order derivatives were computed by convolving the image with the derivatives of a Gaussian kernel of standard deviation σ. Steger (1998) used this technique for automatic road extraction from aerial images. Sato et al. (1997) and Frangi et al. (1998) used the technique for automatic extraction of blood vessels from medical images.

Computation of Vesselness Measure

The input image was then transformed using the vesselness measure (V_0) of Hessian eigenvalues Frangi et al. (1998). Vesselness is a measure of the likelihood of a

pixel belonging to a tubular structure, in this case a plant stem. Vesselness measure was computed using equation 2:

$$V_0 = \begin{cases} 0 & \text{if } \lambda_2 > 0 \\ \exp\left(-\dfrac{R_\beta^2}{2\beta^2}\right)\left(1-\exp\left(-\dfrac{S^2}{2c^2}\right)\right) & \text{otherwise} \end{cases} \tag{2}$$

The vesselness measure consists of two criteria: the "blobness" measure is the ratio of the Hessian matrix eigenvalues, and the second-order "structuredness" is the Frobenius matrix norm of the Hessian matrix.

$$R_\beta = \frac{\lambda_1}{\lambda_2} \tag{3}$$

$$S = \|H\|_F = \sqrt{\sum_{j \leq D} \lambda_j^2} \tag{4}$$

where D is the dimension of the image, in this case $D = 2$. The blobness measure accounts for the deviation from a blob-like structure but cannot distinguish between a line and a plate-like pattern. The ratio attains its maximum for a blob-like structure and is zero whenever $\lambda_1 \approx 0$. The second-order structuredness gives a low response where there is no image structure or where there is low image contrast. Parameters β and c in equation 2 are thresholds that control the filter's sensitivity to R_β and S, respectively. $|\lambda_1| < |\lambda_2|$ are eigenvalues of Hessian matrix H. The vesselness measure was filtered using a threshold to ignore lower responses and highlight the image structures. Figure 1

shows sample images after computation of vesselness measure. The images were

obtained using $\sigma = 1$, $\beta = 0.5$ and $c = 65$. The vesselness measure was set to zero for all

$V_0 < 0.005$.

<div align="center">(a)   (b)   (c)</div>
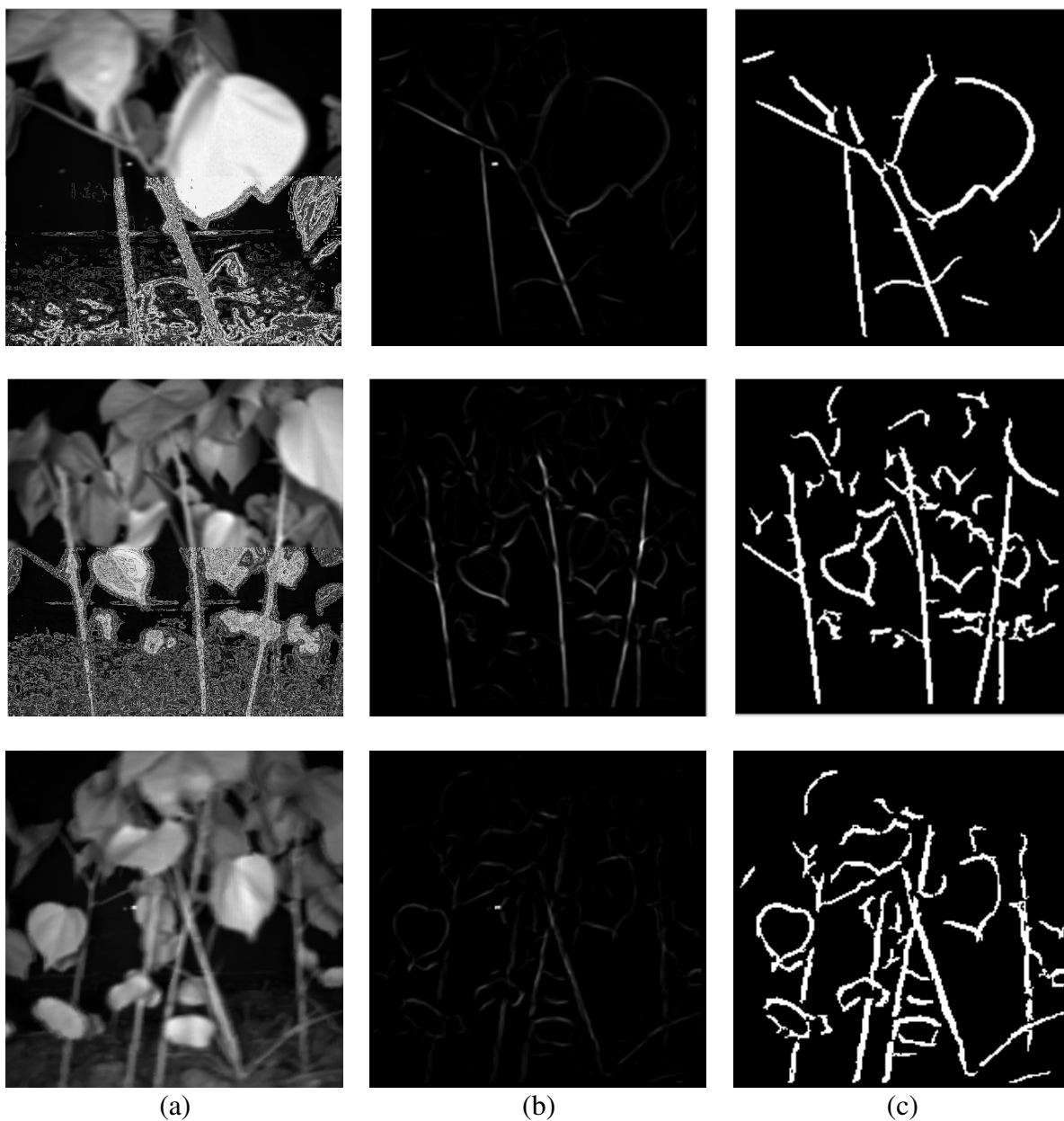
Figure 1. Vesselness measure: (a) amplitude images of cotton plants; (b) outputs of vesselness measure computation; (c) outputs after vesselness measure was filtered.

Curvilinear Structures Detection

The filtered image was then used to detect center lines. At the center of line profile, the first directional derivative in the direction perpendicular to the line, $\hat{n}$, should be zero and the second directional derivative should be a large absolute value (Steger, 1998), 1998). In 2D image, the direction perpendicular to a line is given by:

$$\hat{n} = \left(n_x, n_y \right) \text{ with } \left\| \left(n_x, n_y \right) \right\|_2 = 1 \tag{5}$$

which is the unit eigenvector corresponding to the eigenvalue of maximum absolute value. A quadratic polynomial is used to determine whether the first derivative along $\left(n_x, n_y \right)$ vanished within the given pixel. The point is given by:
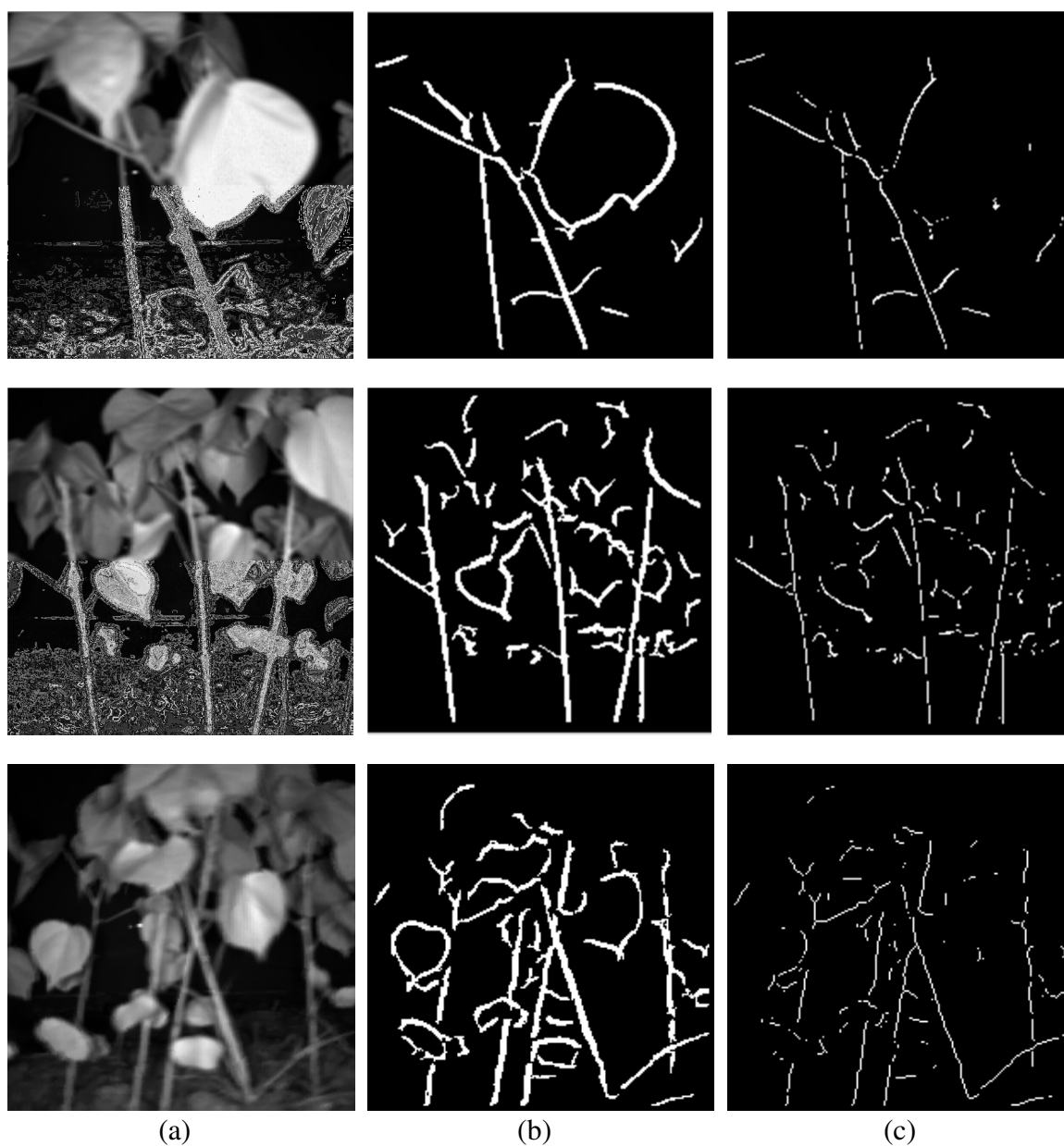
$$\left(p_x, p_y \right) = \left(tn_x, tn_y \right) \tag{6}$$

where

$$t = -\frac{I_x n_x + I_y n_y}{I_{xx} n_x^2 + 2I_{xy} n_x n_y + I_{yy} n_y^2} \tag{7}$$

If $\left(p_x, p_y \right) \in \left[-\frac{1}{2}, \frac{1}{2} \right] \times \left[-\frac{1}{2}, \frac{1}{2} \right]$, i.e., if zero-crossing occurs within pixel boundaries, then it is declared a line point. Figure 2 depicts the images after center lines were detected.

| (a) | (b) | (c) |

Figure 2. Center line detection: (a) amplitude images; (b) filtered vesselness measure, and (c) center lines on vesselness measure

<u>Edge Linking and Line Fitting</u>

In the next step, Steger curves were thinned to obtain single pixel wide curves.

Ends and junctions of the curved were then determined. "Hop-along" method (Jain,

Kasturi, & Schunck, 1995) was used for line fitting. For this purpose, ordered edge list was extracted using 8-way connected component based curve tracing. The hop-along algorithm steps along an ordered edge list and either appends edges to the existing calculated line if the edge points follow the same direction, or starts a new line if there is a significant change in direction of the edge points. Hence, a curve is represented as a sequence of straight lines joined end-to-end. A line segment parameterized by the coordinates of the end points is given by:

$$x(y_1 - y_k) + y(x_k - x_1) + y_k x_1 - y_1 x_k = 0 \tag{8}$$

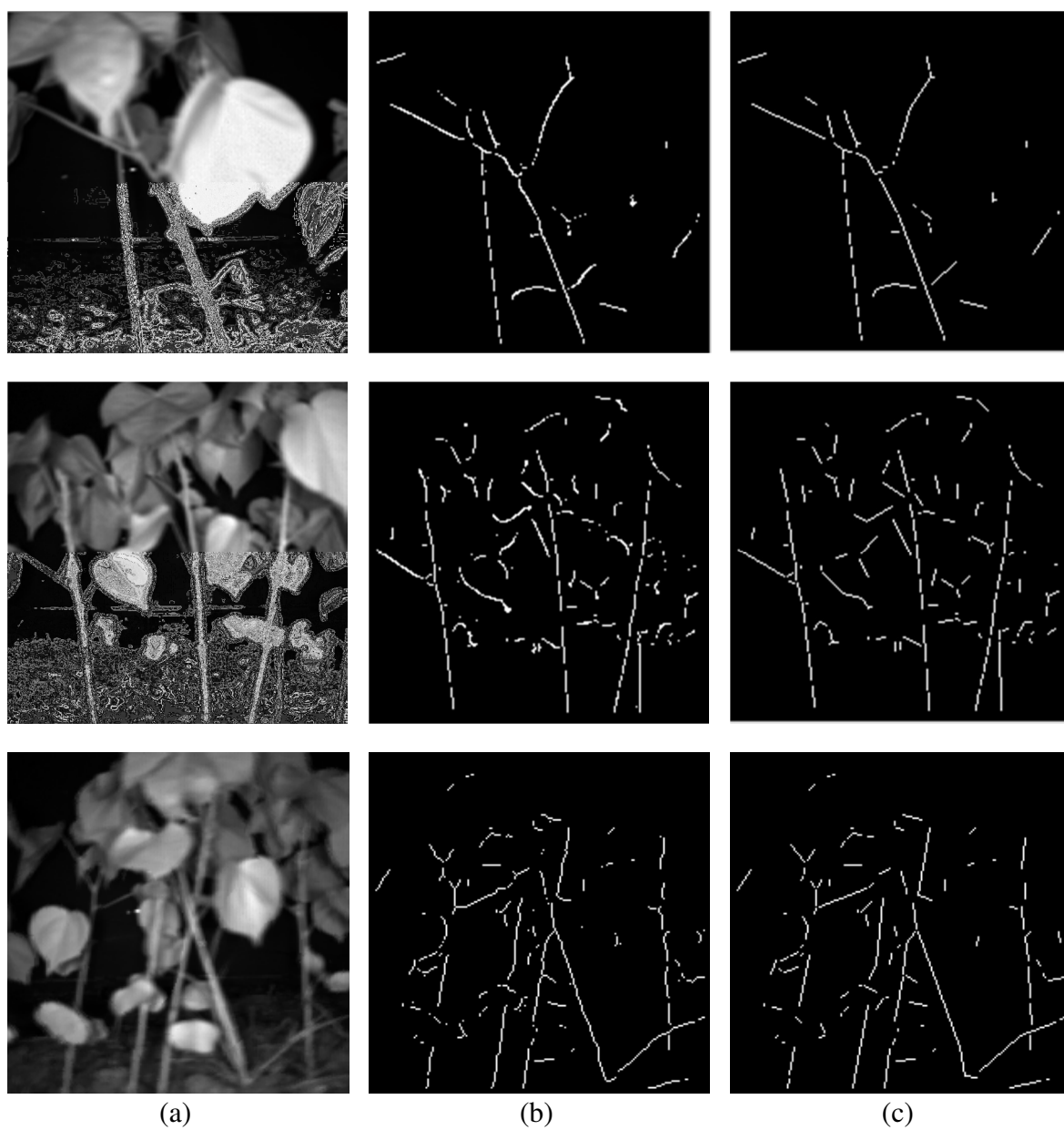The distance of any point (x_i, y_i) from the line segment is $d = \dfrac{r}{D}$, where

$$r = x_i(y_1 - y_k) + y_i(x_k - x_1) + y_k x_1 - y_1 x_k \tag{9}$$

and

$$D = \sqrt{(x_1 - x_k)^2 + (y_1 - y_k)^2} \tag{10}$$

Normalized maximum error, $\varepsilon = \dfrac{\max_i |d_i|}{D}$ was used to measure goodness of fit.

The line segment was split at the edge point which is farthest from the line joining the end points, if ε was above some given threshold. The result of line fitting is shown in figure 3.

(a)	(b)	(c)

Figure 3. Line fitting: (1) amplitude images; (b) Steger curvilinear structures, and (c) fitted center lines.

Stem Detection

In the last step, cotton plant stems were detected using Hough transform (Duda & Hart, 1972). The Hough transform uses a voting mechanism to identify strong linear

features in an image and is effective even in presence of large amount of noise (Jain et al., 1995). Figure 4 depicts cotton plant stems detected on three image samples.

<div align="center">(a)   (b)   (c)</div>
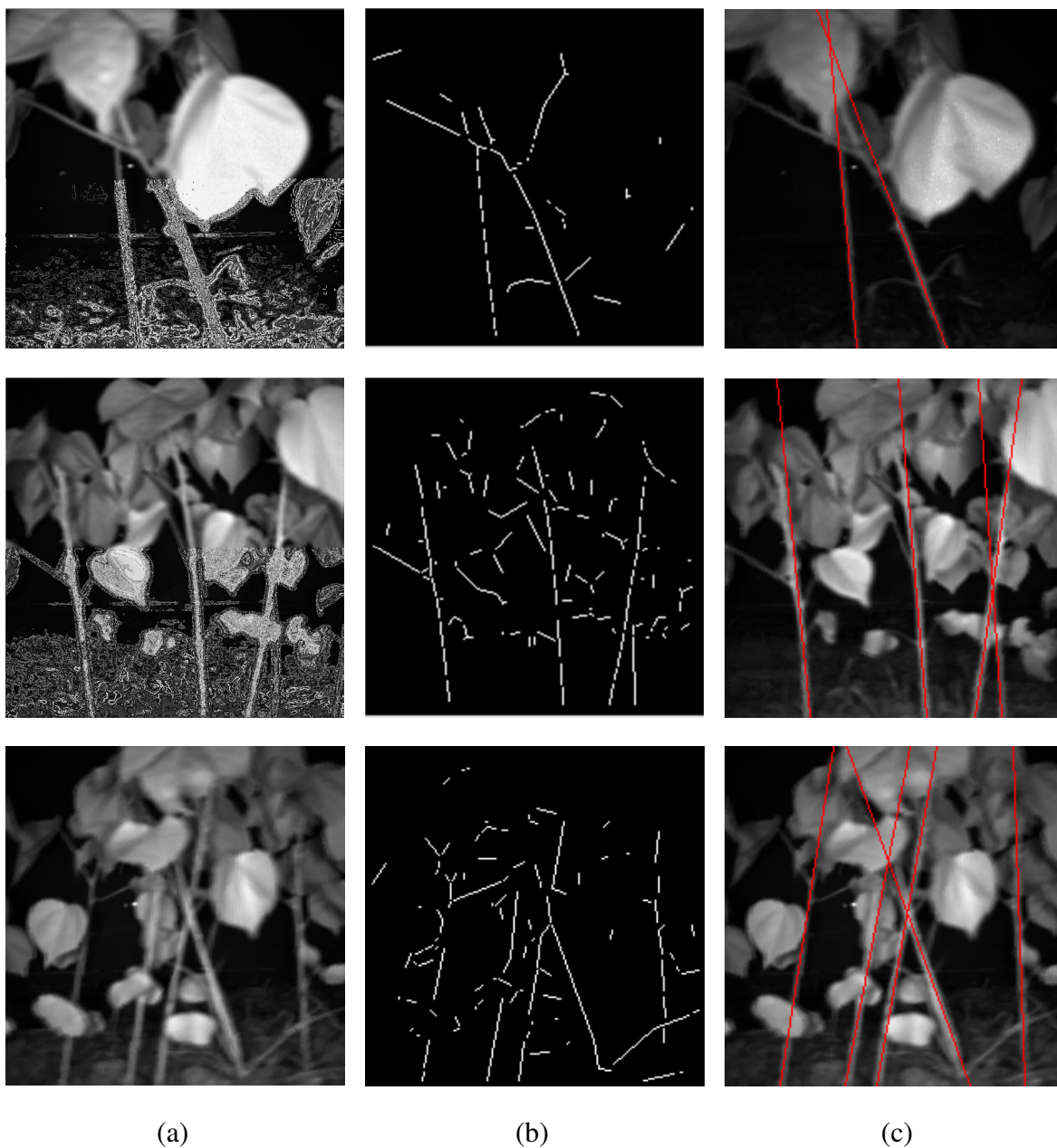
Figure 4. Stem detection: (a) amplitude images; (b) fitted center lines and (c) detected stems.

Each pixel in line fitted image contributes a vote to an element (r_n, θ_n) of an accumulator array of size r by θ entries where

$$r_n = \sqrt{x^2 + y^2} \tag{11}$$

$$\theta = \tan^{-1}\left(\frac{y}{x}\right) \tag{12}$$

The Hough parameters were chosen such that only lines which were within $\pm 15°$ where detected.

Experiments and Results

In a small-scale experiment conducted on a field data, the system detected 93 plants out of 100. The seven plants which went undetected were either too short, or largely occluded by leaves. Figure 5 shows examples of undetected plants. In the top row, the plant on the right was not detected as the stem profile was almost completely occluded by the leaves. In the bottom row, the plant on the left was too short for the system to identify it as a plant.
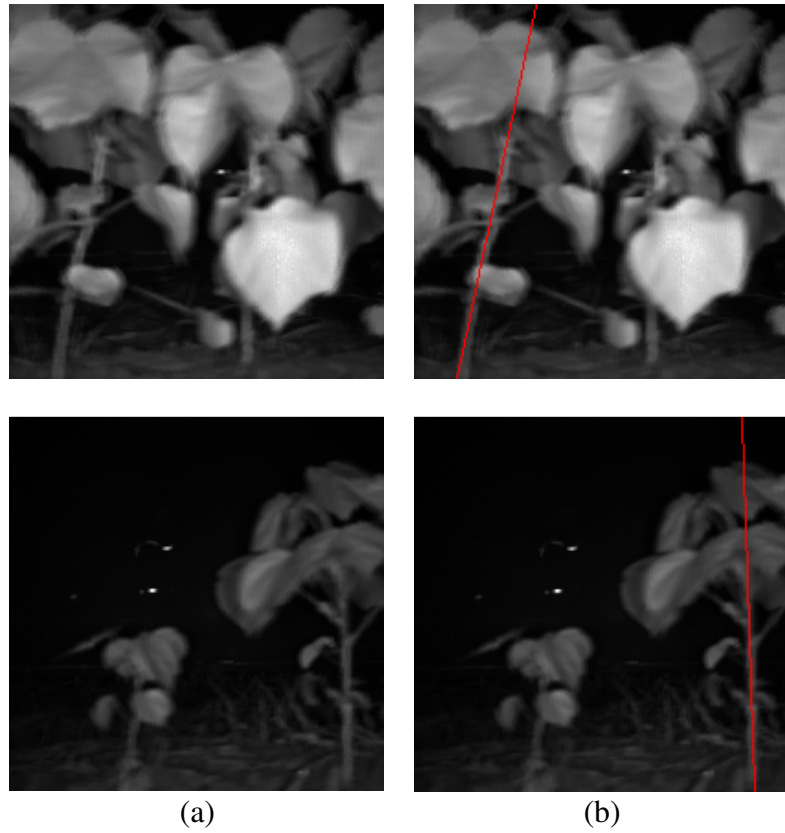
Figure 5. Undetected plants: (a) amplitude images, and (b) occluded and short plants were not detected.

There were two occurrences of false detections in situations where weeds with straight line profile were growing close to the cotton plants. Figure 6 depicts situations where the system detected weeds with straight line profile as cotton plants. The thick blue lines represent false detections.
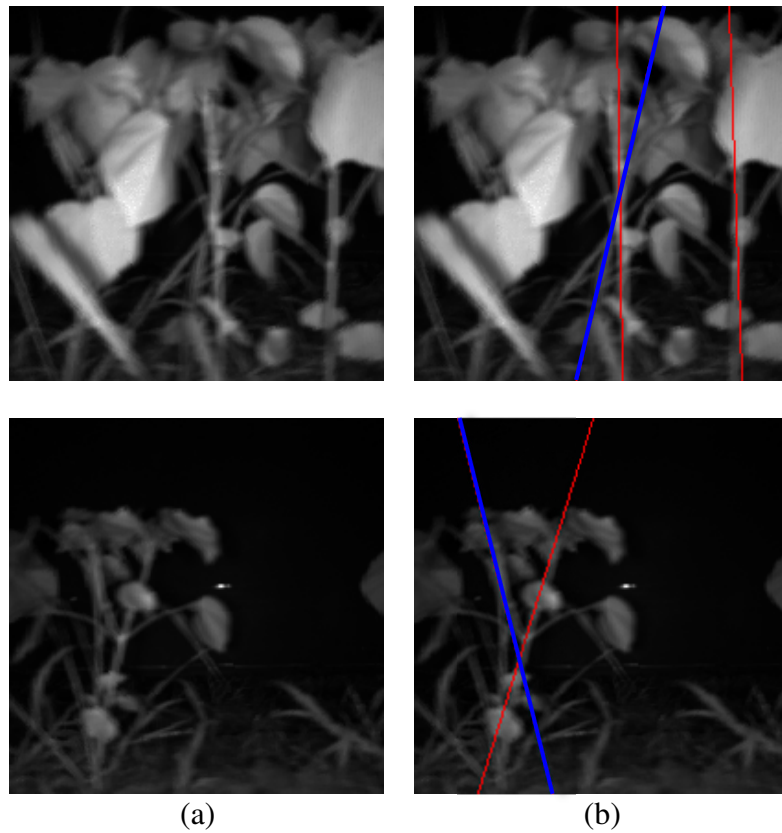
Figure 6. False detections: (a) amplitude images, and (b) weeds caused false detections.

Conclusions

In this paper, image processing algorithms for stem detection for cotton plants were developed using images acquired from light based time-of-flight camera. The system was able to detect 93 plants out of 100 plants, and there were two occurrences of false detection. The system can be used for plant population measurement and with appropriate image mosaicking technique it can also be used for within-row inter-plant spacing measurement.

References

Duda, R.O. & Hart, P.E., 1972. Use of Hough transformation tondetect lines and curves in pictures. Communications of the ACM 15, 11-15.

Frangi, A.F., Niessen, W.J., Vincken, K.L. & Viergever, M.A., 1998. Multiscale vessel enhancement filtering. Medical Image Computing and Computer-Assisted Intervention - Miccai'98 1496, 130-137.

Jain, R., Kasturi, R. & Schunck, B., 1995. Machine vision. McGraw-Hill, Sydney.

Jin, J. & Tang, L., 2009. Corn plant spacing sensing using real-time stereo vision. Journal of Field Robotics 26, 591-608.

McCarthy, C.L., Hancock, N.H. & Raine, S.R., 2009. Automated internode length measurement of cotton plants under field conditions ASABE 52, 2093-2103.

Nakarmi, A.D. & Tang, L., 2012. Automatic inter-plant spacing sensing at early growth stages using a 3D vision sensor. Computers and Electronics in Agriculture 82, 23-31.

Sato, Y., Nakajima, S., Atsumi, H., Koller, T., Gerig, G., Yoshida, S. & Kikinis, R., 1997. 3D multi-scale line filter for segmentation and visualization of curvilinear structures in medical images. Cvrmed-Mrcas'97: First Joint Conference - Computer Vision, Virtual Reality and Robotics in Medicine and Medical Robotics and Computer-Assisted Surgery 1205, 213-222.

Shrestha, D.S. & Steward, B.L., 2003. Automatic corn plant population measurement using machine vision. Transactions of the Asae 46, 559-565.

Steger, C., 1998. An unbiased detector of curvilinear structures. Ieee Transactions on Pattern Analysis and Machine Intelligence 20, 113-125.

Sudduth, K. A., S. J. Birrell, & M. J. Krumpelman. 2000. Field evaluation of a corn population. In Proc. 5th International Conference on Precision Agriculture, CD–ROM. T. C. Robert, R. H. Rust, and W. E. Larson, eds. Madison, Wisc.: ASA, CSSA, and SSSA.

Tang, L. & Tian, L.F., 2008a. Real-time crop row image reconstruction for automatic emerged corn plant spacing measurement. Transactions of the Asabe 51, 1079-1087.

Tang, L. & Tian, L.F., 2008b. Plant identification in mosaicked crop row images for automatic emerged corn plant spacing measurement. Transactions of the ASABE 51, 2181-2191.

CHAPTER 5

TRACKING LAYING HENS USING A 3D VISION SENSOR AND RADIO
FREQUENCY IDENTIFICATION TECHNOLOGY

A manuscript written to be submitted to Computer and Electronics in Agriculture

A. D. Nakarmi[1], L. Tang[1,2], H. Xin[1]

Abstract

Space needs for laying hens without affecting their natural behaviors is one of the most debatable topics among egg producers and advocates of animal welfare. Quantification of stocking density effect on natural behaviors of laying hens is hence deemed vital. Offline video analysis is one of the most common approaches used to track and register laying hen behaviors. However, such manual video analysis techniques are labor and time intensive. Needless to say, the number of target objects that can be tracked simultaneously is limited to a small number. In this paper, we propose a novel method for tracking of multiple laying hens using a sensor fusion approach. Image processing techniques were employed on top view images captured by a state-of-the-art time-of-flight (TOF) of light based 3D vision sensor for identification as well as tracking of individual hens housed in a 1.2 m by 1.2 m pen. A Radio Frequency Identification (RFID) sensor grid consisting of 20 antennas installed underneath the pen was used as a recovery system in situations where the imaging system failed to maintain identities of some hens. Each hen was uniquely tagged with a passive RFID transponder which was

[1] Department of Agricultural and Biosystems Engineering, Iowa State University, Ames, IA 50011, USA
[2] Corresponding author. Phone: 515-294-9778; Fax: 515-294-6633; e-mail: lietang@iastate.edu

attached to the lower part of its leg.

Introduction

Visual monitoring of laying hen movements for behavioral analysis appears to be unsatisfactory for several reasons. First, presence of human observers may affect behavior and movement of laying hens. Second, during night time when lights are off, it is difficult to observe their movements. Third, it is time and labor intensive task to observe laying hens for a prolonged period of time. Video cameras can be used to avoid the effects of human presence on laying hen behaviors and movements. Similarly, infrared cameras can be used for low or no light conditions. The time consuming nature of human analysis of video recordings, however is still a problem. Therefore, a system that automatically tracks individual laying hens and extracts their behavior and movement data is valuable.

Monitoring laying hens is particularly difficult as their behaviors are flexible and their movements cannot be expected to follow regular paths. The behavior of laying hens consists of periods of walking, feeding, and drinking interspersed by resting and less frequent activities including wing flapping, dust bathing, perching, nesting and social interaction.

Tracking multiple laying hens for behavior monitoring is a challenging task with interesting features from computer vision perspective. Segmenting laying hens from the

background can be difficult as the litter on which the hens live can often be of similar intensity as that of their feathers. Laying hens tend to flock together, and because laying hens are not highly mobile animals, difficulty in separating individual hens can persist for prolonged time. Conversely, certain hens may make sudden and quick motor patterns, thereby creating discontinued trajectory, which can create difficulties in tracking as well.

Literature on classical multi-target tracking is based on the use of data-association after foreground detection in the image. Uchida et al. (2000) proposed a robust method for tracking many pedestrians by viewing from an upper oblique angle. They extracted individuals by background subtraction. When pedestrians overlapped each other, they tracked targets robustly based on their trajectories. However, poultry do not move for long time periods while remaining in contact and they alter trajectories randomly.

Computer vision has been applied to tracking animals. Sumpter et al. (1997) tracked a group of animal at high frame rate. Sergeant et al. (1998) developed a poultry tracking system in which a camera was placed above poultry. They detected poultry silhouettes based on color information and segmented the silhouettes of poultry by using the information on the contours of the silhouette. Fujii et al. (2009) used a computer vision technique based on particle filters to track multiple laying hens. However, their system was not able to track laying hens for prolonged period of time.

The objective of the study was to develop a tracking system capable of tracking individual laying hen housed in a group. As a part of a larger project the tracking system

can be used for automatic quantification of stocking density effect on certain laying hen

behaviors.

Materials and Methods

The laying hens tracking system consisted of hardware and software subsystems.

The hardware subsystem consisted of a mechanical framework of experimental pen,

electronic devices (imaging system, RFID components, and communication modules),

and a computer. The software subsystem consisted of data acquisition component and

offline data processing component. Figure 1 shows a schematic diagram of the tracking

system.
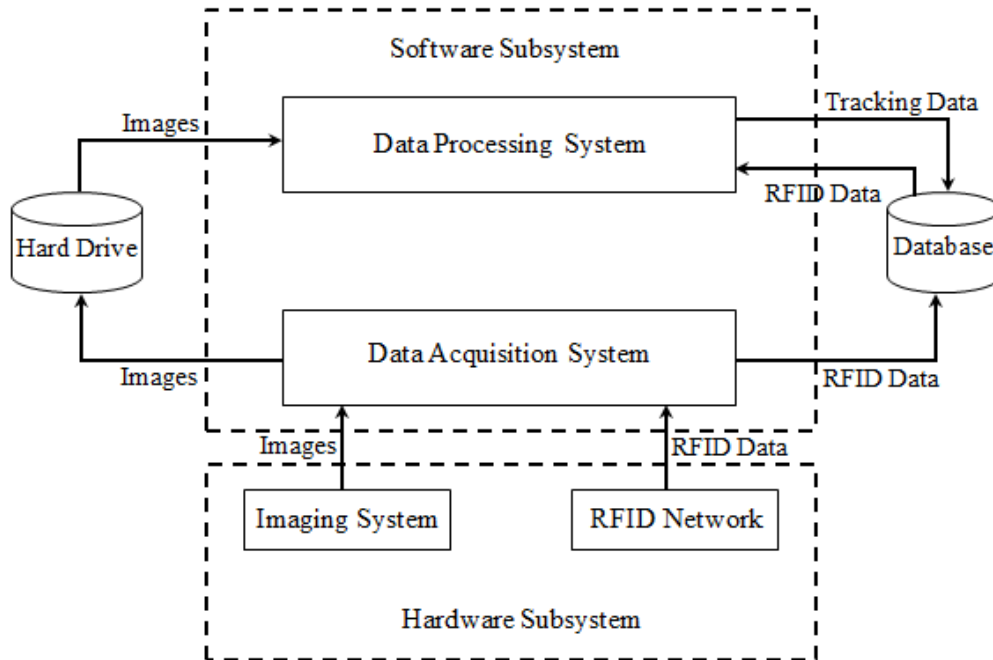
Figure 1. A schematic diagram of laying hens tracking system

Experimental Pen Design

A 1.2 m by 1.2 m pen was designed to house multiple laying hens (figure 2). A 61 cm long feeder was attached outside the north wall, and a water source was mounted on the south wall from inside. A 1.2 m by 0.31 cm long nestbox was placed just outside the east wall. Two entrances to the nestbox were at the north and the south side. The nestbox entrances were 15 cm above the floor. A perch was placed inside the pen 20 cm from the west wall and 25 cm above the floor. Saw dust was used as substrate material on the pen. Accumulated litter was cleaned every 2 weeks.

(a)   (b)
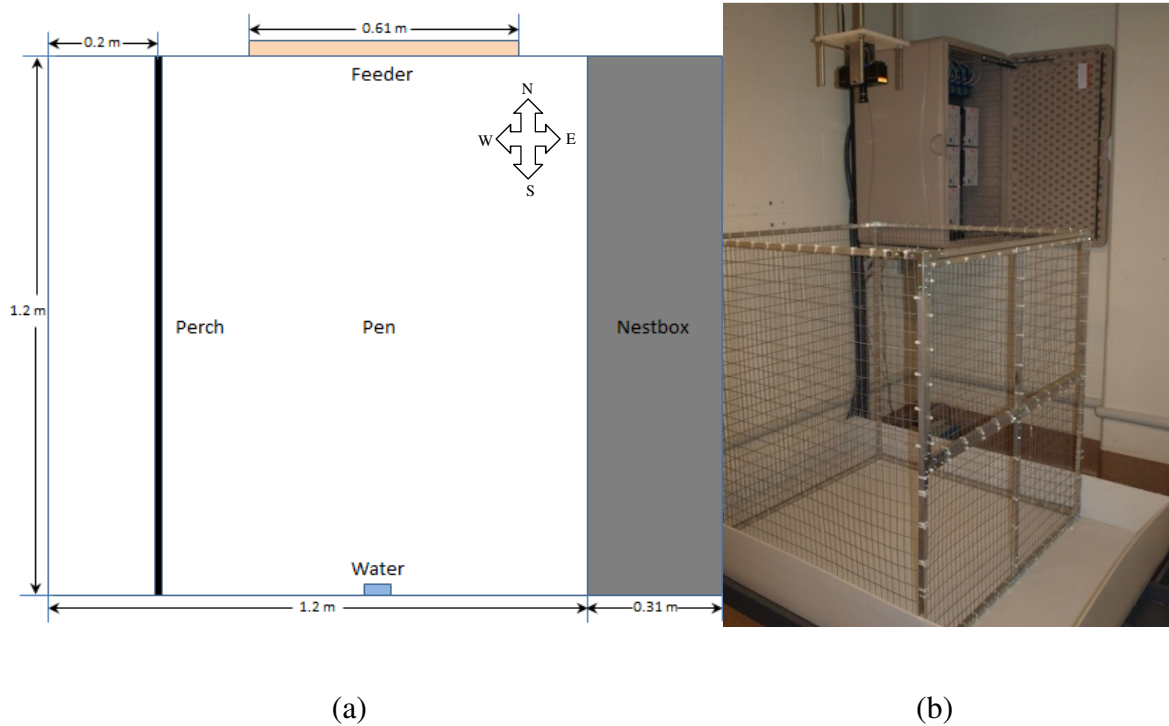
Figure 2. 1.2 m by 1.2 m pen: (a) layout of the pen with nest-box and perch, and (b) actual pen before adding nestbox and perch

RFID Antenna Network Design and Interfacing

A total of 20 antennas (RI-ANT-G02E-30, Texas Instruments, USA) were used to create an antenna grid with 18 antennas laid underneath the floor and other antennas were mounted beneath the entrances to the nest box. The 18 antennas on the floor were 30 cm apart from center to center. Due to close proximity of operation, antennas severely interfered with each other. Walls wrapped with aluminum foil were created around each antenna to reduce the interference. However, this reduced read range of the antenna significantly, from 28 cm to 9 cm, which resulted in dead regions between antennas where the antennas would not detect any tags. Figure 3 shows layout of 18 antennas installed on the floor. The inner circles represent the read range of the antennas during operation, and the dead regions are shown in black.

(a)   (b)
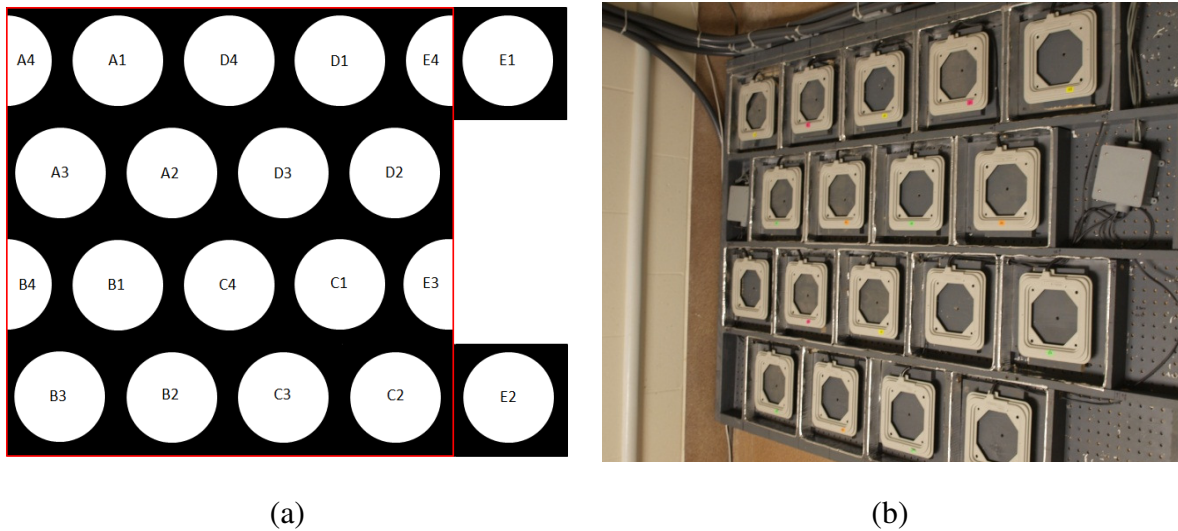
Figure 3. RFID antenna grid: (a) antenna layout with 5 clusters labeled A through E, and (b) 18 antennas installed on the floor

A 4-antenna cluster was created which was then connected to a RFID reader (RI-STU-251B, Texas Instruments, USA) via a 4-channel multiplexer (RI-MOD-TX8A, Texas Instruments, USA). Five such clusters were created. Figure 4 shows a layout of the cluster and interfacing of the cluster with other devices used in the RFID system. The communication protocol between the 4-channel multiplexers and the RFID readers was RS485. The readers were configured to work in Master/Slave synchronization scheme, with the first reader working as the Master and all others as the slaves. This configuration allowed the system to read all 20 antennas in less than half a second. With a 4-channel multiplexer 5 antennas, one from each cluster could be read simultaneously.
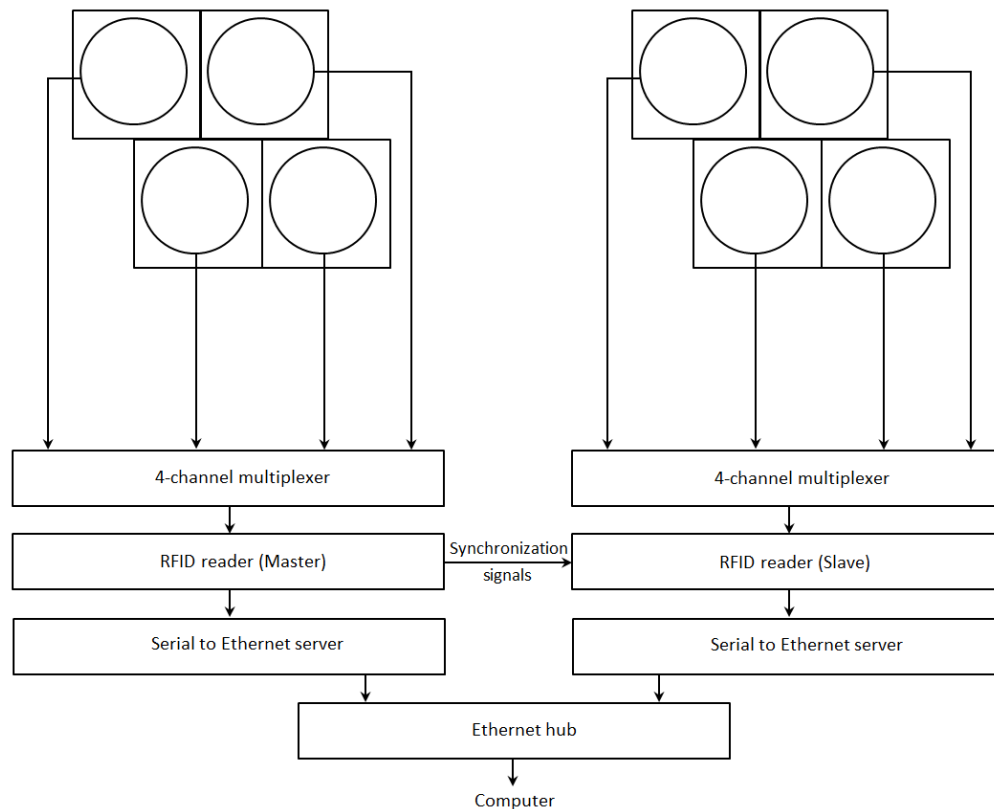
Figure 4. A schematic diagram of 4 antenna cluster with master/slave synchronization configuration between RFID readers

The RFID readers were connected to serial to Ethernet servers (VESR901, B&B Electronics, USA), and finally interfaced to the computer using an off-the-shelf Ethernet hub. Each serial to Ethernet server was assigned a unique IP address. The communication protocol between the RFID readers and the serial-to-Ethernet servers was RS485, while TCP/IP was the Ethernet protocol used for interfacing the RFID clusters with the computer. Figure 5 shows the instrumentation used in RFID network.
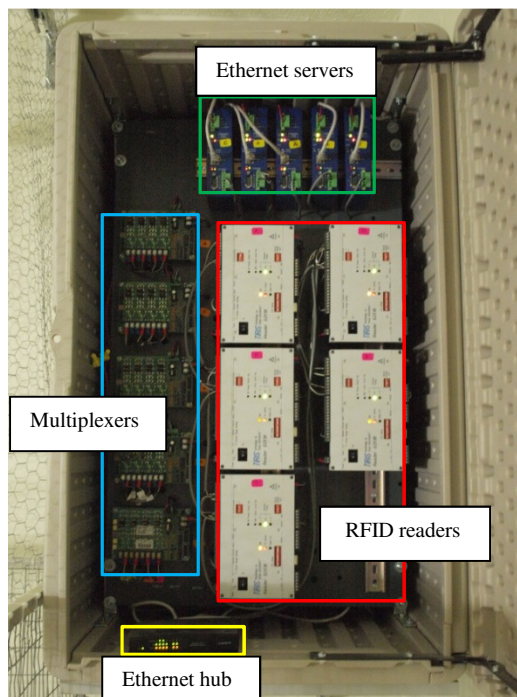
Figure 5. RFID system instrumentation

Imaging Device and Interfacing

A state-of-the-art 3D imaging sensor, CamCube3^{TM} (PMDTec, Germany), based on TOF (time of flight) of light principle was mounted ~1.85 m from the floor to cover

1.2 m by 1.2 m pen area. The imaging sensor was connected to the computer using USB2.0 communication protocol.

Software Development

As previously stated, the software subsystem consisted of two components: data acquisition and offline data processing. The data acquisition component consisted to two independently running threads, one for image acquisition and the other for RFID data acquisition.

Data Acquisition System

Multithreading programming technique allowed the data acquisition system to handle multiple tasks simultaneously, in order to ensure maximum data acquisition speed since multiple RFID antennas were required in this application. Multithreading programming with uniquely configured device IPs enabled the computer to scan data from RFID readers in different threads. The RFID readers kept transmitting RFID tag numbers to TCP/IP socket, and the computer did not have to poll each RFID reader, which essentially enabled the system to operate at a maximum sampling speed. The image acquisition thread acquired images at ~5 FPS. Each frame was sequentially numbered and stored in the user specified file path.

The RFID data acquisition thread was run first and manually ensured that all the devices were working correctly. The image acquisition thread was then run. The main program thread then created a record for each RFID tag that consisted *ImagePath*: user

specified path where the images were stored, *ImageNo*: frame number, *TagID*: RFID tag

number, *AntennaID*: RFID antenna that read the tag, and *TimeStamp*: time at which the

frame was captured. The records were stored into the *RFID* data table in the database.

Data Processing System

The offline data processing component primarily consisted of image processing

algorithms. The images were read from the user specified folder and were processed for

hen detection. For each frame corresponding RFID data was fetched from the RFID data

table in the database. The centroid of a detected hen was used to locate the closest RFID

antenna, which in turn was used to associate the hen with its corresponding RFID tag.

For each processed frame, the system created a tracking record that consisted

ImagePath, *ImageNo*, *HenID*: 1 through 5 for SD5, and 1 through 10 for SD10, *TagID*,

CentroidX: x-coordinate of hen pixel mass, *CentroidY*: y-cordinate of hen pixel mass,

MajorAxisLength: major axis of the ellipse fitted on the hen pixel mass,

MinorAxisLength: minor axis of the ellipse fitted on the hen pixel mass, *Heading*:

heading direction of the hen (0-359 degrees), and *TimeStamp*. The records were then

stored into the *Tracking* data table in the database.

Image Processing Algorithm Overview

The images were subjected to background subtraction method for foreground

detection. The foreground image was filtered using anisotropic diffusion filter which

essentially helped in enhancing object edges. The filtered image was then segmented

using modified watershed algorithm. Regions in close vicinity were merged to form laying hens on the first frame. In subsequent frames, overlapping of pixels between the previously identified hen regions and currently segmented watershed regions were used to detect laying hens. As the frames were captured at 5 FPS, between frames movements of the hens were limited therefore the algorithm sufficiently tracked the hens.

Noise Reduction

In order to alleviate over-segmentation caused by contaminated noises in watershed transform, usually a filter is employed that can effectively reduce noise and preserve important edge information. Although linear filtering can reduce noise in the image, it usually causes blurring and possibly fusing of important edges. Perona and Malik (1990) and Gilboa et al. (2001) reported that diffusion filters were more effective in smoothing noise while preserving necessary edge information. In this study, a diffusion filter (Gilboa et al., 2001) was adopted to reduce the noise effect (figure 6).

(a)   (b)
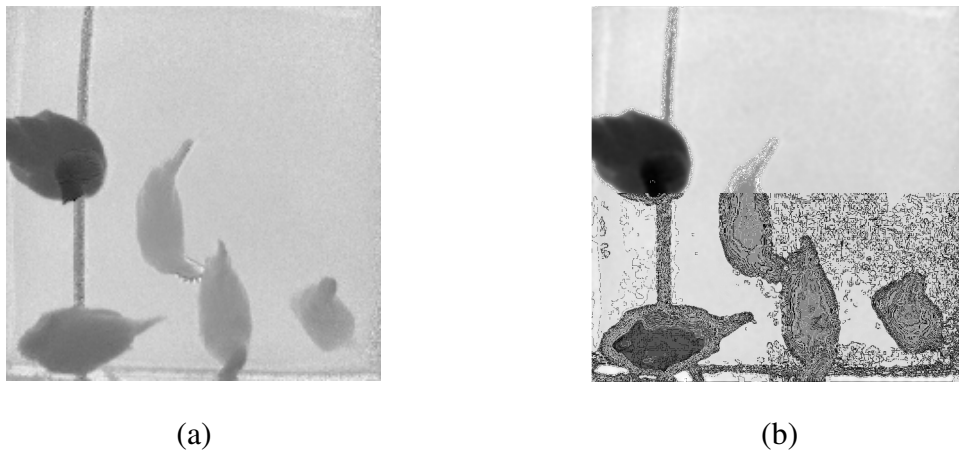
Figure 6. Noise reduction: (a) original distance image, and (b) image after application of anisotropic diffusion filter

Foreground Detection and Gradient Computation

A background subtraction technique was used to detect foreground objects. An image of the pen was taken without laying hens in it and it was subtracted from the image with hens to segment out foreground. A median filter was used to eliminate smaller regions from the foreground image. Foreground pixels were grouped to form connected components. In the first frame, area threshold was used to decide if a connected component contained one or multiple hens. For subsequent frames, its vicinity was scanned to see if there were other hens around that region in previous frame. Figure 7 depicts foreground objects detected after background subtraction.

(a)   (b)   (c)
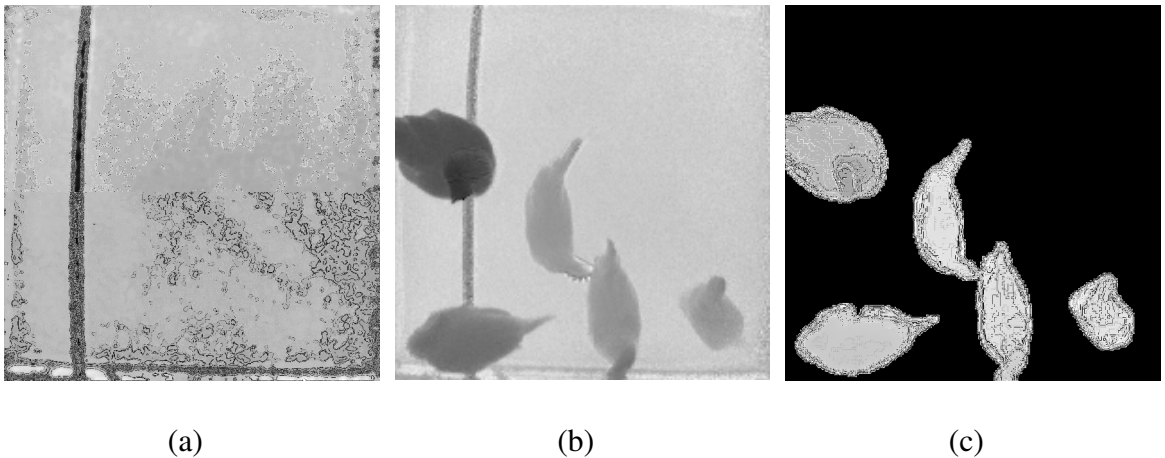
Figure 7. Foreground detection: (a) background image; (b) image with laying hens, and (c) detected foreground hens.

The components which were larger and could be formed from multiple hens were selected for further processing. In the next step, Sobel gradient operator was used to compute a gradient magnitude image. The operator used two 3×3 kernel which were convolved with the original image to calculate approximations of the derivatives, in

horizontal (equation 1) and vertical (equation 2) directions, respectively. The resulting

gradient approximations were then combined to compute the gradient magnitude

(equation 3). The gradient magnitude image was then used for watershed transformation.

Figure 8 shows gradient magnitude computed on selected foreground objects, which

were then subjected to watershed transformation.

$$G_x = \begin{bmatrix} 1 & 0 & -1 \\ 2 & 0 & -2 \\ 1 & 0 & -1 \end{bmatrix} * I \tag{1}$$

$$G_y = \begin{bmatrix} 1 & 2 & 1 \\ 0 & 0 & 0 \\ -1 & -2 & -1 \end{bmatrix} * I \tag{2}$$

$$G = \sqrt{G_x^2 + G_y^2} \tag{3}$$

where G_x and G_y are gradient approximations in horizontal and vertical directions,

respectively, I is the original image, and G is the gradient magnitude.

| (a) | (b) | (c) |
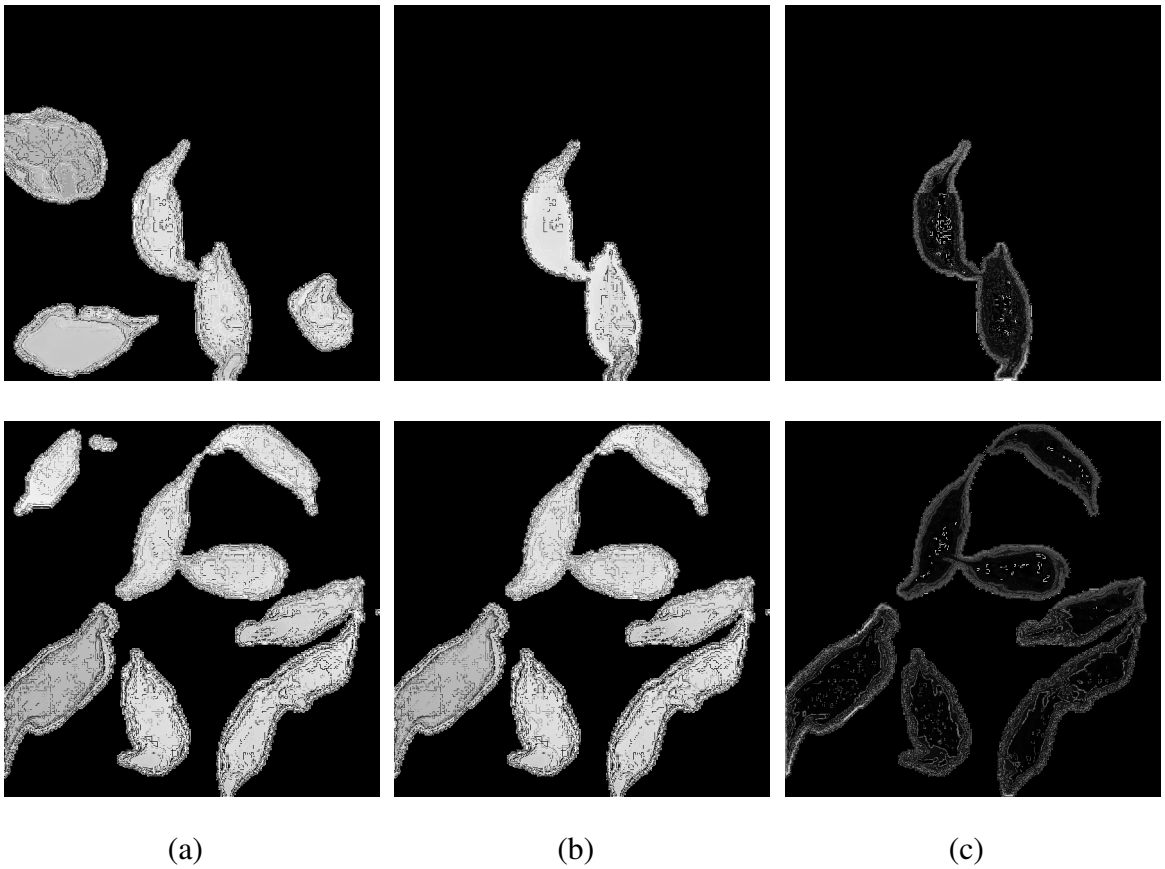
Figure 8. Gradient computation: (a) foreground objects; (b) objects selected for gradient computation based on size, and (c) gradient magnitude image. Top row for laying hens at SD5 and bottom rows for SD10.

Foreground Segmentation

When multiple hens flocked together, it was challenging to separate them before they could be tracked. Edge-based segmentation methods require strong edge information for good segmentation results, which was not always the case, when hens come in contact of each other, due to the texture of their feathers. The watershed transformation on the other hand works well in such situations, but is plagued with slower computation and over-segmentation problems.

A watershed transformation is an image operation based on mathematical morphology that is also regarded as the rain falling on a landscape with each drop dripping down the steepest path toward a body of water called catchment basin. Classic watershed algorithms are based on successive complete scannings of the image under processing. At each step, all the pixels are scanned one after another in a predetermined order, generally a progressive scan or an interlaced scan. These algorithms do not run in a fixed number of iterations, and this number is often very large. The fast watershed algorithm proposed by Vincent and Soille (1991), on the other hand, is designed such that it does not require scanning the entire image at every iteration. Rather, it allows random access to the pixels of an image and direct access to the neighbors of a given pixel, thereby significantly increasing the efficiency. The fast watershed algorithm is summarized below.

Employing the previously described analogy, when a water drop flows down along a relief, it will flow into the region minimum. Vincent and Soille (1991) watershed segmentation method is based on immersion simulations; starting from the lowest altitude, the water will progressively fill the different catchment basins of the image. There are two steps involved in the immersion algorithm: sorting and flooding. In the sorting step, the image pixels are sorted in ascending order according to their grayscale values, which enables a direct access to the pixels at a certain gray level. The minimum and maximum grayscale values, h_{min} and h_{max}, respectively, are also computed. In the flooding step, the algorithm progressively floods the catchment basins of the image. The algorithm is composed of fast computation of geodesic influence zones and breadth-first

scanning of all pixels in the order of altitude (their grayscale values), thereby assigning a

distinct label to each minimum and its associated catchment basin. This process is

implemented level-by-level using a FIFO (first-in-first-out) queue of pixels. The output

is an image demarcated by the label of the catchment basins. A dam is built to prevent

the basins from merging when two floods originating from different catchment basins

meet.

Let $I : D_I \rightarrow \mathbb{N}$ be a grayscale image, with $h_{\min}$ and $h_{\max}$ the minimum and

maximum gray levels, respectively. Starting at the gray level $h = h_{\min}$, the catchment

basins with the minima of I are successively expanded up until $h = h_{\max}$. Let X_h denote

the union of the set of catchment basins computed at level h. A connected component of

the threshold set T_{h+1} at level $h + 1$ can either be a new minimum, or an extension of a

catchment basin in X_h: in the latter case geodesic influence zone of X_h within T_{h+1},

$IZ_{T_{h+1}}$, is computed, resulting in an update X_{h+1}. Let MIN_h denote the union of all

regional minima at altitude h. The recursive algorithm explained above is defined in

equation 4 and 5.

$$X_{h_{\min}} = \{ p \in D_I \mid I(p) = h_{\min} \} = T_{h_{\min}} \tag{4}$$

$$X_{h+1} = MIN_{h+1} \bigcup IZ_{T_{h+1}}(X_h), \quad h \in [h_{\min}, h_{\max}) \tag{5}$$

The watershed transform of I, $W(I)$, is the complement of $X_{h_{\max}}$ in D_I, i.e., the set

of points of D_I which do not belong to any catchment basin, and is given by equation 6.

$$W(I) = D_I \setminus X_{h_{\max}} \qquad\qquad (6)$$

According to recursive equations 1 and 2, it is the case that at level $h + 1$ all non-basin pixels (i.e., all pixels in T_{h+1} except those in X_h) are potential candidates to get assigned to a catchment basin in step $h + 1$. Therefore, it allows the pixels with gray level $h' \leq h$ which are not yet part of a basin after processing level h, are merged with some basin at the higher level $h + 1$.

(a)   (b)
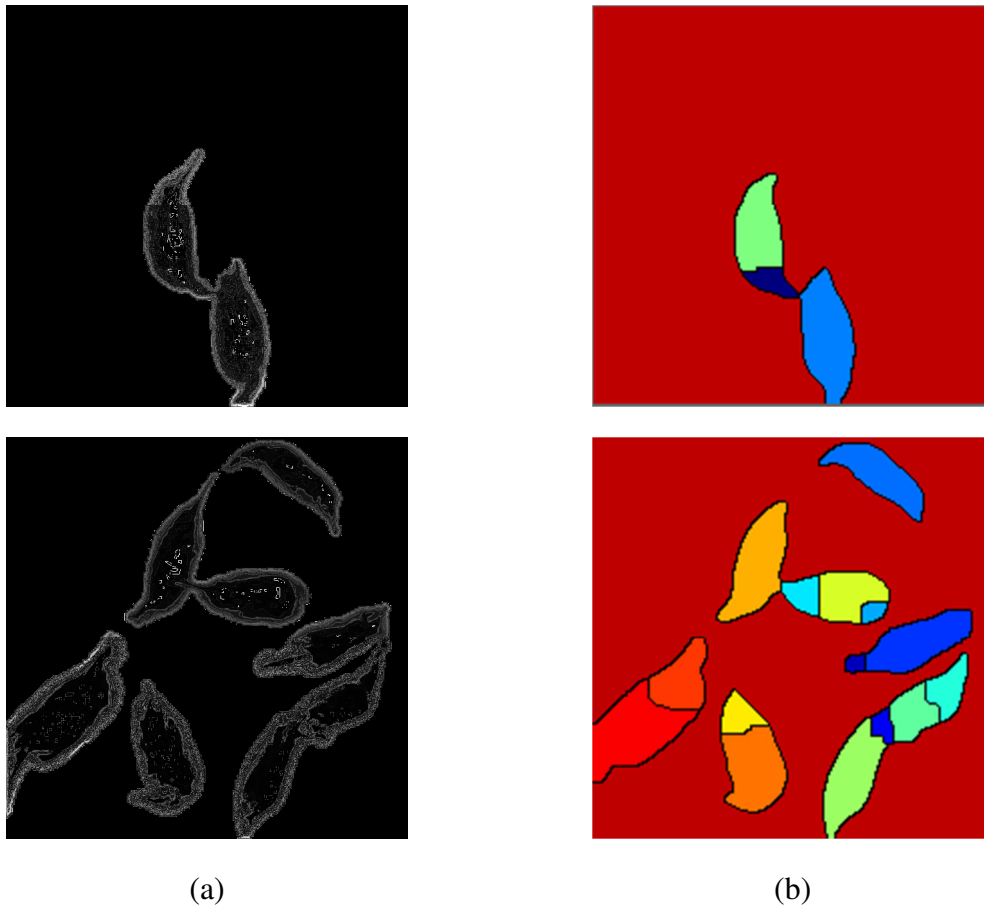
Figure 9. Segmentation using watershed transformation: (a) gradient magnitude image, and (b) image after watershed transformation with black watershed lines and catchment basins in color. Top row for laying hens at SD5 and bottom row for SD10.

Pixels which, in a given iteration, are equidistant to at least two nearest basins may provisionally be labeled as "watershed" pixels. However, in the next iteration this label may change again. A definitive labeling of a pixel as "watershed" pixel can only happen after all levels have been processed. Figure 9 shows watershed transformation results with watershed lines in black and catchment basins in color. Fast watershed segmented algorithm, however still suffers from over-segmentation problem. Therefore, the segmented watershed partitions need to be merged to form individual hen regions.

Vision-based Tracking

After watershed transformation of the foreground image, on the very first frame, the regions in close vicinity were merged to form laying hen regions. Large partitions were considered as probable hen regions and merging of such partitions were avoided. Area and orientation information along with mean height were used during the process. In subsequent images, overlapping between the previously identified hen regions and watershed regions were used to merge regions and form individual hens. As the images were acquired at ~5 FPS, the relative movements of the hens between consecutive frames were limited, and the algorithm, in most cases, was able to track individual hens. When the hens made sudden quick movements, it was difficult to associate watershed regions to previously identified hens. In such situations, information from RFID antenna network was used to recover the identities of lost birds. RFID network was also used in recovering hen identities when multiple hens were in next-box and one more exited the

nest-box. The vision system was unable to maintain hen identities in such situations. The system would then maintain a separate list to restore information of the hens without identities. As soon as the RFID system picked up their tags and their identities were recovered, the corresponding information saved in the list was merged to the main list that stored the tracking information. Figure 10 shows hens detected and identified in groups of 5 and 10, respectively. Figure 11 shows laying hens identified in different frames in groups of 5 and 10, respectively.

(a)   (b)
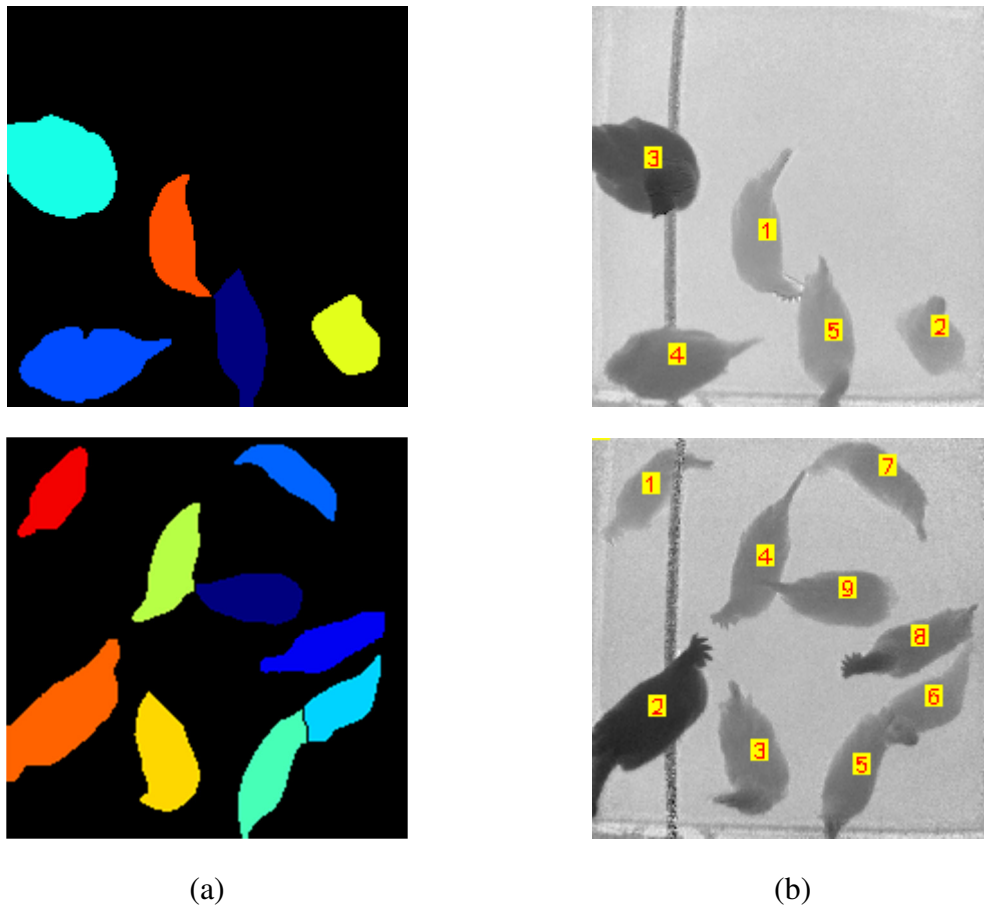
Figure 10. Hen detection and identification: (a) segmented hens, and (b) hens labeled for tracking. Top row for hens at SD5 and bottom row for SD10.
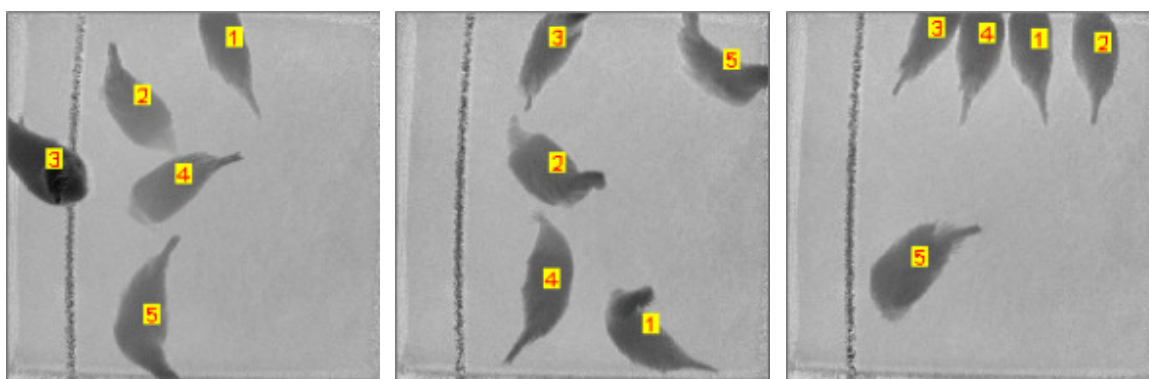
(a)
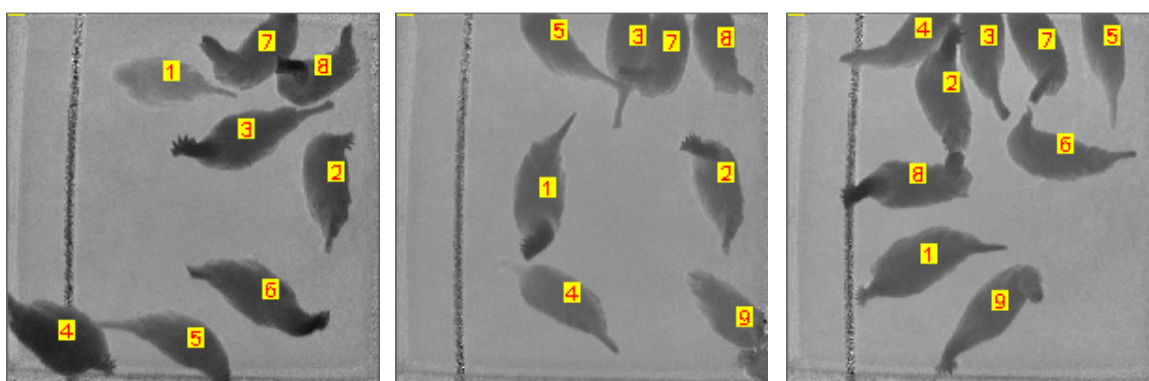
(b)

Figure 11. Laying hen identification at different times: (a) from left to right, five hens identified in frames numbers 0, 1000, and 4000, respectively, and (b) from left to right, ten hens identified in frames numbers, 0, 500, and 1000, respectively.

Hen Identity Recovery using RFID Antenna Network

A passive RFID glass transponder (RI-TRP-WEHP-30, Texas Instruments, USA) with a unique number was taped around the lower part of the hen's leg. When the hen stands within the read range of an antenna, the tag number is read and its approximate position is known based on the location of the antenna that reads the tag. The RFID antenna network therefore was helpful in locating the hens in situations when the visual tracking failed to correctly track them. The RFID antenna network was also used to track

hens moving in and out of the nestbox. When multiple hens were in the nestbox and one of them appeared in the camera view, it was not possible to maintain the identity if the hen, until its tag was read by one of the antennas.

Experiments and Results

Figure 12 shows the error distribution between the manually located centroids and those generated automatically, where in total 600 images from each stocking densities were used for the comparison. Frames where the software detected more than 5 cm travel was used, which accounted for 95 centroids in case of 5 hens and 176 centroids in case of 10 hens, respectively. From this distribution, 95% of the centroids lie within 4 pixels, i.e., less than 4 cm, of the manually selected centroids. It was also noted that the manual selection of centroids were expected to exhibit an error of ± 3 pixels.

Figure 13 and Figure 14 depict the comparison of manually extracted trajectories and software generated trajectories for laying hens housed in groups of 5 and 10, respectively. In case of 10 hens, one of the hens was in nest-box through out the image sequence. The filled circles represent the positions of the laying hens at the first frames, while the filled diamonds represents the positions at the last frames. It can be seen in these figures that the manual and the software generated trajectories are essentially the same.
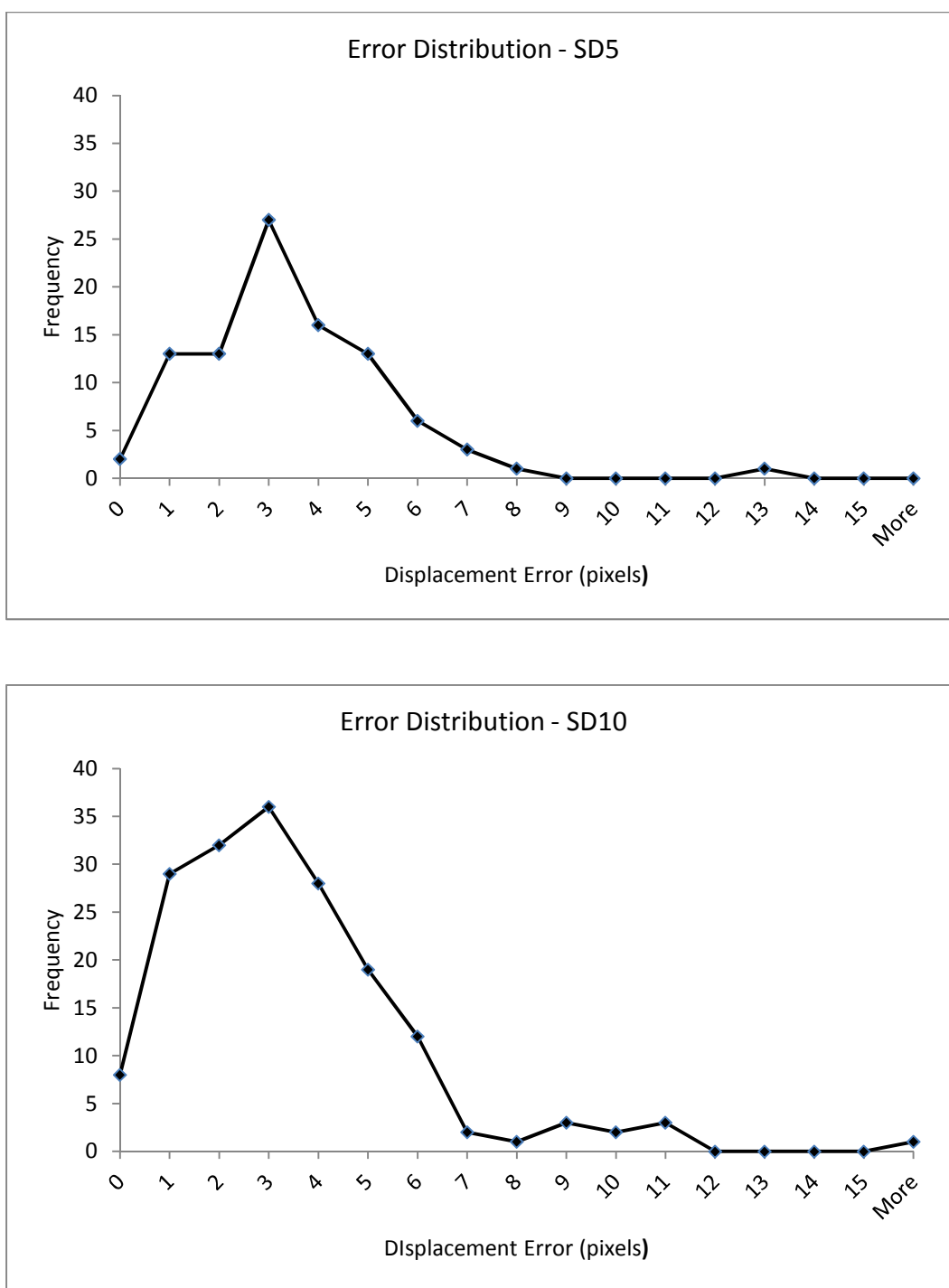
**Figure 12.** Error distribution between manually extracted and software detected centroids.
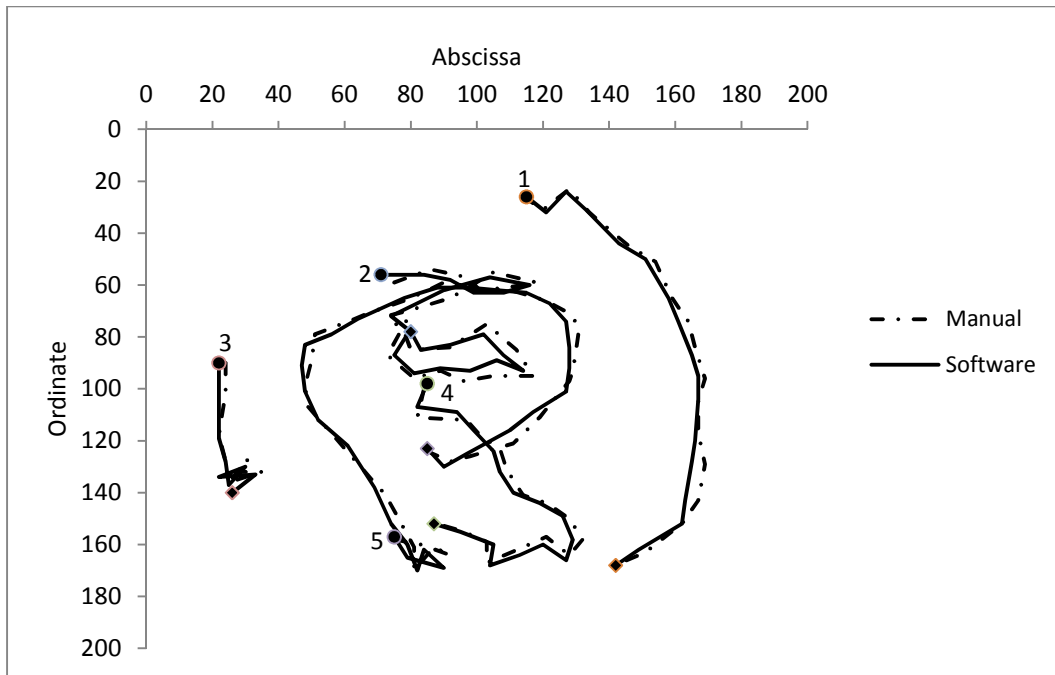
Figure 13. Trajectories of laying hens at SD5.
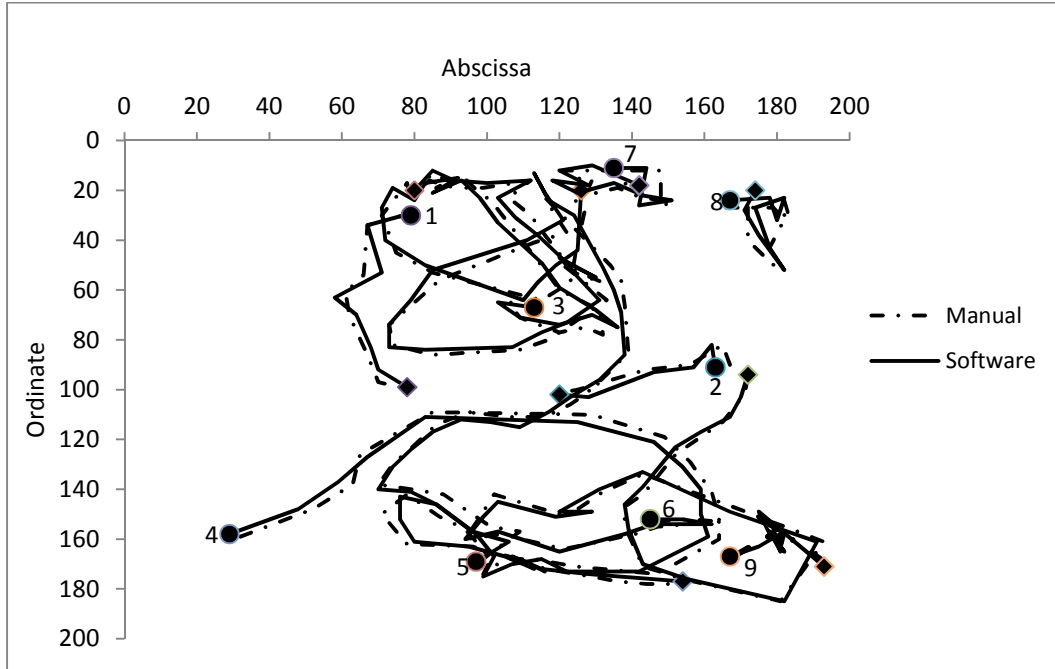
**Figure 14.** Trajectories of laying hens at SD10.

The visual tracking of the laying hens appeared to work simply using frame to frame correspondence based on overlapping of pixels between consecutive frames given that the hens were correctly identified in the first frame. There were situations where visual tracking was unable to maintain the identities of the hens. One such case is shown in Figure 15, where one of the hens in the nest-box exited and appeared on the main floor.

(a)   (b)

(c)   (d)
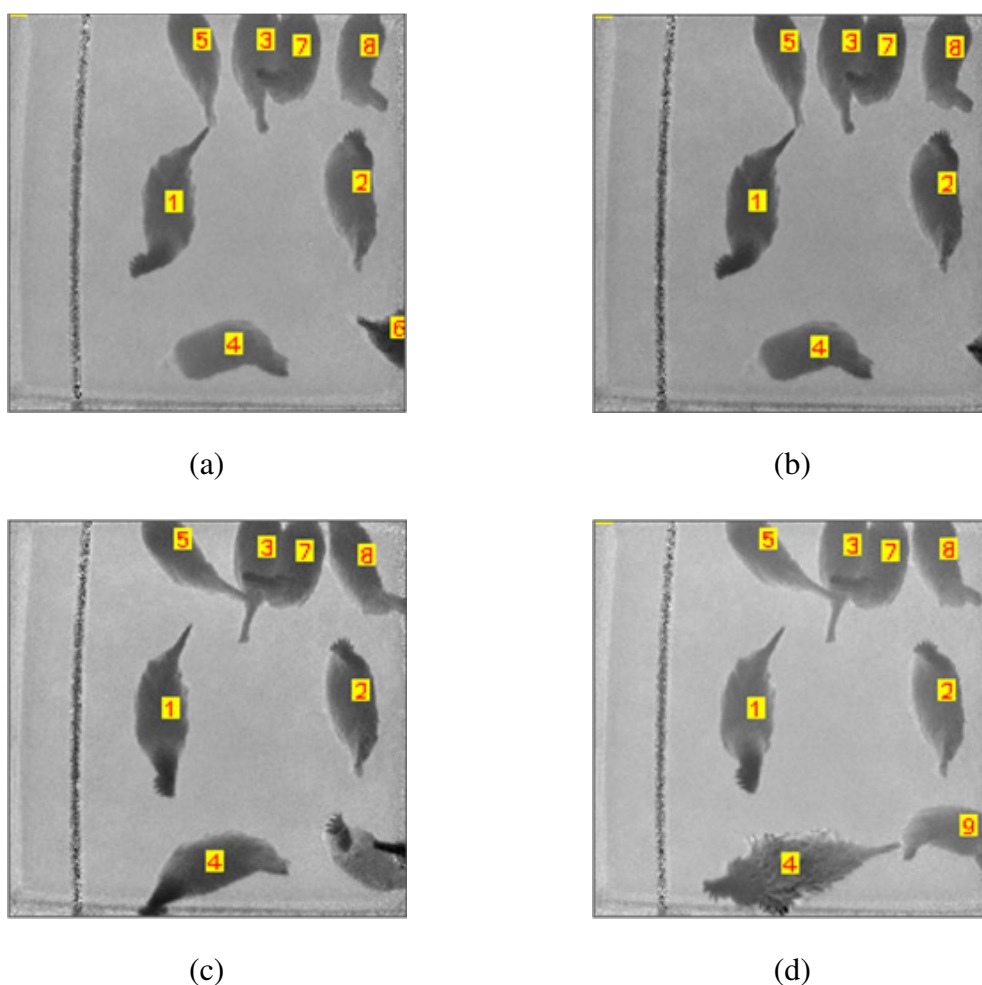
Figure 15. Recovering hen identity when one of the hens in nest-box exited: (a) in frame 401 hen 6 was enter the next-box; (b) in frame 402 hen 6 entered the nest-box; (c) in frame 475 one of the hens in the next-box exited, and (d) in frame 484 the hen that exited the nest-box was identified as hen 9

In this particular scenario, the visual tracking system did not know which hens among those in the nest-box exited while it still kept track of the hen but without identifying which hen it was. Once the RFID system detected the tag attached to the hen, the system then maintained its identity. The tracking data associated with hen, between the frame it lost its identity and the frame when RFID system recovered its identity, was temporarily stored in a separate table in the database. Once its identity was recovered, this data was then moved into the main data table where the tracking data of hens were correctly associated with their identities.

In another case, when certain hens made sudden quick movements, the visual system failed to keep track of the hens bu simply using frame to frame correspondence based on overlapped pixels. In one particular scenario shown in figure 16, hen 6

(a)   (b)
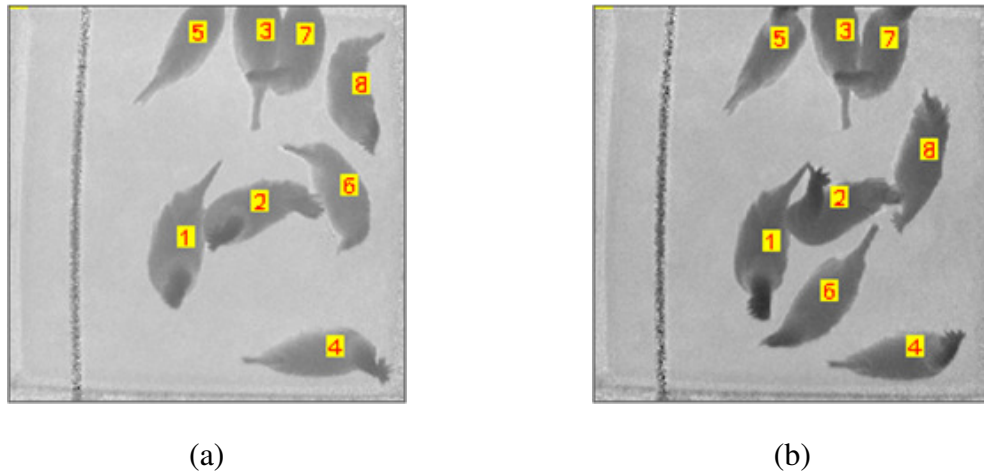
Figure 16. Maintaining hen identification when it made a sudden quick movement: (a) frame 651 before hen 6 made a sudden movement, and (b) in frame 652, hen 8 appeared at hen 6's location in frame 651. Identities of the two hens were maintained with the help of RFID network

appeared to make sudden quick movement between two consecutive frames and when frame to frame correspondence was used hen 8 was misidentified as hen 6. In this case as well, the RFID system was used to recover the identities of the hens as it was able to read the tags attached to the hens at their correct positions.

Conclusions

As a part of a larger project aimed at automatic quantification laying hen behaviors for the purpose of stocking density effect, we developed a sensor fusion approach to track laying hens housed in groups of 5 and 10. Due to the varying nature of appearance related to their posture and their social behavior of performing activities in groups, detecting individual laying hens housed in groups was a difficult task. The image processing techniques developed based on the depth images however was able to satisfactorily detect and identify individual hens with the occasional help from the developed RFID system, when necessary. The developed tracking system can be used in extracting behaviors of laying hens, and thereby is useful for automatic quantification of stocking density effects on certain behaviors such as locomotion, feeding, drinking and nesting.

Acknowledgements

References

Fujii, T., Yokoi, H., Tada, T., Suzuki, K., Tsukamoto, K., & Ieee. (2009). Poultry Tracking System with Camera Using Particle Filters. *2008 Ieee International Conference on Robotics and Biomimetics, Vols 1-4*, 1888-1893.

Gilboa, G., Zeevi, Y.Y., Sochen, N.A., 2001. Complex diffusion processes for image filtering. Scale-Space and Morphology in Computer Vision, Proceedings 2106, 299-307.

Perona, P., Malik, J., 1990. Scale-space and edge detection using anisotropic diffusion. IEEE Transactions on Pattern Analysis and Machine Intelligence 12, 629-639.

Sergeant, D., Boyle, R., Forbes, M., 1998. Computer visual tracking of poultry. Computers and Electronics in Agriculture 21, 1-18.

Sumpter, N., Boyle, R.D., Tillett, R., 1997. Modelling collective animal behaviour using extended point-distribution models, University of Leeds, School of Computer Studies.

Uchida, K., Miura, J., Shirai, Y., 2000. Tracking multiple pedestrians in crowd, Proc. Workshop of Machine Vision and its Applications, Tokyo, Japan, pp. 533-536.

Vincent, L., Soille, P., 1991. Watersheds in digital spaces: an efficient algorithm based on immersion simulations. IEEE Transactions on Pattern Analysis and Machine Intelligence 13, 583-598.

CHAPTER 6

AUTOMATIC QUANTIFICATION OF LAYING-HEN BEHAVIORS USING A 3D
VISION SENSOR AND RADIO FREQUENCY IDENTIFICATION TECHNOLOGY

A. D. Nakarmi[1], L. Tang[1], H. Xin[1,2]

Abstract

Stocking density of laying hens in egg production remains an area of investigation from the standpoints of ensuring hen's ability to perform natural behaviors and production economic efficiency. It is therefore of socio-economic importance to quantify the effect of stocking density on laying hens behaviors and thus wellbeing. Video recording and manual video analysis is the most common approach used to track and register laying hen behaviors. However, such manual video analyses are resource intensive and are prone to human error. The number of target objects that can be tracked simultaneously is also limited to a small number. In this study, we explore a novel method for automatic quantification of certain behaviors of individual laying hens in a group-housed setting (1.2 m × 1.2 m pen), such as locomotion, perching, feeding, drinking and nesting. Image processing techniques are employed on top-view images captured with a state-of-the-art time-of-flight (ToF) of light based 3D vision camera for identification as well as tracking of individual birds in the group with a passive Radio Frequency Identification (RFID) system. Each hen is tagged with a unique RFID

[1]. Department of Agricultural and Biosystems Engineering, Iowa State University, Ames, IA 50011, USA
[2]. Corresponding author. Phone: 515-294-4240; Fax: 515-294-4250; E-mail: hxin@iastate.edu

transponder attached to the lower part of her leg. A RFID sensor grid consisting of 20 antennas installed underneath the pen floor is used as a recovery system in situations where the imaging system fails to maintain identities of the birds. Spatial as well as temporal data are used to extract the afore-mentioned behaviors of each bird. To test the performance of the tracking system, we examined the effects of two stocking densities and perching space on bird behaviors, 2880 cm^2-hen^{-1} vs. 1440 cm^2-hen^{-1} and 24.4 cm vs. 12.2 cm per hen perch, corresponding to five hens vs. ten hens in the 1.2 m × 1.2 m pen, respectively. The system is able to discern the impact of the physical environment (space allocation) on behaviors of the birds. Of particular interest is that the two stocking densities tested did not affect the characteristics of hen's movement.

Keywords: Laying hen, Stocking density, Behavior monitoring, 3D vision, RFID

Introduction

Spatial requirement for laying hens and its impact on their welfare remains one of the most debatable topics among egg producers and advocates of animal welfare. With the 2012 European Union ban on conventional cages for laying hens and recent developments in the U.S., non-cage or alternative housing systems are likely to become more predominant (Zimmerman et al., 2006). The United Egg Producers (UEP) and consumer food chain McDonald's put forward welfare guidelines in 2000. The UEP guidelines recommended that cage floor space be increased over a five-year period ending in 2008 from the U.S. industry standard of 348 cm^2-hen^{-1} to a range of 432 to 555

cm^2-hen^{-1} (UEP, 2000). While McDonald's Recommended Welfare Practices call for cage floor space of 465 cm^2-hen^{-1} (McDonald's, 2000). The European Union (EU) on the other hand, recommended cage floor space for conventional cages to be 550 cm^2-hen^{-1} until 2012 (Hy-Line, 2003). Without large-scale experiments, it is difficult to assert if increasing the cage floor space actually improves the welfare of laying hens. A broad range of different potential indicators of welfare needs to be considered before the effect of stocking density (SD) can be assessed.

Researchers have explored many possible indicators of welfare and methods of measurement. Behavior is one such important indicator of animal welfare. Xin and Ikeguchi (2001) developed a measurement system to quantify feeding behavior of individual poultry in order to study effects of biophysical factors such as light, ration, noise, and thermal variables. Gates and Xin (2001) developed and tested algorithms for determining individual feeding statistics and pecking behavior from time-series recordings of feed weight. Puma et al. (2001) developed an instrumentation system to study dynamic feeding and drinking behaviors of individual birds. Persyn et al. (2004) used the measurement system and computational algorithm developed by Xin and Ikeguchi (2001) to quantify feeding behaviors of pullets and laying hens with or without beak trimming. Cook et al. (2006) adapted and expanded the behavior measurement system and analytical algorithm developed by Persyn et al. (2004) to investigate stocking density effects on feeding behavior of group-housed laying hens. Liu et al. (2013)

developed an instrumentation system to study perching behaviors of group-housed laying hens.

Behavioral characteristics are usually evaluated using audio-visual tools by a human observer which is time and labor intensive, subjective to human judgment and only applicable for a limited observation period (Abrahamsson, 1996). Quantification of animal behavior, and hence animal welfare, in livestock using image processing brings along specific problems. Animal appearance varies according to their posture, which makes processing and interpretation of images difficult (Van der Stuyft, 1991). Researchers have used visual monitoring to study group behaviors of animals. Image processing techniques have been used to monitor the weight distribution in poultry flocks (De Wet et al., 2003; Chedad et al., 2003), spatial distribution of pigs (Shao et al., 1998; Hu and Xin, 2000), and trajectory of a flock of poultry (Vaughan et al, 2000). Monitoring behavior of an individual animal within a group requires tracking of the animal. This problem can be alleviated by constraining the animal of interest so that it is in a standard position with no other animals around. This has been applied on pigs to monitor the weight (Schofield et al., 1999) and back fat (Frost et al., 2004). Leroy et al. (2005) developed automatic computer vision technique to track individual laying hen and detect six different behavior phenotypes, namely standing, sitting, sitting, sleeping, grooming, scratching and pecking. The system study, however, was still conducted to monitor behaviors of individually caged hen. However, for freely moving animals such as laying hens in a cage, constraints are impractical. Sergeant et al. (1998) used an adaptive image segmentation technique to estimate the trajectory of a limited number of

broiler chickens in video images. The correspondences of animals between two subsequent images were determined using a set of simple heuristics. These techniques were further enhanced as model-based tracking, which allows for more robust and accurate shape tracking, including locations on the animal body which are not detectable through image features (Tillett et al., 1997).

The objective of the study was to develop an automatic tracking and behavior monitoring system of individual hens housed in groups. For experimental purpose, the hens were housed in groups of five or ten, where each hen was tracked, and her perching, nesting, feeding/drinking and movement behaviors were monitored.

Materials and Methods

Experimental equipment and setup

A 1.2 m by 1.2 m pen was designed to house multiple laying hens (figure 1). A 61 cm long feeder was attached outside the north wall, and a water source (two nipple drinkers) was mounted on the inside of the south wall. A 1.2 m by 0.31 m nestbox was placed just outside the east wall. Entrances (exits) to the nestbox were kept at the north and the south side. The nestbox entrances were 15 cm above the floor. A perch was placed inside the pen 20 cm from the west wall and 25 cm above the floor. Saw dust was used as bedding material of the pen floor. An identical pen was made to house hens before moving into the test pen for data collection. Fluorescent lighting at the intensity 10-12 lux in the open area and 1-2 lux in the next box was on at 06:00h and off at 22:00h, i.e., 16L:8D. Resource allowance for hens in the experiment is shown in table 1.
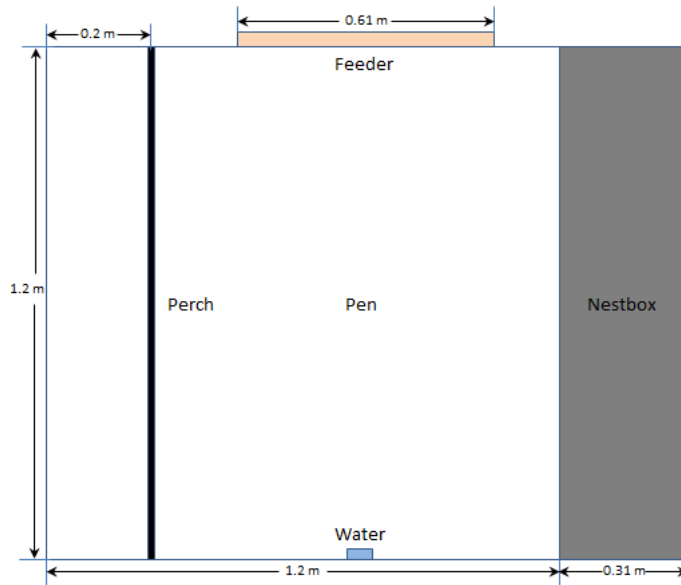
(a)   (b)

Figure 1. A schematic and photographical representation of the experimental pen

Table 1. Resource allowance for hens in the experimental pen compared to conventional cage, aviary, and enriched colony houses

Parameter	Experimental		Conventional	Aviary	Enriched
	SD5	SD10			
Wire mesh floor space (cm^2 hen^{-1})	-	-	568	633	643
Litter floor space (cm^2 hen^{-1})	2880	1400	-	505	-
Nest space (cm^2 hen^{-1})	743.2	371.6	-	86	58
Perch space (cm hen^{-1})	24.4	12.2	-	12.5	11.0
Feed trough space (cm hen^{-1})	12.2	6.1	10.2	10.2	12.0
Nipple drinker（hens drinker^{-1}）	2.5	5	6	8.9	7.5

Laying hens used in this study were 32 weeks old White Leghorns weighing approximately 1.4 kg at procurement. A total of 15 hens were housed in groups of five and ten, respectively, in two identical pens. First, five birds were housed in the test pen and ten birds were housed in the holding pen. After three days of data collection, five other birds from the holding pen were moved into the primary pen, and data were collected for three days with ten birds in the test pen as well. The hens were acclimatized for at least five days between data collection. The hens were fed twice a day at 09:00h and 17:00h. Eggs were collected once a day at 17:00h. The litter was cleaned every 2 weeks.

The images were captured for 18 hours per day, with ten hours of light time and eight hours of dark time. Images were not captured while feeding the hens and collecting eggs from the pen. It was observed that not all eggs were laid in the nest box and occurrence of egg eating was noticed. Therefore, it was necessary for eggs laid on the floor to be collected every day. The hens were then given enough time to settle down before the images were captured. During the capture of each frame, tags read by RFID sensor network were also recorded. The records were stored in the database and accessed later during image processing phase to determine hen locations and identities.

A total of 20 antennas (RI-ANT-G02E-30, Texas Instruments, USA) were used to create an antenna grid with 18 antennas laid underneath the pen floor and the remaining two antennas were mounted beneath the entrances to the nest box. The 18 antennas on the floor were 30 cm apart from each other. Five clusters of 4-antenna were created which were then connected to a RFID reader (RI-STU-251B, Texas Instruments,

USA) via a 4-channel multiplexer (RI-MOD-TX8A, Texas Instruments, USA). Figure 3(a) shows a layout of the clusters and their interfacing with other devices used in the RFID system. The readers were configured to work in Master/Slave synchronization scheme, with the first reader working as the Master and all others as the slaves. This configuration allowed the system to read all 20 antennas in less than 0.5 s. With the 4-channel multiplexers connected to each of the RFID reader, five antennas, one per cluster, could be read simultaneously. The read time per channel of the multiplexer was 0.1 s. The RFID readers were connected to serial to Ethernet servers (VESR901, B&B Electronics, USA), and finally interfaced to the computer using an off-the-shelf Ethernet hub.

A state-of-the-art 3D imaging sensor, Cambube3 (PMDTec, Germany), based on TOF (time of flight) of light principle was mounted above a 1.2 m by 1.2 m pen. The camera was used to capture distance images at ~5 FPS (frames per second). The system was developed in Microsoft Visual Studio 2010 using C#.Net as the primary programming language and Microsoft SQL Server 2008 as the backend database management system.

Overview of the algorithm

The acquired images were processed offline to detect individual birds in the pen. Each hen was tracked and its activity at each frame was extracted and stored in the database for further analysis. The development of the automatic algorithm for behavior extraction consisted of three steps as shown in figure 2. In the image pre-processing step,

the acquired images were treated with a diffusion filter (Gilboa et al., 2001) to reduce image noise while maintaining edge features. The filtered images were then subject to background subtraction to extract foreground objects. Gradient magnitudes of foreground images were then computed. In the second step, Watershed segmentation algorithm based on immersion was employed on gradient magnitude images to divide foreground images into partitions with similar heights. Size of the foreground object was used as the primary criterion to determine whether it was used for Watershed segmentation. Simple heuristics based on centroid, height similarity, orientation, size and major axis length were used to group close by partitions to form hen regions. In the next step, overlapping of the partitions in consecutive images was then utilized to track individual hens. In the last step, spatial information along with heading direction was used to determine hen activity in a given frame. In situations where the visual system was unable to keep track of the hens due to quick sudden movements of the hen, RFID sensor network was used to recover hen identities. For the RFID sensor network to recover the hen identities, the system should already have read the tags attached to the hens. Depending on initial hen locations with respect to RFID antennas, it would take several frames to several hundred frames before all the tags were read. If a hen was on perch, inside next box, or outside the reading range (10 cm radius from the center of the antenna) of its closest RFID antenna, it would not be detected. When more than one hen was inside the next box and one of them exited, the vision system could not determine its identity. The system then maintained a separate list of the unidentified hens. As the

unidentified hen moved along and RFID network read its tag, its identity was then

recovered, and the corresponding data were saved (Nakarmi et al., 2013).

     Centroid of each detected hen area was computed and compared with

corresponding centroids in subsequent frames to calculate hen movements. A list of

centroids was maintained for each hen. When the movement between the centroid in

hand and the last centroid in the list was larger than 5 cm, it was added to the centroid

list. The 5 cm threshold was used to filter out smaller movements, which were

considered to be noise due to erroneous centroid extraction.
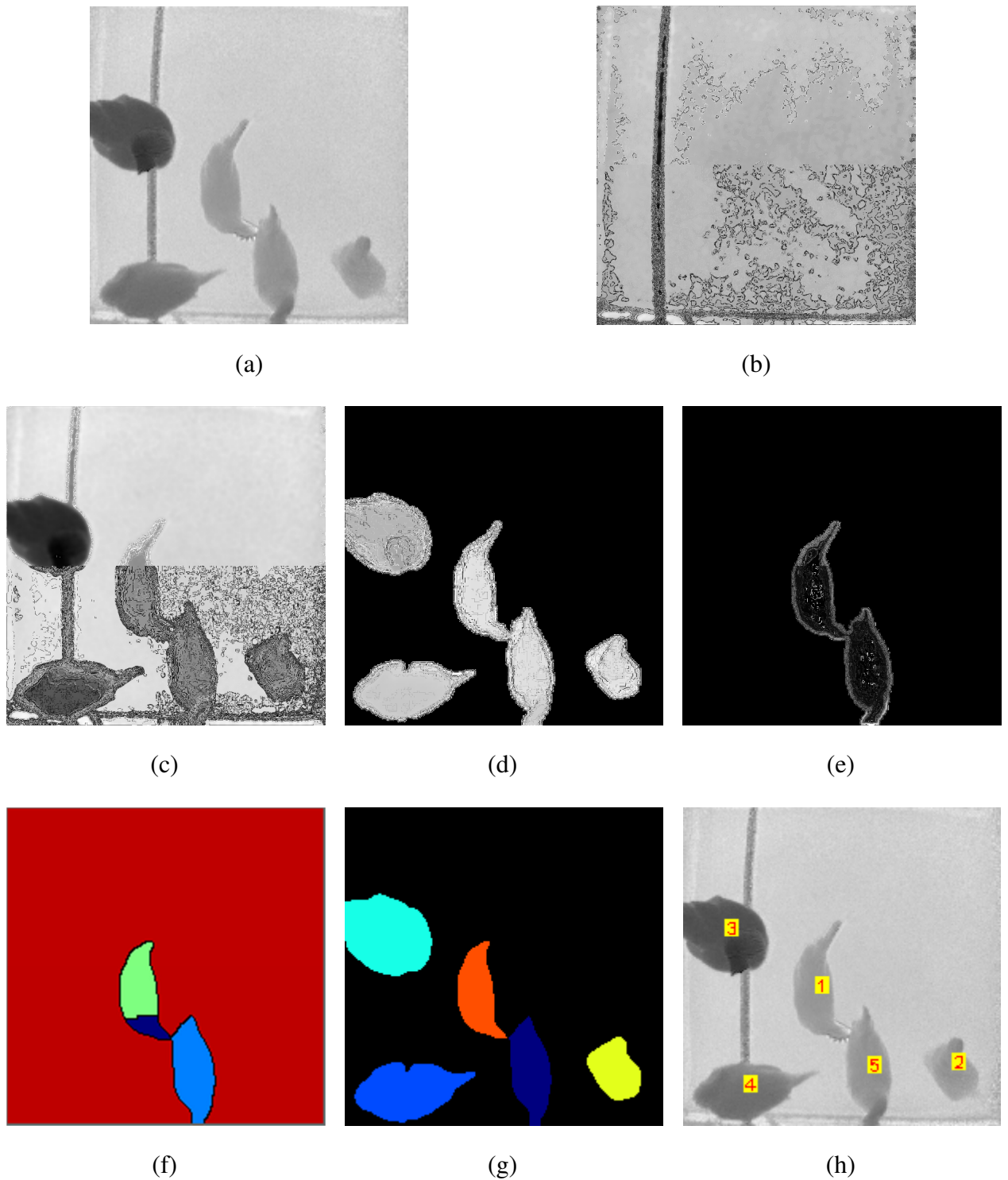
Figure 2. Laying hens identification algorithm: (a) Distance image; (b) Background image; (c) Noise reduced image; (d) Foreground image; (e) Gradient magnitude image; (f) Watershed partitions; (g) Detected hens; (h) Uniquely identified hens

Experiments and Results

The system was able to track individual hens and extract their behaviors such as perching, nesting, feeding, drinking and movement. The SD effect was examined by comparing behavioral data of the same 5 hens used in both the SD levels. Figure 3 shows the time spent by the hens in feeding area on different days. The graph clearly indicates that the hens spent more time in feeding area when housed in a group of 5 than when housed in a group of 10.
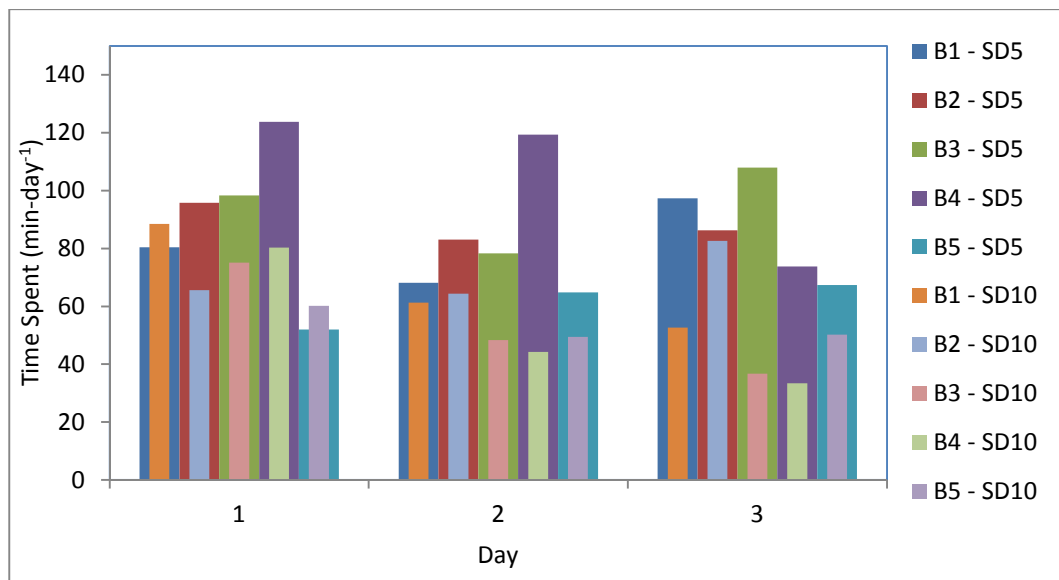

Figure 3. Time spent at feeder by 5 hens on different days when housed at SD5 or SD10

Figures 4, 5, 6 and 7 depict time budgets of perching, nesting, feeding and drinking behaviors, respectively. The shaded block along the horizontal axis indicates the dark hours of the day. Figure 4 clearly shows that the hens spent longer time on perch at night than during the day. The data also show that the hens spent 348 ± 240 min-hen^{-1}-day^{-1} and 265 ± 158 min-hen^{-1}-day^{-1} on perch when housed at SD5 and SD10,

respectively, presumably due to the available perch space. Similarly, figure 5 depicts time budget of nesting behavior. The hens spent longer time in nest box between 10:00h and 11:00h and the time spent in nest box slowly declined. It was observed that only 3-4 hens spent most of their time on perch at night, while some hens spent entire time in nest box or on floor at night despite having enough perch space. The data revealed that the hens spent 99 ± 165 min-hen^{-1}-day^{-1} and 78 ± 142 min-hen^{-1}-day^{-1} in nest box when housed at SD5 and SD10, respectively. Figure 6 shows time budget of feeding behavior. The feeding behavior seems consistent throughout the day, with nearly zero activity at night. It can be seen that the hens spent 87 ± 21 min-hen^{-1}-day^{-1} and 60 ± 17 min-hen^{-1}-day^{-1} in feeding area when housed in groups of 5 and 10, respectively. Similarly, as shown in figure 7, drinking behavior seems consistent throughout the day and was nearly zero at night. The hens spent 32 ± 12 min-hen^{-1}-day^{-1} and 27 ± 11 min-hen^{-1}-day^{-1} in drinking area when housed at SD5 and SD10, respectively.
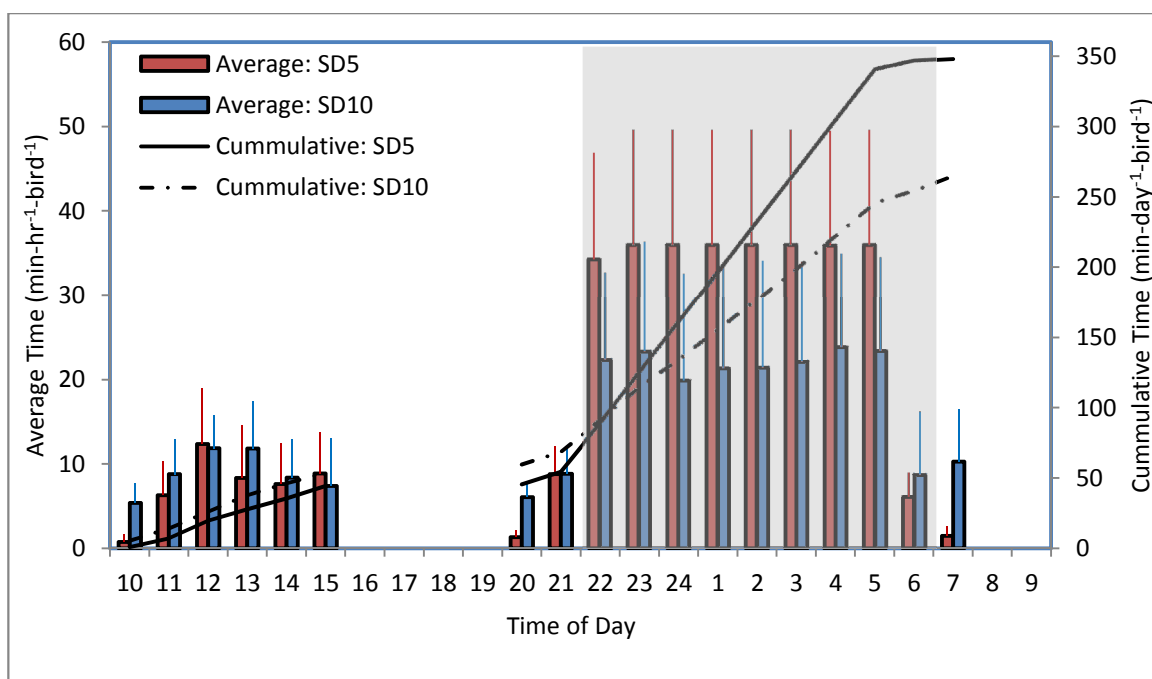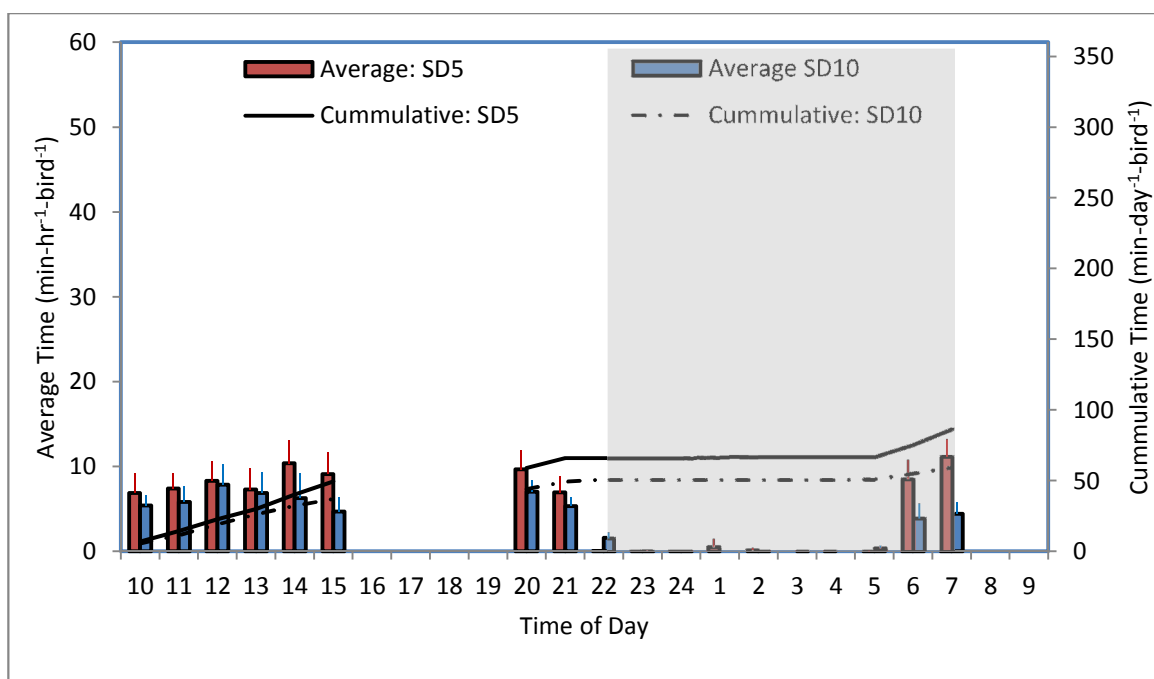
Figure 4. Perching-behavior time budget of hens housed in group of 5 or 10 hens
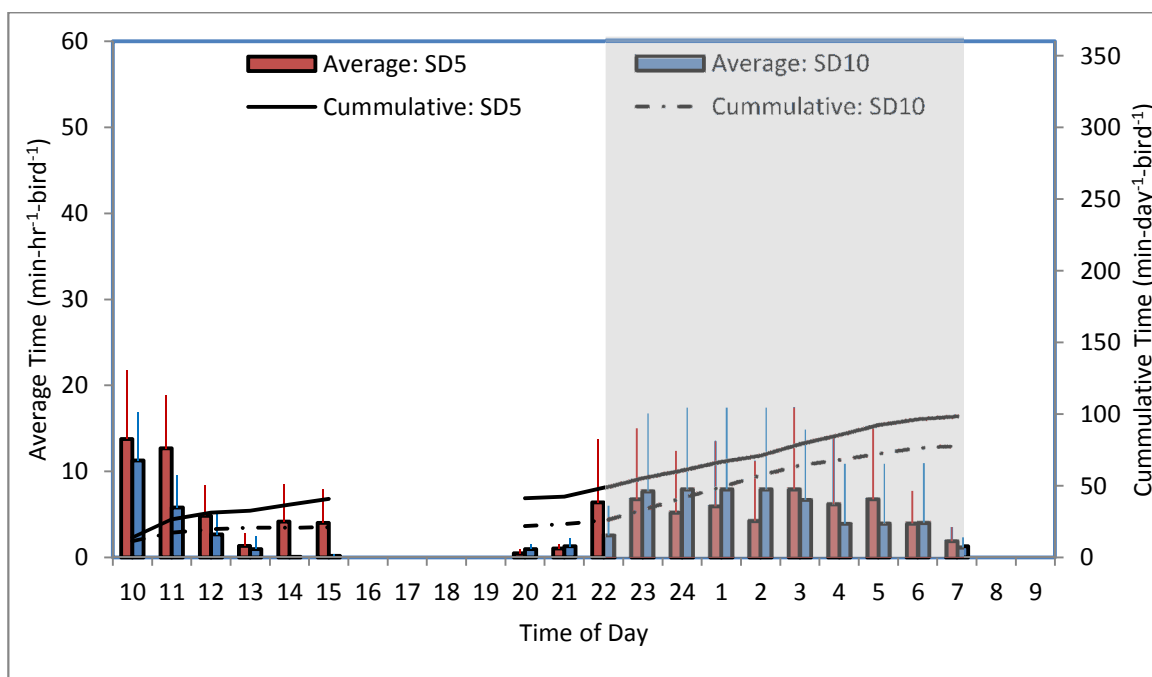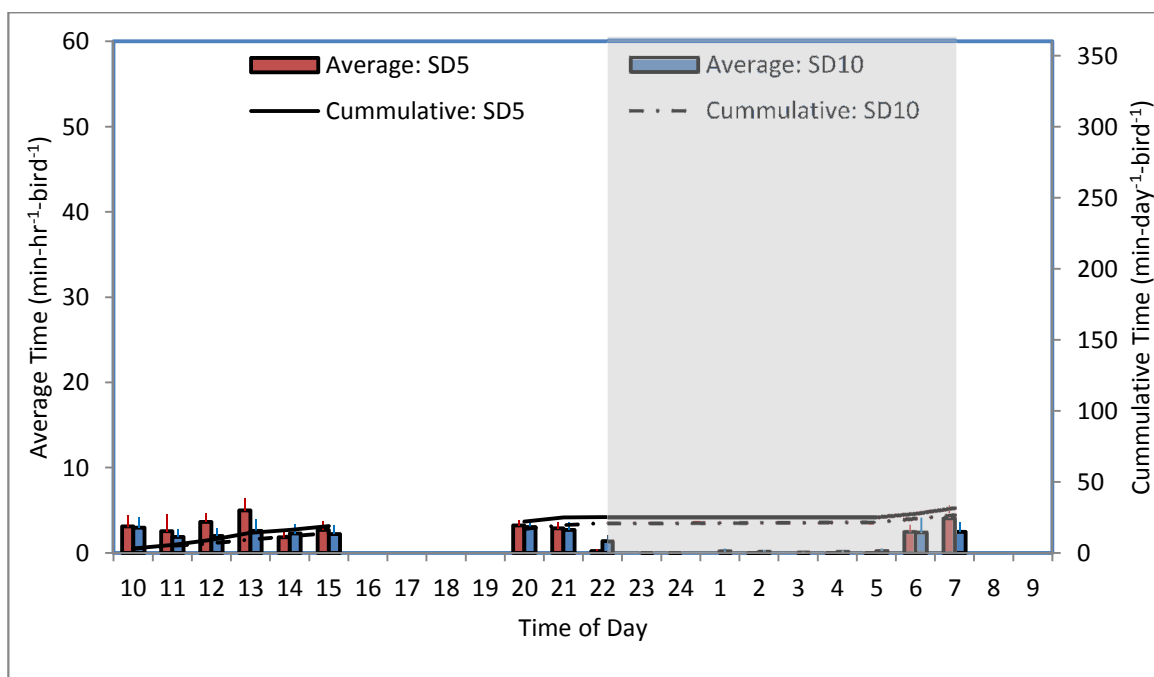

**Figure 5.** Nesting-behavior time budget of hens housed in group of 5 or 10 hens

Figure 6. Feeding-behavior time budget of hens housed in group of 5 or 10 hens


Figure 7. Drinking-behavior time budget of hens housed in group of 5 or 10 hens

Figure 8 depicts time budget of movement. The hens seemed to move 499 ± 236 m-hen^{-1}-day^{-1} and 540 ± 160 m-hen^{-1}-day^{-1} when housed in group of 5 and 10, respectively.
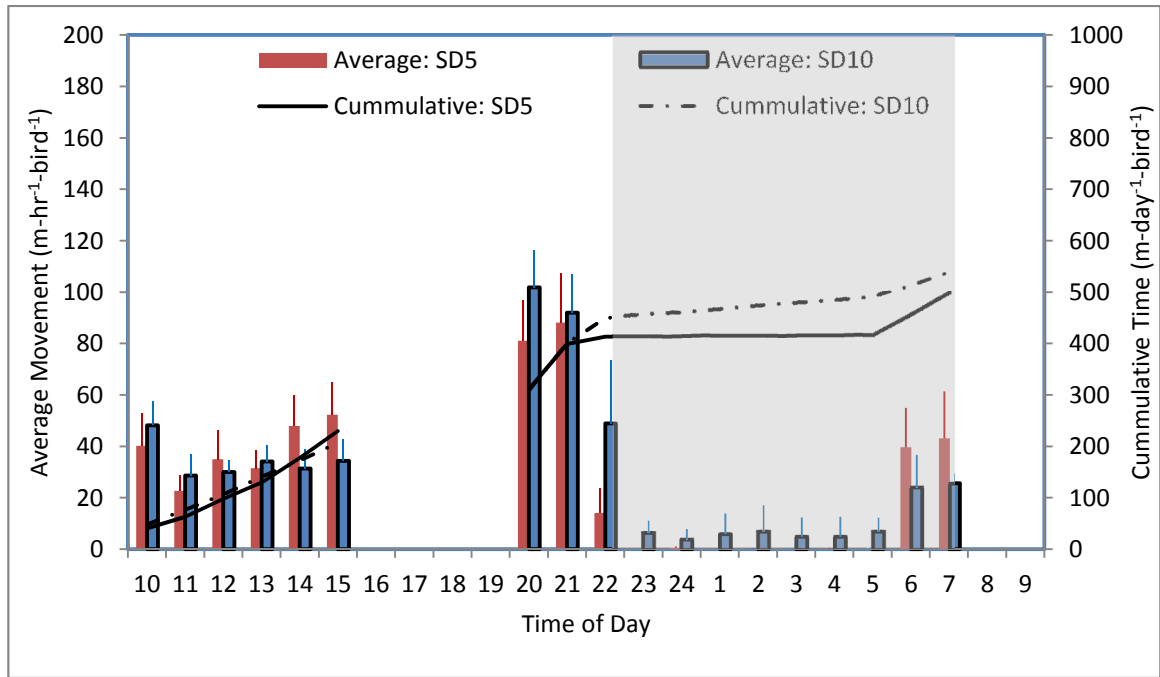
Figure 8. Movement time budget of hens housed in group of 5 or 10 hens in a 1.2 m × 1.2 m pen

Figure 9 shows comparison between distributions of movement by the hens housed at SD5 and SD10 filtered at 5 cm to ignore smaller movements which could be the result of erroneous centroid extraction. It was observed that about 90% of the movements made by the hens during the day (10 hr-day^{-1}) were less than 10 cm long when they were housed in group of 5, while about 85% of the movements were less than 10 cm long when housed in group of 10.
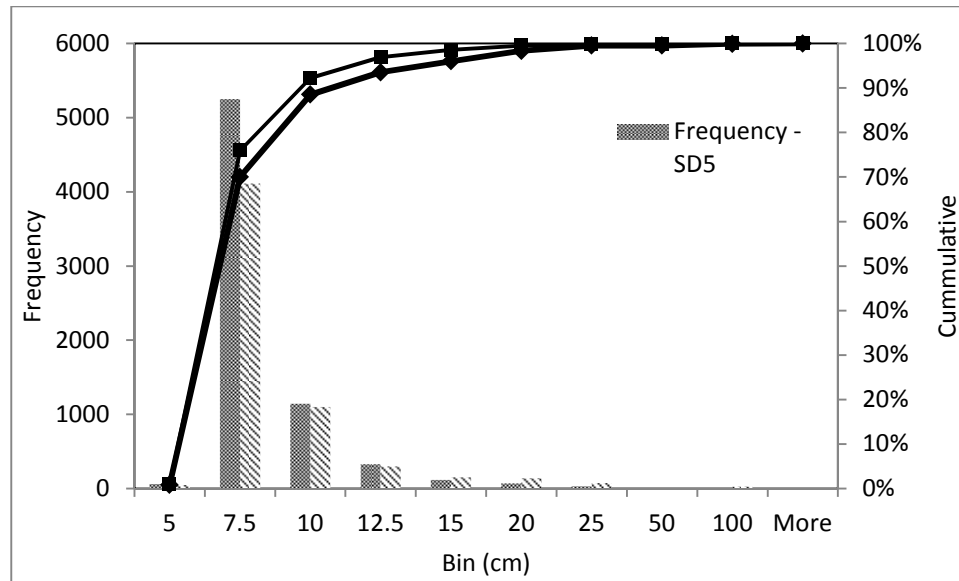
Figure 9. Comparison of movement by hens housed at stocking density of 5 or 10 in a 1.2 m × 1.2 m pen.

Figure 10 shows average time spent by the hens performing different activities. The same 5 hens on average spent 32% and 25% of their time on perch when housed in groups of 5 and 10, respectively. Similarly, the hens on average spent 9% and 7% of their time in nest box, and 8% and 6% of their time in feeding area when housed in groups of 5 and 10, respectively. The hens spent 3% of their time in drinking area in both the stocking densities. For the remaining of the time, 48% and 60%, the hens performed activities such as standing, walking and sitting when housed at SD5 and SD10, respectively.
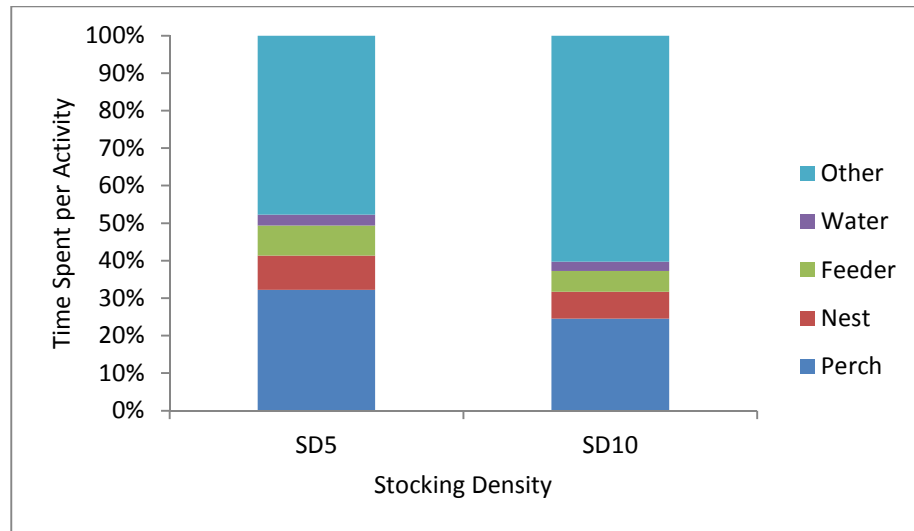
Figure 10. Average time spent by birds performing different activities

The statistical analysis of the data showed that SD effect was significant on perching behavior of the laying hens (P = 0.0023). The hens spent more time on perch at SD5 (348 min) compared to SD10 (265 min). This is not surprising because of the limited perch space. Similarly, SD effect was prominent on feeding behavior (P < 0.0001), 87 min at SD5 and 60 min at SD10. The increased pressure for feeding space was seen on hens in SD10. On the other hand, SD effect was insignificant on nesting or drinking behaviors (P = 0.3597 and 0.1366, respectively). The result also show that SD did not affect movement of the hens for the given floor space of 1.2 m × 1.2 m (P = 0.2422).

Table 2. Stocking density effect on laying hen behaviors.

Behavior	Stocking Density Effect
Perching	Yes (p=0.0023)
Nesting	No (p=0.3597)
Feeding	Yes (p<0.0001)
Drinking	No (p=0.1366)
Movement	No (p=0.2422)

Conclusions

In this study, we developed a system that automatically extracts behaviors, such as locomotion, perching, nesting, feeding and drinking, of hens housed in groups of 5 and 10, thereby quantifying stocking density effects on their behaviors. The system has been demonstrated to track and maintain identities of individual hens, which is critical for extraction of time budgets of individual hen behaviors. This unique tracking system will enhance researchers' ability to examine the impact of physical and management factors on behaviors and well-being of group-housed animals.

Acknowledgements

References

Abrahamsson, P. 1996 Furnished cages and aviaries for laying hens: effects on production, health and use of facilities. Swedish University of Agricultural Sciences. Upsala. Department of Animal Nutrition and Management. Report 234.

Chedad, A., Aerts, J.-M., Vranken, E., Lippens, M., Zoons, J. & Berckmans, D. 2003 Do heavy broiler chickens visit automatic weighing systems less than lighter birds? *British Poultry Science*, 44(5): 663-668.

Cook, R. N., Xin, H., Nettleton, D. 2006 Effects of Cage Stocking Density on Feeding Behaviors of Group-Housed Laying Hens. *Transactions of ASABE*. Vol: 49(1): 187-192

De Wet, L., Vranken, E. & Berckmans, D. 2003 Computer-assisted image analysis to quantify daily growth rates of broiler chickens. *British Poultry Science*, 44(4): 524-532.

Frost, A. R., French, A. P., Tillett, R. D., Pridmore, T. P., Welch, S. K. 2004 A vision guided robot for tracking a live, loosely contrained pig. *Computers and Electronics in Agriculture*, 44(2): 93-106.

Gates, R.S. and H. Xin. 2001. Comparative analysis of measurement techniques of feeding behavior of individual poultry. ASAE Meeting Paper No. 01-4033. St. Joseph, Michigan.

Hy-Line International. 2000. Hy-Line Variety W-36 Commercial Management Guide. West Des Moines, IA: Hy-Line International

Hu J., Xin H. 2000 Image-processing algorithms for behavior analysis of group-housed pigs. *Behavior Research Methods Instruments & Computers*, 32(1): 72-85.

Leroy, T., Vranken, E., Van Brecht, A., Struelens, E., Sonck, B., Berckmans, D. 2006. A Computer Vision Method for On-line Behavioral Quantification of Individually Caged Poultry. *Transactions of ASABE*, Vol. 49(3): 795-802.

Liu, K., Xin, H., Shepherd, T., Zhao, D., Yang, Z., Carlson, K. 2013. Evaluation of Hen Preference for Hexagonal or Round Perches. ASABE Meeting, Kansas City, Kansas.

McDonald's. 2000. *Recommended Welfare Practices: Egg Laying Hens Guidelines*. Oak Brook, Illinois. McDonalds's Corporation.

Nakarmi, A. D., Tang, L, Xin, H. 2013. Tracking Laying Hens using a 3D Vision Sensor and Radio Frequency Identification Technique, ASABE Meeting, Kansas City, Kansas.

Perona, P., Malik, J. 1990. Scale-space and Edge Detection using Anisotropic Diffusion. *IEEE Transactions of Pattern Analysis and Machine Intelligence*. 12(7): 629-639.

Persyn, K.E., H. Xin, D. Nettleton, A. Ikeguchi, and R.S. Gates. 2004. Feeding behaviors of laying hens with or without beak trimming. *Transactions of the ASAE*. 47(2): 591-596.

Puma, M.C., H. Xin, R.S. Gates, and D.H. Burnham. 2001. An instrumentation system for studying feeding and drinking behavior of individual poultry. *Applied Engineering in Agriculture*. 17(3): 365-374.

Schofield, C. P., Marchant, J. A., White, R. P., Brandl, N. & Wilson, M. 1999 Monitoring pig growth using a prototype imaging system. *Journal of Agricultural Engineering Research*, 72: 205-210.

Sergeant, D., Boyle, R. & Forbes, M. 1998 Computer visual tracking of poultry. *Computers and Electronics in Agriculture*, 21(1): 1-18.

Shao, J., Xin, H. & Harmon, J. D. 1998 Comparison of image feature extraction for classification of swine thermal comfort behaviour. *Computers and Electronics in Agriculture*, 19(3): 223-232.

Tillett R. D., Onyango C. M., Marchant J. A. 1997 Using model-based image processing to track animal movements. *Computers and Electronics in Agriculture*, 17(2): 249-261.

UEP. 2000. *Animal husbandary guidelines for U.S. Egg laying Flocks*. Atlanta, Georgia. United Egg Producers.

Van der Stuyft, E., Schofield, C. P., Randall, J. M., Wambacq, P. & Goedseels, V. 1991 Development and application of computer vision for use in livestock production. *Computers and Electronics in Agriculture*, 6: 243-265.

Vaughan R., Sumper N., Henderson J., Frost A., Cameron S. 2000 Experiments in automatic flock control. *Robotics and autonomous systems*, 31(1-2): 109-117.

Xin, H. and A. Ikeguchi. 2001. Characterization of feeding behavior of growing broilers – A Research Report. Iowa State University, Ames, Iowa, USA.

Zimmerman, P. H., Linderberg, A. C., Pope, S. J., Glen, E., Bolhuis, J. E. and Nicol, C. J. 2006. The effect of stocking density, flock size and modified management on laying hen behavior and welfare in a non-cage system. *Applied Animal Behavior Science*.101(111-124).

CHAPTER 7

CONCLUSIONS AND RECOMMENDATIONS

Conclusions

In this study, computer-vision and image-processing techniques were applied to develop automatic inter-plant spacing-sensing of corn plants at early growth stages and automatic quantification of stocking-density effects on certain laying-hen behaviors including locomotion, perching, nesting, feeding, and drinking.

The automatic inter-plant spacing-sensing system for corn plants used a light-based time-of-flight (TOF) vision sensor mounted on a three-wheeled image acquisition platform. The platform was designed in such a way that the effects of direct sunlight and wind were reduced and it could therefore be used at any point of time in a given day. The system was capable of accurately detecting corn plants between v2 and v4 in their growth stages (20-35 cm tall), and of measuring inter-plant distances. The major challenges encountered were attributed to long plant canopies occluding the stem profile, multiple plants emerging at the same location, and uneven emergence of the plants that led to a misidentification rate of up to 4%. While the multi-view approach used helped reduce effects of long canopies and could detect doubles, the system still missed considerably late-emerging plants.

The system for automatic quantification of stocking-density effects on laying-hen behaviors was developed using a sensor-fusion approach. A vision system was used as a primary sensor for tracking multiple laying hens and extracting their behaviors, while the

RFID antenna grid was used as a recovery mechanism to help maintain identities of laying hens when the vision system failed to do so. Tracking multiple laying hens was a challenging task from a computer-vision perspective since, a) the hens had similar images; 2) the hens appeared to differ in different frames based on their postures; 3) the nesting hens entered and exited the scene; and 4) some hens were partially or fully occluded when they were positioned beneath the perching hens. The hens were exposed to a photo period of 16 hours starting at 6:00h. They were fed twice a day at 9:00h and 17:00h pm and eggs were removed once a day during the evening feeding session. Images and RFID data were acquired for 18 hours per day for a total of 3 days for each stocking density. Data was not collected from 8:00h to 10:00h in the morning and from 16:00h to 20:00h in the evening to allow the hens to settle down after being disturbed during feed refilling and egg removal. The hens were extremely disturbed during the egg removal process because an operator had to use a probe to pull eggs from the cage floor. The statistical analysis of the data revealed that the stocking-density effect was significant with respect to perching and feeding behaviors of the laying hens, but was insignificant with respect to their nesting and drinking behaviors as well as to their locomotion.

Recommendations

Inter-plant Spacing Sensing

The developed within-row inter-plant spacing sensing system was capable of accurately detecting stem centers of corn plants which lying within $\pm 15°$ from vertical and at least 20 cm tall. The multi-view approach helped the system to detect doubles and to reduce the effect of long-hanging canopies that occluded stem profiles.

- The images acquired from the field were processed offline. The acquisition frame rate was about 18 frames per second and the processing rate was about 6 frames per second. For the system to be capable of real-time operation, the algorithm must be optimized and/or implemented in hardware.

- To keep the misidentification rate low, the system was designed to ignore plants shorter than 20 cm. The system was incapable of distinguishing between weeds and corn plants. A sophisticated object-recognition algorithm could help eliminate this shortcoming.

- The image-acquisition platform was pushed manually in the direction of the crop row. In the future this platform could be modified to mount on a tractor or on an auto-guidance system provided with a path-planning algorithm.

Hen Behavior Monitoring

The hen-behavior monitoring system developed for automatic quantification of stocking-density effects on laying-hen behaviors was capable of tracking individual laying hens and extracting their behaviors in each frame.

- The images were acquired at about 5 frames per second and the offline processing rate was about 3 frames per second. For the system to be capable of working in real-time, the algorithm must be optimized and/or implemented in hardware.

- Feed refilling and egg removal were not mechanized, so the researcher was required to enter the laboratory twice a day. The egg-removal process was extremely disturbing to the hens and they were therefore given several hours to settle down after this activity. In the future, to support data collection over a full 24-hour interval, the feed refilling and egg-removal processes must be mechanized.

- The system was able to extract certain laying-hen behaviors such as perching, nesting, feeding, drinking, and locomotion. These behaviors were basically extracted using spatial information of the laying hens from the vision and RFID data. To extract other typical laying behaviors such as wingflapping and preening, a dynamic model of each behavior must be developed.